



UNIVERSIDAD DE INVESTIGACIÓN DE TECNOLOGÍA EXPERIMENTAL YACHAY

Escuela de Ciencias de la Tierra, Energía y Ambiente

**TÍTULO: Sequence stratigraphy of the central part of the
Ecuadorian Coastal Basins combining seismic and well-log
data.**

Trabajo de integración curricular presentado como requisito para la
obtención del título de Geóloga

Autora:

Ortega Cumbicus Alejandra Nathalia

Tutor:

M.Sc. Pérez Roa Richard

Co-Tutor:

PhD. Vázquez Taset Yaniel

Urcuquí, Junio 2024

Autoría

Yo, **ORTEGA CUMBICUS ALEJANDRA NATHALIA**, con cédula de identidad 1104414931, declaro que las ideas, juicios, valoraciones, interpretaciones, consultas bibliográficas, definiciones y conceptualizaciones expuestas en el presente trabajo; así cómo, los procedimientos y herramientas utilizadas en la investigación, son de absoluta responsabilidad de la autora del trabajo de integración curricular. Así mismo, me acojo a los reglamentos internos de la Universidad de Investigación de Tecnología Experimental Yachay.

Urcuquí, Junio 2024.

Alejandra Nathalia Ortega Cumbicus

CI: 1104414931

Autorización de publicación

Yo, **ORTEGA CUMBICUS ALEJANDRA NATHALIA**, con cédula de identidad 1104414931, cedo a la Universidad de Investigación de Tecnología Experimental Yachay, los derechos de publicación de la presente obra, sin que deba haber un reconocimiento económico por este concepto. Declaro además que el texto del presente trabajo de titulación no podrá ser cedido a ninguna empresa editorial para su publicación u otros fines, sin contar previamente con la autorización escrita de la Universidad.

Asimismo, autorizo a la Universidad que realice la digitalización y publicación de este trabajo de integración curricular en el repositorio virtual, de conformidad a lo dispuesto en el Art. 144 de la Ley Orgánica de Educación Superior.

Urcuquí, Junio 2024.

Alejandra Nathalia Ortega Cumbicus

CI: 1104414931

Dedication

To my beloved family, especially my sister, Gabriela, and my parents, Danilo and Maty, I cannot help but recognize the fundamental role you have all played in my life. To my faithful feline companions Danna, Catalino, and Mio, with your comforting presence, you have been my solace in times of stress and uncertainty. You have filled my life with joy, love, and companionship. Each of you has contributed to this achievement in your own special way.

Alejandra Nathalia Ortega Cumbicus

Acknowledgment

I am deeply grateful to my advisor, Richard Pérez, and co-advisor, Yaniel Vázquez, for their support, invaluable guidance, and endless patience throughout the development of this thesis. Their insightful feedback, constructive criticism, and encouragement have been fundamental to accomplishing my project. I would also like to extend my gratitude to Mariela Rodríguez and Germán Merino for their valuable insights and feedback on the final work.

I want to express my deepest gratitude to my family for their unwavering love, support, and understanding throughout this journey and for always supporting and caring for me. I thank my parents for giving me their wisdom; their encouragement has been a constant source of motivation for me.

Moreover, I thank all my professors who have taught me and helped me grow academically during my career. I thank my friends Martina, Luis, Karol, Sebas, Vicky, Bolo, and Darwin for cheering and accompanying me throughout this journey. I thank my boyfriend, Wil, for his unconditional love and support and for helping me in my personal growth. I am deeply grateful to all who have positively impacted me and helped me present this work.

Alejandra Nathalia Ortega Cumbicus

Resumen

La estratigrafía secuencial permite una evaluación profunda de una cuenca mediante el análisis de los ambientes deposicionales de las facies, y este proyecto tiene como objetivo realizar un estudio de la cuenca costera central del Ecuador utilizando datos sísmicos y de registro de pozos con el fin de proporcionar más información para la exploración de hidrocarburos en esta área. De esta manera, podría ser posible encontrar una reserva probada de hidrocarburos para aumentar la producción de petróleo o gas natural del país, que ha mostrado valores bajos de producción en los últimos años. Para esta secuencia estratigráfica de la cuenca fue necesaria una mejora de los datos utilizados para obtener una buena aproximación al modelo real; por esta razón, se aplicó una eliminación de ruido self-supervised y un spectral blueing a los datos sísmicos, al igual que los datos de registro de pozos también recibieron un procesamiento para crear una traza sintética que se ajustara mejor a un modelo del subsuelo. Además, se realizó un análisis geohistórico para comprender la evolución de la cuenca mediante el estudio de la subsidencia de la cuenca. Por lo tanto, esta evaluación de la cuenca de la parte costera central del Ecuador podría ser utilizada para un estudio de exploración de hidrocarburos.

Palabras Clave:

Estratigrafía secuencial, Self-supervised denoising, Amarre sísmica-pozo, Seismic spectral blueing (SSB), Exploración de hidrocarburos.

Abstract

Sequence stratigraphy allows a profound basin assessment by a broader depositional framework of the facies. This project aims to comprehensively analyze Ecuador's central coastal basin using seismic and well-log data to provide more information for exploring hydrocarbon in this area. In this way, it could be possible to find a proven hydrocarbon reserve to increase the production of oil or natural gas, which has shown low production values over the past few years. For this sequence stratigraphic of the basin, an improvement of the data used was necessary to get a good approach to the real model; for this reason, self-supervised denoising and spectral blueing were applied to seismic data, and the well-log data as well received processing for creating a synthetic trace that better fit the subsurface model. In addition, a geohistorical analysis was made to understand the evolution of the basin by analyzing its subsidence. Therefore, this basin assessment from the central coastal part of Ecuador could be used to study hydrocarbon exploration.

Keywords:

Sequence stratigraphy, Self-supervised denoising, Seismic well tie, Seismic spectral blueing, Hydrocarbon exploration.

Contents

Dedication	iii
Acknowledgment	iv
Resumen	v
Abstract	vi
Contents	vii
List of Tables	x
List of Figures	xi
1 Introduction	1
1.1 Background	1
1.2 Problem Statement	3
1.3 Objectives	6
1.3.1 General Objective	6
1.3.2 Specific Objectives	7
1.4 Geographical Setting	7
2 Theoretical Framework	10
2.1 Sequence Stratigraphy	10
2.2 Seismic Data	16
2.3 Well-log Data	18
2.4 Seismic-well tie	21

3	Geological Framework	24
3.1	Manabí basin	25
3.2	Lithostratigraphic units of Manabí basin	30
4	Methodology	39
4.1	Data Available and software	40
4.2	Geophysical work	41
4.2.1	Analysis of the frequency and resolution of seismic data, extraction of wavelets and development of synthetic seismograms (Phase I). . .	41
4.2.2	Seismic data improvement: denoising, spectral blueing	44
4.2.3	Development of synthetic seismograms (Phase II)	46
4.2.4	Seismic Interpretation	46
4.3	Geological work	47
4.3.1	Digitalization and filtering of well-log data	48
4.3.2	Correlation of wells in the study area	48
4.3.3	Definition of stratigraphic sequences	49
5	Results and Discussion	50
5.1	Enhancement of seismic and well-log data	50
5.2	Seismic interpretation	52
5.2.1	Basement (BS)	54
5.2.2	Seismic sequence 1 (SS-1)	55
5.2.3	Seismic sequence 2 (SS-2)	57
5.2.4	Seismic sequence 3 (SS-3)	61
5.2.5	Seismic sequence 4 (SS-4)	63
5.2.6	Seismic sequence 5 (SS-5)	65
5.2.7	Seismic sequence 6 (SS-6)	67
5.2.8	Correlation Panel	70
5.3	Basin Analysis	72
5.3.1	Geo-historical results and basin fill evolution	72
6	Conclusions	82

Bibliography	85
Appendices	91
Appendix 1.	92

List of Tables

4.1	Data available in the study area for the creation of synthetic seismograms	44
4.2	Combination of the parameters for the denoising process	45
4.3	Seismic characteristics of the interpreted sequences for the 11 lines. These characteristics are generally evaluated according to the parameters described in the chapter 2 and an example is present in Fig. 4.5	47
5.1	Correlation coefficients of the synthetic seismograms for the three wells before (phase I) and after (phase II) the improvement of data.	53
5.2	Analysis of the horizons, generally described according to their frequency, amplitude, and continuity.	54

List of Figures

1.1	Trend of the oil production of Ecuador from 2000 to 2022. (Central Bank of Ecuador, 2023)	4
1.2	The total value of exportations of Ecuador of 2022 and the representation in percentage. (OEC, 2022)	5
1.3	Cross-section of Ecuador with W-E orientation, representing subduction of Nazca plate under American plate, the major terranes and main basins systems. Manabí basin is pointed with the red arrow. Modified from Cediél et al. (2003)	7
1.4	Location map of the area of study (blue rectangle) in Manabí basin, Ecuador showing the height variations, with the seismic lines (black lines) and wells (red points) used for this analysis, also the counties seats (brown rectangles) and main faults (red lines). It also shows the location of Fig. 5.1 and Fig. 5.19.	9
2.1	Types of stratigraphic unconformities. Modified from (Falcón, 2005)	12

2.2 Sequences types, systems tracts and bounding surfaces defined relative to the base-level and the TR curves. Abbreviations: SU = subaerial unconformity; c.c. = correlative conformity; BSFR = basal surface of forced regression; MRS = maximum regressive surface; MFS = maximum flooding surface; R = transgressive wave-ravinement surface; IV = incised valley; (A) = positive accommodation (cf. base-level rise); NR = normal regression; FR = forced regression; LST = lowstand systems tract; TST = transgressive systems tract; HST = highstand systems tract; FSST = falling stage systems tract; RST = regressive systems tract; DS = depositional sequence; GS = genetic stratigraphic sequence; T-R = transgressive regressive sequence. Taken from Eriksson et al. (2006) 13

2.3 System tracts and sequence boundaries nomenclature. Keys: RSL=relative sea level; T=transgression; R=regression; FR=forced regression; LNR=lowstand normal regression; HNR=highstand normal regression; LST=lowstand systems tract; TST=transgressive systems tracts; HST=highstand systems tract; FSST=falling-stage systems tract; RST=regressive systems tract; T-R=transgressive-regressive; MFS=maximum flooding surface; MRS=maximum regressive surface. Taken from Octavian et al. (2011) 15

2.4 Seismic line uninterpreted from Taranaki basin, New Zealand with the two-way time in seconds and depth with meters. Taken from Al-Masgari et al. (2021) 17

2.5 Reflections configuration of some seismic facies from the Taranaki basin of New Zealand. Taken from Al-Masgari et al. (2021) 18

2.6 Stratigraphic cross-section and well correlations with the SP record between the boreholes in Manabí basin with N-S orientation. Taken from Benitez (1995) 19

2.7 Synthetic seismogram from a well of a study in El Salto field, Venezuela, with a correlation coefficient of 0.486. Taken from Pérez and Richard (2015) 22

3.1	Geological map of coastal basins of Ecuador from Guayaquil Gulf to Esmeraldas, illustrating the main faults, basins and cordilleras of the coast, with the seismic lines (black lines) and the three wells (blue circles) analyzed delimited for the area of this study (dashed line). Other wells on the coast are represented by red circles. Modified from (Carrillo et al., 2022)	26
3.2	Seismic profile of line 553 with NW-SE orientation with the six seismic units and the regional discordance (Ub to U5). Taken from (Villitanga, 2020) . .	27
3.3	Stratigraphy of Manabí basin according to the Chone-1 drilling information and Reyes and Michaud (2012), the biozones according to Benitez (1995); Ordóñez et al. (2006), seismic sequences and unconformities codes analyzed in this work, the paleoenvironment from Ordóñez et al. (2006); Benitez (1995), the lithology according to Benitez (1995); Reyes and Michaud (2012)	32
4.1	Workflow of the methodology of this project describing the geophysical and geological activities to develop for the improvement of the seismic-well tie.	40
4.2	Survey spectrum of the seismic data. A) Survey the spectrum of seismic data before processing data. B) survey spectrum after applying spectral blueing.	42
4.3	Time-Depth chart of Ricaurte well, used to create the first synthetic seismograms of the three wells.	43
4.4	Synthetic seismogram of the first phase from Ricaurte-1 well shows the velocity, depth, density, gamma ray record, wavelet, synthetic trace and the trace with the correlation coefficient (r) at the last column.	44
4.5	Seismic interpretation example of line 1 (see location in Fig. 1.4) with NW-SE orientation, crossing line 9, line 3, Ricaurte-1 well and line 11. Faults (black lines), stratigraphic sequences and unconformities are represented. .	48
5.1	Portion of a seismic line 1 with NW-SE orientation (Fig. 1.4) that crosses the line 9. A) Seismic raw data B) Data denoised with proof 6 of 32x32 pixels, with no extra noise and SB The yellow line represents the top of SS-5, and a fault is found at the northwestern part (black line.)	51

5.2	Well-log of GR, SP and resistivity ILD records of Ricaurte-1. A) Segment of data scanned from logs of Ricaurte-1 well of 340 m. B) Segment of well data digitalized of Ricaurte-1 from -1.40 to -0.60 s. Some of the first part of the records (SP) were skipped because of the distortion of superficial conditions	52
5.3	Seismic line 10 with SW-NE orientation (see location in Fig. 1.4). Above the data without interpretation, and below the seismic line with the sequences and unconformities identified. Faults are represented with red lines.	53
5.4	Transgressive-Regressive cycles of the second order from the Gamma Ray record of Ricaurte well and the correlation with the seismic sequences, seismic portion of line 1 (see Figure 1.4 for location) from this work with its time in two-way traveltime, eustatic changes of Haq et al. (1987) , the mega-sequences of Barba (2018) , the geological formations that Ricaurte-1 cut and the lithology from Benitez (1995) ; Reyes and Michaud (2012)	55
5.5	Isopach map of the basement (BS) in the study area showing two-way travel time in s (TWT).	56
5.6	Isopach map of SS-1 in the study area showing the two-way traveltime (TWT) of the seismic waves in s.	58
5.7	Isochore map of SS-1 and the basement showing the two-way traveltime (TWT) of the seismic waves in s.	59
5.8	Isopach map of SS-2 in the study area showing the two-way traveltime (TWT) of the seismic waves in s.	60
5.9	Isochore map of SS-2 and SS-1 showing the two-way traveltime (TWT) of the seismic waves in s.	61
5.10	Isopach maps of each sequence (BS, SS-1, SS-2, SS-3, SS-4, SS-5, SS-6) in the study area showing the two-way traveltime (TWT) of the seismic waves in s.	62
5.11	Isopach map of SS-3 in the study area showing the two-way traveltime (TWT) of the seismic waves in s.	63
5.12	Isochore map of SS-3 and SS-2 values showing the two-way traveltime (TWT) of the seismic waves in s.	64

5.13	Isopach map of SS-4 in the study area showing the two-way traveltime (TWT) of the seismic waves in s.	66
5.14	Isochore map of SS-4 and SS-3 values showing the two-way traveltime (TWT) of the seismic waves in s.	67
5.15	Isopach map of SS-5 in the study area showing the two-way traveltime (TWT) of the seismic waves in s.	68
5.16	Isochore map of SS-5 and SS-4 values showing the two-way traveltime (TWT) of the seismic waves in s.	69
5.17	Isopach map of SS-6 in the study area showing the two-way traveltime (TWT) of the seismic waves in s.	70
5.18	Isochore map of SS-6 and SS-5 values showing the two-way traveltime (TWT) of the seismic waves in s.	71
5.19	Correlation panel of the three wells Calceta-1, Chone-1, Ricaurte-1. Formation's code: KCy = Cayo Fm., KGq = Guayaquil Fm., EZp = Zapallo Fm., OPr = Playa Rica Fm., OMT = Tosagua Gp, MAg= Angostura Fm. with its depositional setting, and the unconformities U-0, U-1, U-2, U-3, U-4. Fault in red line	72
5.20	Geohistorical graphic of Ricaurte-1 well. Formation's code: KCy = Cayo Fm., KGq = Guayaquil Fm., EZp = Zapallo Fm., OPr = Playa Rica Fm., OMT = Tosagua Fm. It shows the seismic sequences SS-1, SS-2, SS-3, SS-4, SS-5, which correspond to each formation, and the unconformities U-0, U-1, U-2, U-3, U-4.	73
5.21	Geohistorical graphic of Chone-1 well. Formation's code: KCy = Cayo Fm., KGq = Guayaquil Fm., EZp = Zapallo Fm., OPr = Playa Rica Fm., OMT = Tosagua Fm. It shows the seismic sequences SS-1, SS-2, SS-3, SS-4, SS-5, which correspond to each formation, and the unconformities U-0, U-1, U-2, U-3, U-4.	75

5.22 Geohistorical graphic of Calceta-1 well. Formation’s code: KCy = Cayo Fm., KGq = Guayaquil Fm., EZp = Zapallo Fm., OPr = Playa Rica Fm., OMT = Tosagua Fm. It shows the seismic sequences SS-1, SS-2, SS-3, SS-4, SS-5, which correspond to each formation, and the unconformities U-0, U-1, U-2, U-3, U-4. 78

5.23 Geohistorical graphic of three wells (Ricaurte-1, Chone-1, Calceta-1). Formation’s code: KCy = Cayo Fm., KGq = Guayaquil Fm., EZp = Zapallo Fm., OPr = Playa Rica Fm., OMT = Tosagua Fm. It shows the seismic sequences SS-1, SS-2, SS-3, SS-4, SS-5, which correspond to each formation, and the unconformities U-0, U-1, U-2, U-3, U-4. 79

1 Synthetic seismogram of Ricaurte-1 well after the improvement of data. . . 92

2 Synthetic seismogram of Chone-1 well after the improvement of data . . . 92

3 Synthetic seismogram of Calceta-1 well after the improvement of data . . . 93

Chapter 1

Introduction

1.1 Background

Sequence stratigraphy is a relatively new concept in the interpretation of stratigraphy. Initially, it was called seismic stratigraphy, but it also has other applications than just seismic. In 1949, Sloss and his coworkers proposed the term “sequence,” which refers to the sedimentary periods separated by unconformities (Koutsoukos, 2005). Nowadays, it is known as sequence stratigraphy, and it studies the time and space correlations of the facies. Stratigraphy has many applications, including chemostratigraphy, biostratigraphy, magnetostratigraphy, and chronostratigraphy. In the beginning, the facies were correlated by their lithology. However, geologists realized that a better correlation could be made by combining time and the lithology of facies. It was sustained by H. E. Wheeler with the chrono-lithostratigraphic chart, facilitating the regional correlations in the stratigraphy sequence (Koutsoukos, 2005).

Sequence stratigraphy is based on tectonic, sea level changes, and other factors that modify the depositional environment. The sedimentary cycles are divided by sequence boundaries and surfaces between different systems tracts. Unconformities-bounded differentiate onlap, toplap, system tracts such as highstand system tracts (HST), low stand system tracts (LST), transgressive system tract (TST), etc. (Koutsoukos, 2005). Also, Galloway (1989) presents the flooding-surface bounded as another boundary surface in basis analysis.

Finally, sequence stratigraphy could be defined as the interpretation of sedimentary

cycles found in stratigraphic patterns caused by the variation in factors such as sediment supply, sediment accommodation, tectonism, climate, uplift, sea level changes, and subsidence (Posamentier and Allen, 1999). The difficulty in describing a sequence stratigraphy model is the extensive dependence on many variables because of the complexity of the relationships with the environment. Besides, Posamentier and Allen (1999) propose a list of basic geological principles important for sequence stratigraphy, such as the state of equilibrium of natural systems, Walther's Law and the sedimentation supply and accommodation rate reflected in the patterns of the strata.

A sequence is a basic unit in sequence stratigraphy, and it is defined according to its type (Catuneanu, 2020). For this reason, a sequence is generally described as a "succession of strata deposited during a full cycle of change in accommodation and sediment supply" by Catuneanu et al. (2009). This definition implies that the same surface boundary delimits a sequence at the base and top. The sequence scales go from parasequences to megasequences based on their duration, geographical extension and thickness (Catuneanu, 2020). This stratigraphic sequence follows the principles stated by Posamentier and Allen (1999), like that the main amount of sediment comes from hinterland areas and is deposited in sedimentary basins with the help of the abovementioned factors. A sedimentary basin is an area in the Earth's crust covered by several meters of sedimentary rocks filled during millions of years, and they are important because hydrocarbon mainly forms in sedimentary basins (Selley and Sonnenberg, 2023).

Ecuador has different sedimentary basins, such as the intermountain basins from the Inter-Andean valley, the foreland system at the Oriente basin and the forearc basins in the coastal region. From these basins, some have been extensively studied for exploration and exploitation of hydrocarbons, like the Oriente basin, which is well documented due to the relevance of oil fields found at the back-arc basins of the Andean system (Lonsdale, 1978); meanwhile, the coastal region only is studied in depth at the Progreso Basin, but there is limited information of Manabí or Esmeralda's basins.

1.2 Problem Statement

The exploration activities do not indicate the presence of hydrocarbon in Manabí. However, this zone is well-known as a potential reservoir of hydrocarbons. In the 1940 -1967 period, there were intense explorations in different regions of the country. Some of these areas correspond with foreland (Oriente basin), forearc (Manabí, Esmeraldas, Borbón) sedimentary basins ([Banco Central del Ecuador, 1990](#)). Even though these environments are not common for hydrocarbon, some studies present hydrocarbon reservoirs in this type of basin ([Carrillo et al., 2022](#)). For instance, the research of [Hessler and Sharman \(2018\)](#) demonstrated that the forearc basin has the potential to be exploitation fields of the hydrocarbon systems associated with subduction zones worldwide. The authors concluded that the shared characteristics of these productive basins include the distance to the continental arc, large-scale structures, time to evolve, and development conditions for causing reservoirs of hydrocarbons. For example, the Progreso basin, which is adjacent to Manabí, was the first exploited basin for oil and gas in Ecuador, and it shared geological formation with the Manabí basin from Miocene to the Pleistocene ([Reyes and Michaud, 2012](#)).

Since hydrocarbons are materials that cannot be recovered by nature in a human timescale, the value of these resources increases in their importance for society ([Smith, 2006](#)). The British Petroleum Statistical Review of World Energy and the Energy Information Administration (EIA) data held that the global oil-proven reserves total around 1,650,585,140,000. Global consumption is 35,442,913,090 barrels per year so that it could last until 2067 (around 44 years more), according to data from 2016 ([Worldometer, 2017](#)). However, it needs to consider the oil reserves that have yet to be discovered [Worldometer \(2017\)](#). According to the Energy Information Administration, in 2020, the proven reserves of natural gas were 7257 trillion cubic feet (TCF). The global consumption is 136.325 TCF so that the natural gas will last around 53 years ([EIA, 2023](#)). Further, the global oil demand increased to 103 million barrels per day in June 2023, according to the International Energy Agency ([International Energy Agency \(IEA\), 2023](#)). Haitham Al Ghais, the Secretary-General of the Organization of Petroleum Exporting Countries (OPEC), forecasts a rise in the global demand for oil to 2045 with 110 million barrels per day (OPEC, [2023](#)).

For Ecuador, the proven reserves sum up to 8300 million, and a production of 138 million gives around 59 years for oil production with data of 2021. Also, Ecuador's exportation value was \$36B, of which the 30.8% (\$11.1B) was from crude petroleum, which represents the higher percentage from the exportation of the country, and the 4.64% (\$1.67B) was refined petroleum, in 2022 consistent with the Observatory of Economic Complexity (OEC, 2022). For this reason, Ecuador could still take advantage of the exportation of these resources for at least the next 50 years. Besides, oil production will increase from 172.6 million barrels in 2021 to 175.5 million barrels in 2022. Its costs will rise from 2021 to 2022, from an average of \$62 to \$85.8 per barrel (Central Bank of Ecuador, 2023). Although the last year has a rise in production, the production values do not are as high as they were before the pandemic from 2020, as Figure 1.1 shows.

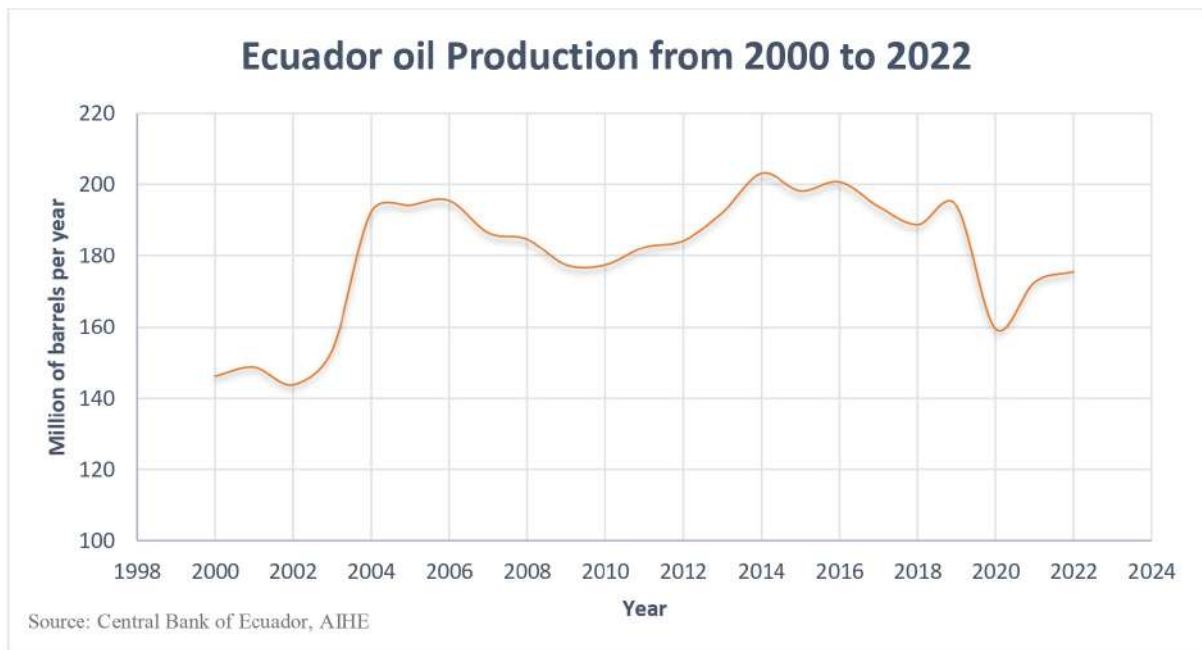


Figure 1.1: Trend of the oil production of Ecuador from 2000 to 2022. (Central Bank of Ecuador, 2023)

Furthermore, the Gross Domestic Product (GDP) of the country increased by 0.1% with the primary support of the oil production income that improved by 26.8% for 2022. The oil industry represents 14.4% of the total GDP of 2022 (Central Bank of Ecuador, 2023).

However, hydrocarbon exploitation has decreased in energy generation compared to “clean” energies, such as geothermal, solar, or wind energy. Even with the increase in re-

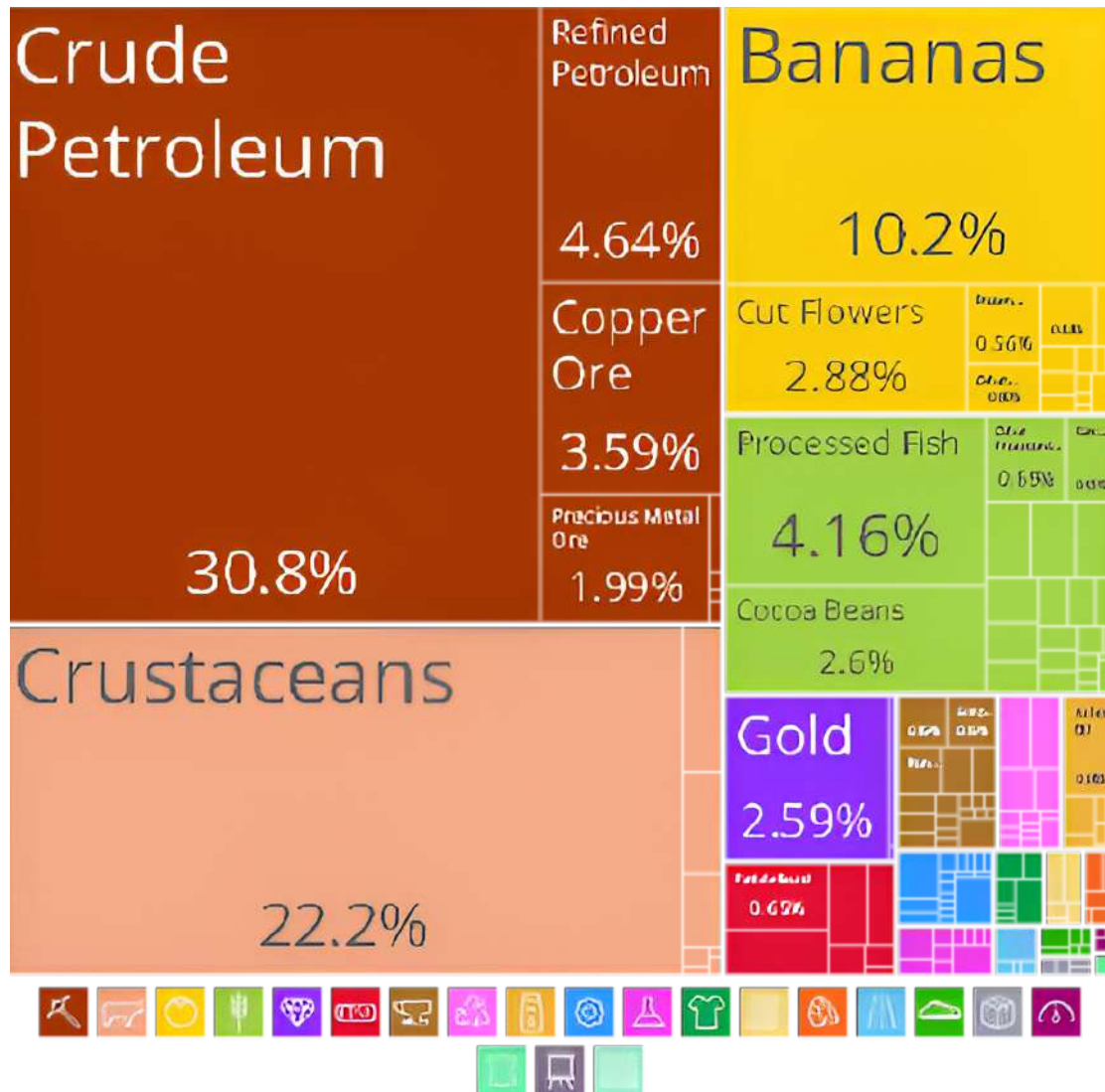


Figure 1.2: The total value of exportations of Ecuador of 2022 and the representation in percentage. (OEC, 2022)

newable resources, hydrocarbons will still have a high value for around 40 years. Moreover, the main exportation from Ecuador is crude oil (Fig. 1.2), and cutting off this revenue would mean 30.8% (\$11.1 B) less of the country's exportation. (OEC, 2022).

The studies in the coastal region are mainly focused on the SW basin of Ecuador's coast because the first explorations in the Manabí basin were not rewarding, so they stopped in 1975 (Banco Central del Ecuador, 1990). Aizprua (2021) details some hydrocarbon potential in Santa Elena and the Guayaquil-Tumbes basin. However, Petroamazonas has started a project to reconsider the hydrocarbon potential of the zone (Aizprua, 2021). Nevertheless, previous studies have not considered the comprehensive analysis of the processed data

to enhance the sequence stratigraphic interpretation. Furthermore, socio-political issues in the country have led to a decline in oil and gas production. For example, the protection initiative of the Yasuní National Park, where the Ishpingo-Tambococha-Tiputini (ITT) block, an important site for hydrocarbon exploitation, is located, as well as the strike of 2022, which resulted in the closure of 961 wells.

For this reason, exploring other places of hydrocarbon potential, like coastal basins (Manabí, Esmeraldas, Borbón) for exploitation is fundamental to recovering oil production and covering the demand enough to continue or increase the income from hydrocarbon resources. Some studies in the coastal basins were made by oil companies, so the reports remain unpublished and classified. Even so, some papers with academic approach established the basis for the analysis of these basins such as [Lonsdale \(1978\)](#); [Benitez \(1995\)](#); [Deniaud \(1998, 2000\)](#); [Hernández et al. \(2020\)](#); [Aizprua et al. \(2020\)](#); [Aizprua \(2021\)](#); [Carrillo et al. \(2022\)](#); [Hernández et al. \(2024\)](#) in agreement with these oil companies. For instance, [Benitez \(1995\)](#) studies the geodynamic evolution of the coastal basins, or [Deniaud \(1998\)](#) studies the tectonic-sedimentary evolution of the coastal basins using the seismic and well data provided by the oil companies, but with primary processing of this data. Currently, the studies used the seismic data with gravity and magnetometry surveys like [Hernández et al. \(2020\)](#) processed 2D seismic data with a deconvolution of Tau-P domain and pre-stack noise attenuation; or [Carrillo et al. \(2022\)](#) which tie the seismic with the well data. It gives reasons to continue the investigations on the coastal region of Ecuador. Rethinking the approach to correct the seismic and well-log data using filtering and deep learning techniques can increase the subsurface knowledge. Therefore, combining improved seismic and well-log data could allow a better interpretation and generate a sequence stratigraphic model of the Manabí basin that may be suitable for hydrocarbon reservoir identification.

1.3 Objectives

1.3.1 General Objective

To enhance the understanding of the geological model of the Manabí basin by applying geophysical methods and sequence stratigraphy theory.

1.3.2 Specific Objectives

- Improve quality data by applying digitalization and filtering of well-log data and denoising and spectral blueing to seismic data.
- Interpret seismic data to create structural, isopach and isochore maps.
- Propose a stratigraphic sequence model and generate the geo-historical graphics to enhance understanding of the evolution of the basin.

1.4 Geographical Setting

Ecuador has a foreland basin system to the eastern (Oriente basin), and there is a system of forearc basins at the west (coastal basins) formed by the accretion of oceanic terranes. These are the Manabí basin, Borbón basin, Manta-Jama basin, Valdivia basin and Progreso basin (Deniaud, 2000). These basin systems are divided by the Western Cordillera, the Cordillera Real at the east, and the Inter-Andean valley between the cordilleras (Fig.1.3). The Manabí basin, where the study area is located, is part of the forearc basins of Ecuador. These extend throughout the coastal region from Guayaquil (south) to San Lorenzo (north) and from the coastal margin (west) to Western Cordillera (east), and the main basins in this area are Progreso at the south, Manabí at the central part of coastal basins, Esmeraldas and Borbón at the north part.

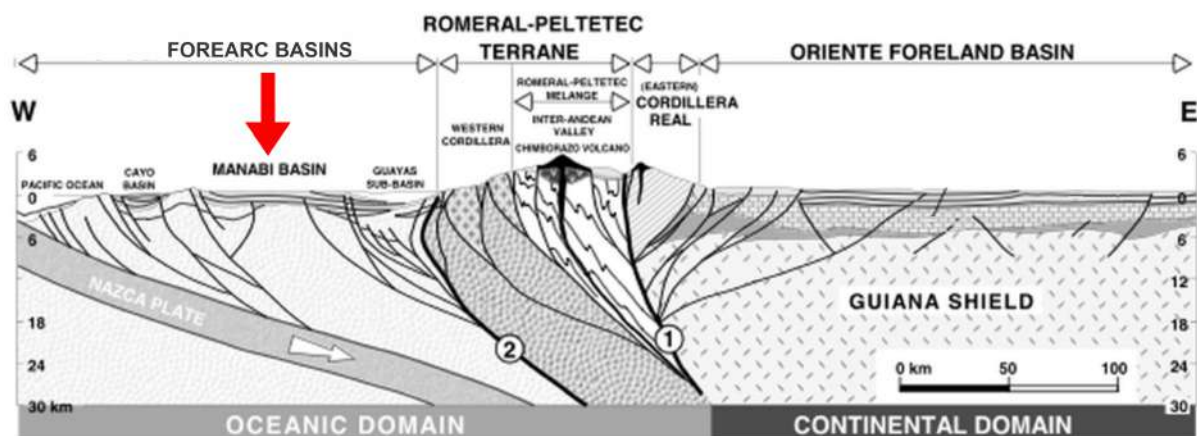


Figure 1.3: Cross-section of Ecuador with W-E orientation, representing subduction of Nazca plate under American plate, the major terranes and main basins systems. Manabí basin is pointed with the red arrow. Modified from Cediel et al. (2003)

The Manabí basin is in the province of the same name with its capital, Portoviejo. This basin is limited to the east with Western Cordillera, at the west with the Jama fault system, to the north limits with the Canandé Fault, and to the south with the Chongón-Colonche Cordillera. It is between 0°N and 2°S latitudes and 79°W to 81°W longitude. However, the study area encompasses 2328.1 km² including Flavio Alfaro, Zapallo, Ricaurte, Chone, Tosagua, Calceta and Rocafuerte counties (Fig. 1.4) that covers just the central-western part of the basin that limits Bahía de Caráquez at the west, at the south with cantonal capital Rocafuerte town, and at the north with the Jama system fault, where the seismic line 1 reached the Jama county. This area was selected to analyze due to its integration of three wells connected by 11 seismic lines, facilitating the production of high-quality seismic-well ties.

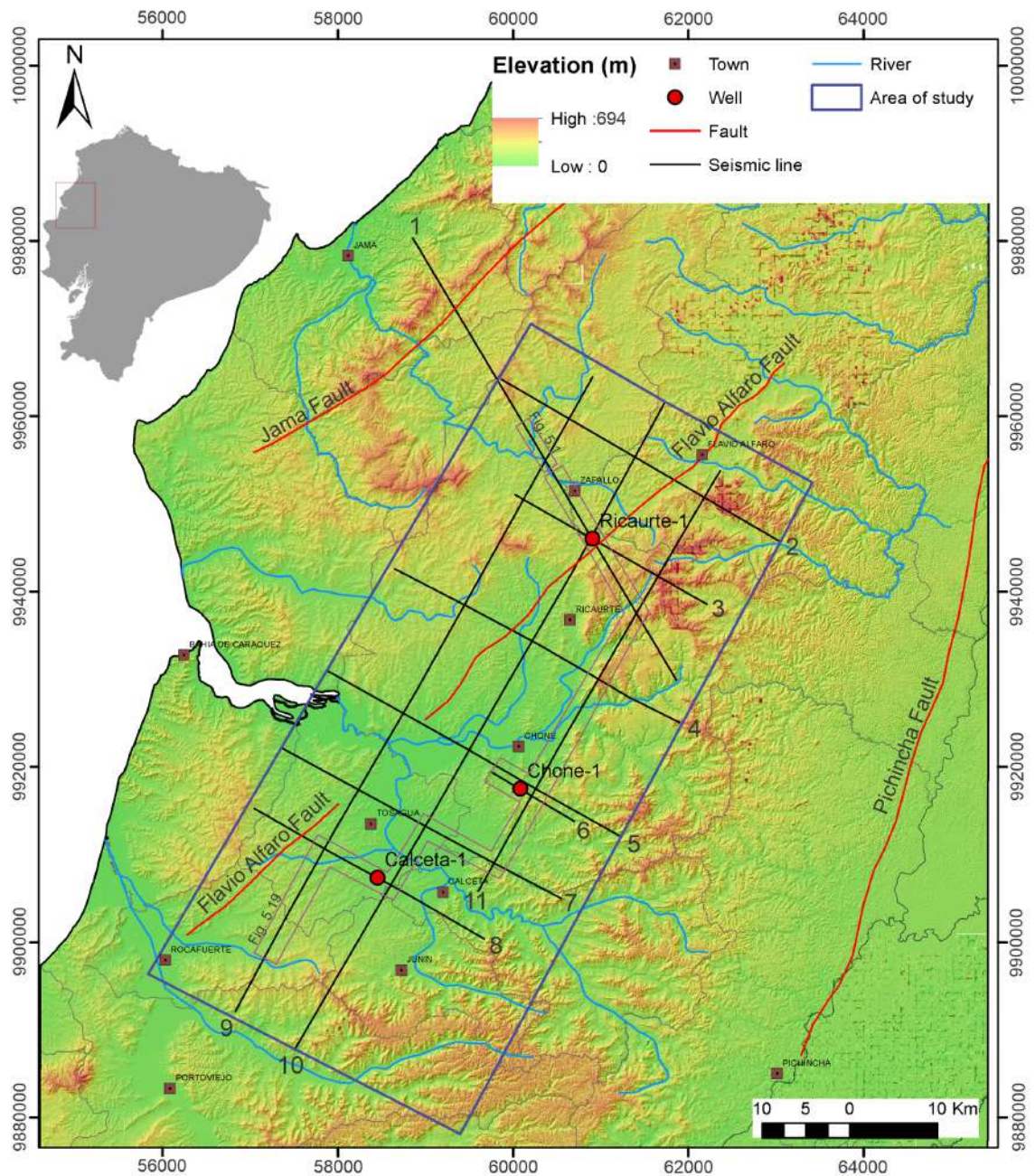


Figure 1.4: Location map of the area of study (blue rectangle) in Manabí basin, Ecuador showing the height variations, with the seismic lines (black lines) and wells (red points) used for this analysis, also the counties seats (brown rectangles) and main faults (red lines). It also shows the location of Fig. 5.1 and Fig. 5.19.

Chapter 2

Theoretical Framework

2.1 Sequence Stratigraphy

According to the Society for Sedimentary Geology website, stratigraphy studies the rock layer's succession and composition variations. Sequence stratigraphy (SS) is defined as a branch of sedimentary stratigraphy that studies the order of deposition of strata successions, providing more accurate interpretation and better prediction of lithofacies heterogeneity. The focus is studying the distribution and architecture of sedimentary sequences and interpreting the processes and events that have impacted their deposition and subsequent changes ([STRATA SEPM, 2013](#)).

Sequence stratigraphy allows the identification and correlation of surfaces and strata that reflect significant changes in the depositional environment and are visible in the sedimentary record. These surfaces, known as sequence boundaries, could be identified with lithologic changes, erosional surfaces, or changes in sedimentary structures. Recognizing and correlating these surfaces allows the sedimentary record to be divided into packages known as depositional sequences, which are the essential elements of sequence stratigraphy. However, SS has disadvantages in interpreting surfaces and terminology due to the broad scope that can vary among interpreters and models. These disadvantages could be avoided by following a workflow to analyze the sequences ([STRATA SEPM, 2017](#)).

Sequence stratigraphy could be the approach to studying groups of sedimentary units separated by sudden changes caused by specific events or factors affecting time-rock relationships ([Posamentier and Allen, 1999](#)). These factors mainly include tectonism as the

movement of the sea floor (Octavian et al., 2011); relative sea level, defined by Posamentier and Allen (1999) as the sea surface level relative to the point of the sea floor; accommodation that is the available space for the sediments to fill; eustasy is the position of the sea surface relative to a specific point as the center of the Earth (Posamentier and Allen, 1999); subsidence, which is defined as the sinking of the basin parallel and responsible for space for accommodation (National Oceanic and Atmospheric Administration, 2019); uplift, that is the elevation of the sea floor (Posamentier and Allen, 1999); and sediment supply is the rate of sediments enter to the basin, which is mainly controlled by climate and tectonism (Octavian et al., 2011). Sea level changes, for instance, determine the deposition and erosion of surfaces, generating different strata geometries; one example is the transgression when sea levels rise (STRATA SEPM, 2013).

Depositional sequences are distinguished by their internal architecture, which reflects the correlation between base-level changes. These sequences can be subdivided into system tracts, representing specific portions of the depositional sequence delineated based on sedimentary facies, sedimentary structures, and their position within the overall stratigraphic framework (STRATA SEPM, 2017). However, Posamentier and Allen (1999) mentioned that the depositional sequences will not be the term to use. Instead, this sequence can be defined as a stratigraphic unit of successions of system tracts bounded by unconformities. (Posamentier and Allen, 1999). A good recognition and interpretation of system tracts are essential to understanding the evolution of sedimentary environments and predicting the likely distribution of a reservoir within a basin. For this reason, the interpretation of accommodation successions should be combined with the fundamental laws of stratigraphy, Steno's laws and Walther's law; also, the chronology and sedimentary structures would facilitate the interpretation of the sequences (STRATA SEPM, 2017).

For the analysis of stratigraphic sequences according to STRATA SEPM (2013), the first step is to identify and subdivide the general surface; following, look for strata geometries of the successions; then, distinguish the system tract changing the order of deposition from the youngest to the oldest using back-stripping, which is the analysis of subsidence with tectonic origin from present to the past. Finally, reorganize to the order of the succession. As the unconformities mark the bounding between the sequences, the unconformity is defined as a non-deposition surface that represents a gap in time and divides younger

strata from the older one (Posamentier and Allen, 1999) or as an absence of sedimentation causing a cut-off in the record and time (Falcón, 2005). Falcón (2005) divide these unconformities according to their geometry in parallels and angular. Figure 2.1 shows the main unconformities: paraconformity, disconformity, and angular unconformity.

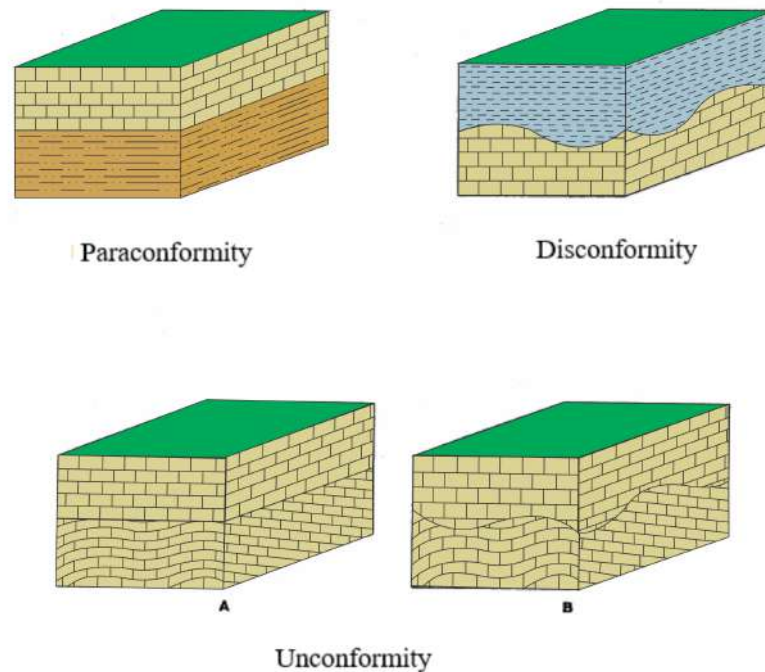


Figure 2.1: Types of stratigraphic unconformities. Modified from (Falcón, 2005)

Depositional Sequence

Octavian et al. (2011) stated that a depositional sequence defines a complete cycle of accommodation changes, including increasing and decreasing accommodation. Still, this sequence needs negative accommodation during its formation, and it is divided by surface bounding (Octavian et al., 2011).

Genetic Stratigraphic Sequence

It is defined by Octavian et al. (2011) as a complete cycle of accommodation. Still, it may have only positive values for the space available in the basin, and it is mainly characterized by the generation of maximum flooding surface (MFS). It is graphically represented in Figure 2.2 with the abbreviation GS.

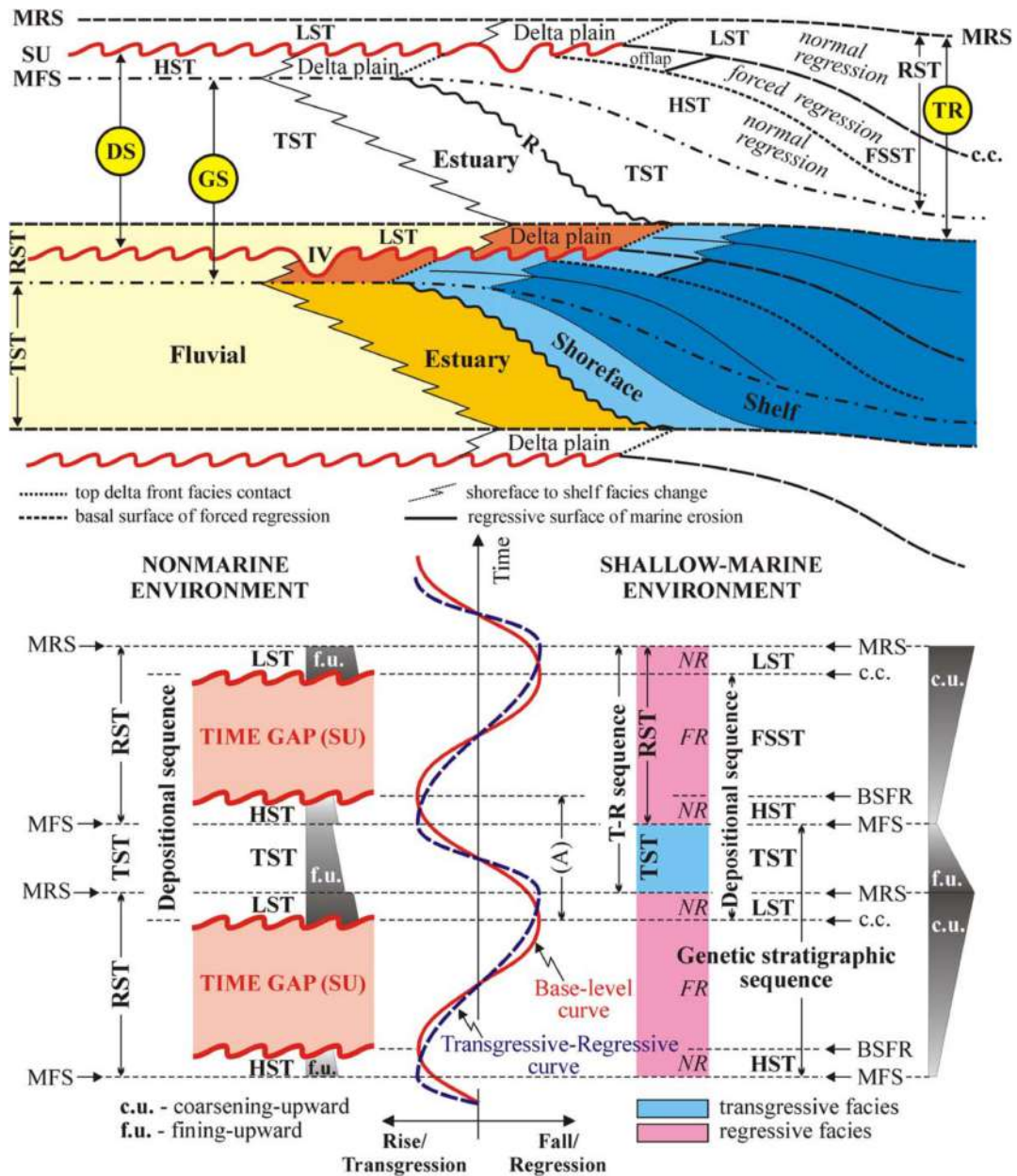


Figure 2.2: Sequences types, systems tracts and bounding surfaces defined relative to the base-level and the TR curves. Abbreviations: SU = subaerial unconformity; c.c. = correlative conformity; BSFR = basal surface of forced regression; MRS = maximum regressive surface; MFS = maximum flooding surface; R = transgressive wave-ravinement surface; IV = incised valley; (A) = positive accommodation (cf. base-level rise); NR = normal regression; FR = forced regression; LST = lowstand systems tract; TST = transgressive systems tract; HST = highstand systems tract; FSST = falling stage systems tract; RST = regressive systems tract; DS = depositional sequence; GS = genetic stratigraphic sequence; T-R = transgressive regressive sequence. Taken from Eriksson et al. (2006)

Transgressive-regressive Sequence (T-R)

It also could be formed during complete cycles of accommodation, but also only dependent on positive accommodation values (Fig. 2.3), which are separated by subaerial unconfor-

mities and maximum regressive surface (Octavian et al., 2011), and it separates a transgressive system tract (TST) at the top from a lowstand system tract (LST) at the base as is illustrated in Fig. 2.2 (SEPM STRATA, 2014).

Falling-Stage System Tract (FSST)

The Falling-Stage Systems Tract (FSST) refers to the deposits that accumulate during a decrease in sea level before the subsequent rise (Fig. 2.3). It is formed by a forced regression and is located directly on the sequence boundary (Fig. 2.2). Depending on sediment supply and sea-level fall, the FSST can have different stacking patterns. The term “falling stage” is commonly used to describe these systems tracts. The FSST is characterized by the erosion of exposed sediment surfaces and the formation of a subaerial unconformity. This unconformity can be overlain by fluvial deposits or reworked by marine features (Octavian et al., 2011; SEPM STRATA, 2014).

Lowstand system tract (LST)

The Lowstand Systems Tract (LST) refers to deposits that form during rising and falling sea level periods (Fig. 2.3). These deposits are found on top of FSST and the corresponding subaerial unconformity as Fig. 2.2 exhibit. LST sediments fill incised valleys and can be part of either the Late Lowstand Systems Tract or the Lowstand Prograding Wedge Systems Tract (Octavian et al., 2011).

Transgressive system Tract (TST)

The Transgressive Systems Tract (TST) includes deposits that form during a period of rising sea levels and are covered by the maximum flooding surface (Fig. 2.2). The TST exhibits back-stepping and onlapping stacking patterns. In cases of higher sediment supply, the parasequences in the TST may show aggradational characteristics (Fig. 2.3) (Octavian et al., 2011).

Highstand system tract (HST)

HST refers to deposits formed when sediment accumulation rates exceed the rate of increase in accommodation during sea-level rise as Fig. 2.3 shows (Octavian et al., 2011). The HST

is positioned on marine sediments and is capped by a subaerial unconformity (Fig. 2.2). Stacking patterns show prograding and aggrading clinofolds, with a top set of fluvial, coastal plain, and delta plain deposits (Octavian et al., 2011).

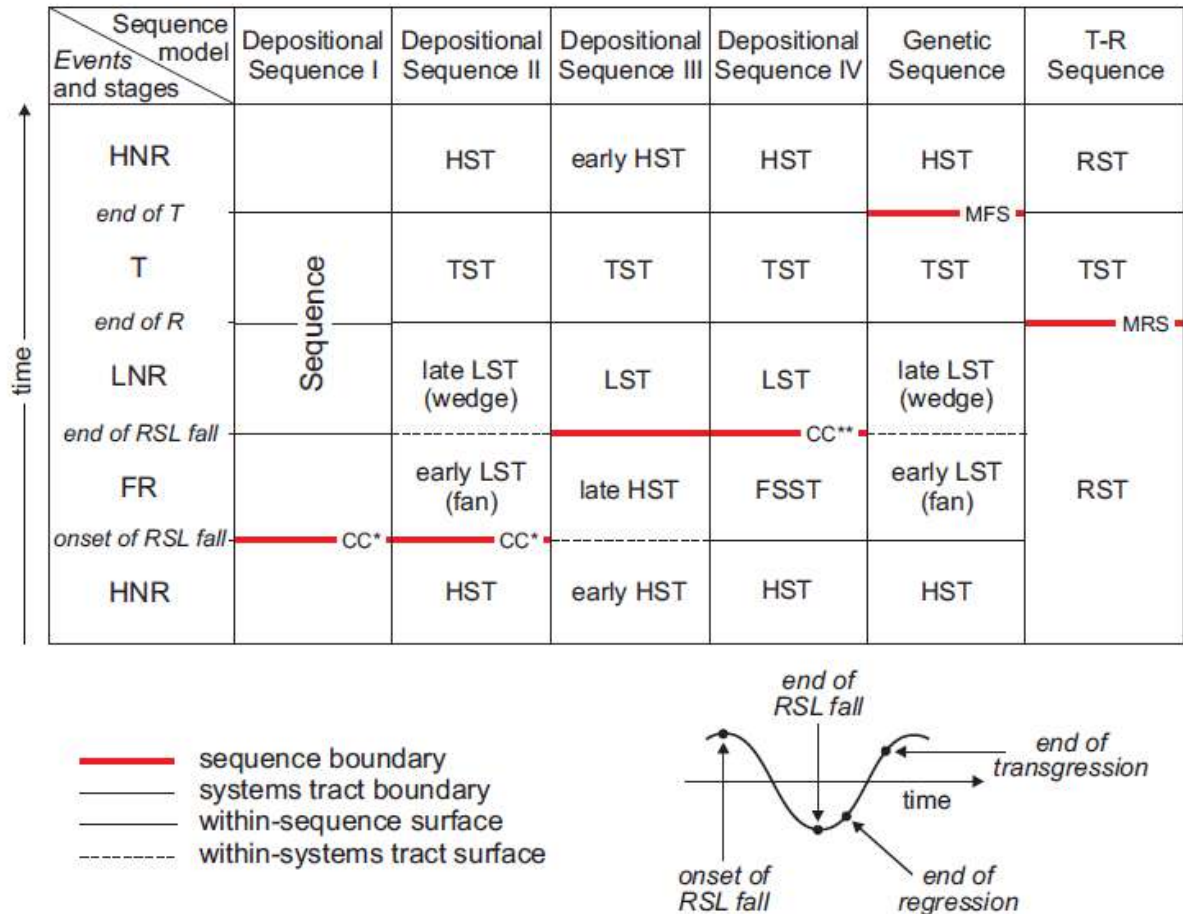


Figure 2.3: System tracts and sequence boundaries nomenclature. Keys: RSL=relative sea level; T=transgression; R=regression; FR=forced regression; LNR=lowstand normal regression; HNR=highstand normal regression; LST=lowstand systems tract; TST=transgressive systems tracts; HST=highstand systems tract; FSST=falling-stage systems tract; RST=regressive systems tract; T-R=transgressive-regressive; MFS=maximum flooding surface; MRS=maximum regressive surface. Taken from Octavian et al. (2011)

Regressive system tract (RST)

RST lies above a Transgressive Systems Tract (Fig. 2.2) and is followed by the initial transgressive surface of the overlying TST (Fig. 2.3). These systems tracts have different stratal stacking patterns and sediment dispersal patterns within the basin, making them relevant to petroleum plays. Sequence stratigraphy can enhance stratigraphic frameworks

for optimizing petroleum exploration and production development (Octavian et al., 2011).

Parasequences

A parasequence is a succession of facies limited by coastal to shallow-water areas (Fig. 2.3). It is bounded by marine flooding surfaces, which indicate an abrupt increase in water depth. Parasequences correspond to individual prograding sediment bodies in siliciclastic coastal to shallow-water settings; meanwhile, in carbonate settings, parasequences correspond to a succession of facies that contain a lag deposit or thin deepening interval followed by a thicker shallowing-upward part (SEPM STRATA, 2014). Although proposed to include all regional meter-scale cycles, the concept is of a parasequence to a unit bounded by marine flooding surfaces (Octavian et al., 2011).

2.2 Seismic Data

Commonly, geophysical methods are used for a comprehensive understanding of a basin by analyzing the subsurface as Hernández et al. (2020); Aizprua (2021); Aizprua et al. (2020); Hernández et al. (2024) did at Manabí basin, but is also used for the prospection of suitable areas for exploitation of hydrocarbons. The most developed method for hydrocarbon exploration is the reflection seismic (Lowrie, 2007). Seismic reflection data became fundamental in the 1960s and 1970s when high-quality multichannel seismic data enabled comprehensive SS analysis (Posamentier and Allen, 1999).

The seismic reflection consists of producing a signal to measure and record the time that it takes a ray to be reflected by the different rock layers and calculate the velocities at those layers; next, this time obtained by the geophones is plotted at a 2D cross-section profile (Lowrie, 2007). The method used for the exploration surveys is the CMP (Common Mid-Point), which is produced in a profile that crosses a geological structure in line, where the geophones are collocated at the same distance, and the shots of signals are made at various points to obtain the trace of reflection of a common point of these shots (Lowrie, 2007). Then, those trace records will be stacked together to get the seismic line; for instance, Figure 2.4 shows a seismic line from research of sequence stratigraphy in the Taranaki basin of New Zealand (Al-Masgari et al., 2021).

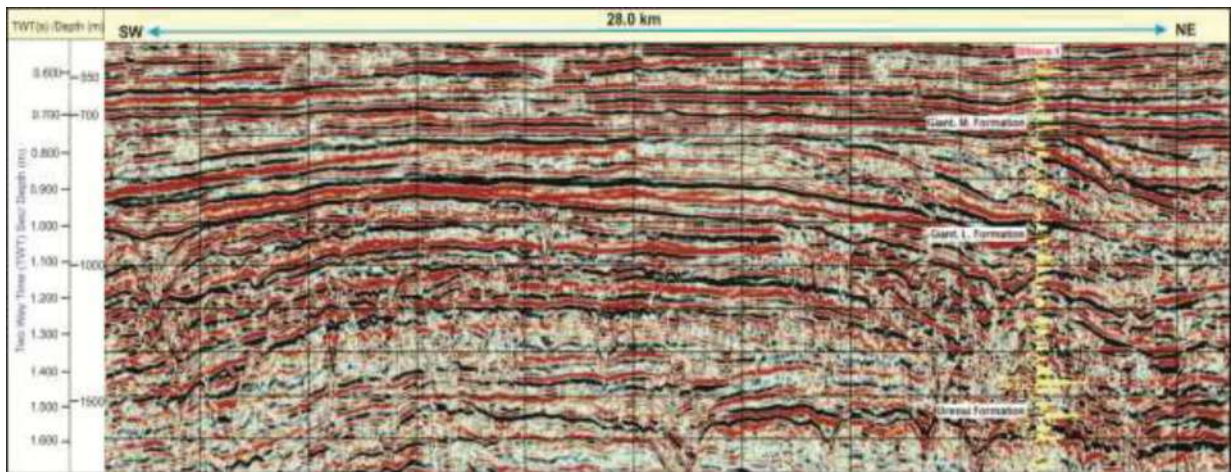


Figure 2.4: Seismic line uninterpreted from Taranaki basin, New Zealand with the two-way time in seconds and depth with meters. Taken from [Al-Masgari et al. \(2021\)](#)

Some important definitions of seismic reflection are frequency, amplitude, continuity, phase and polarity.

Frequency: The thickness of the generated acoustic signal, as shown in Figure 2.5, is usually determined by the frequency spectrum that depends on the type of sources ([Nanda, 2016](#)).

Amplitude: The maximum value at peak-trough of a pulse wavelet corresponds to the maximum value in amplitudes (Fig. 2.5), and it is proportional to the acoustic impedance, which is a rock property of the density times the velocity; so, amplitude allows determining the lithology and its lateral variation ([Nanda, 2016](#)).

Continuity: It is the property of a seismic pulse recognized by traces, and its repetitions of pulses generate continuity of the reflector ([Falc3n, 2005](#)). It is correlated with the homogeneity of a stratum, and it is affected by the noise or specific structures (Fig. 2.5) ([Mitchum, 1977](#))

Phase: It is the delay time from the starting point of the reflection, and it shows continuity as it is independent of amplitude; this phase will be helpful when the continuity is weak and to identify structural characteristics ([Nanda, 2016](#))

Polarity: It represents the sign of the reflectors, and it is interpreted as a positive when a soft rock is overlying a hard rock and negative when the soft rock is underlying the hard rock ([Nanda, 2016](#)).

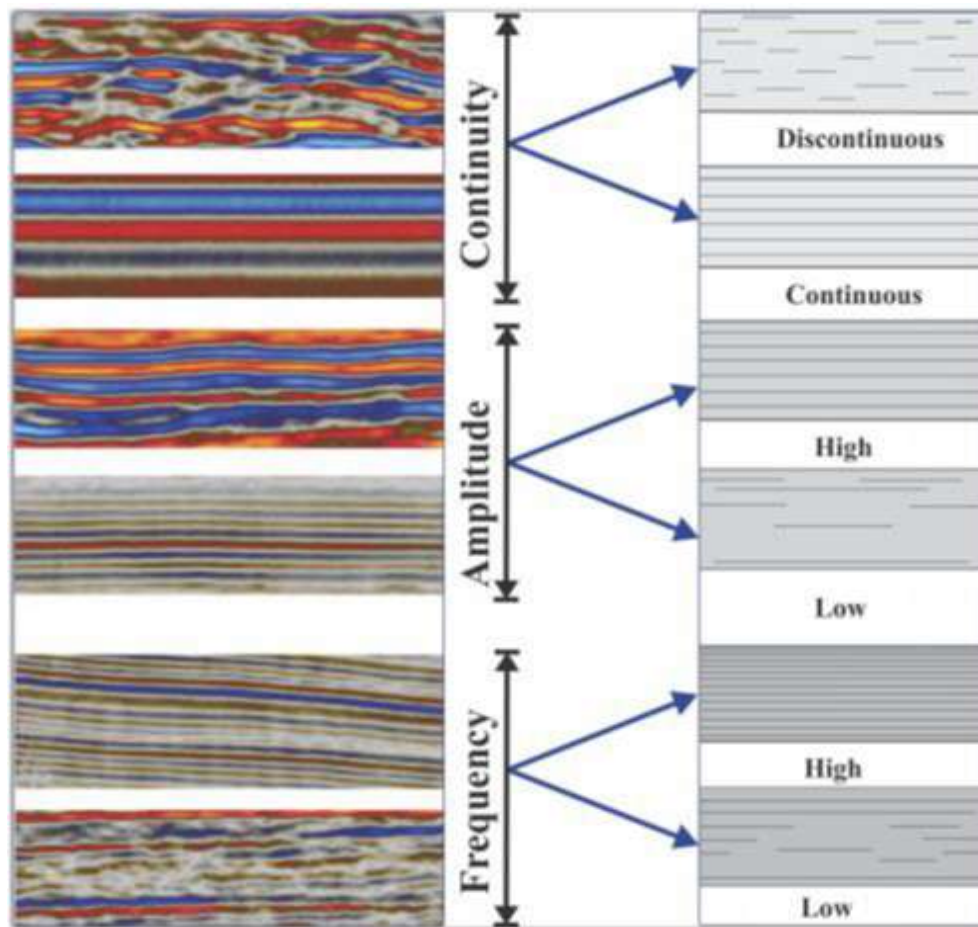


Figure 2.5: Reflections configuration of some seismic facies from the Taranaki basin of New Zealand. Taken from [Al-Masgari et al. \(2021\)](#)

2.3 Well-log Data

Records and measurements obtained from drilling and analyzing wells are known as well-log data. They encompass physical properties like rock types, porosity, permeability, saturation, and wettability encountered during drilling. Well-log data are crucial in understanding subsurface structures, identifying potential oil and gas reservoirs, and making informed decisions in hydrocarbon exploration and production. They also play a vital role in sequence stratigraphy by recording critical surfaces such as transgressive surfaces, maximum flooding surfaces, sequence boundaries, and surfaces between transgressive system tracts and lowstand system tracts, aiding in the differentiation of depositional settings ([Posamentier and Allen, 1999](#)). Moreover, by examining well logs such as gamma-ray, resistivity, and sonic logs, it is possible to identify different lithological units and grain size,

determine boundaries between depositional sequences, and correlate these sequences across different wells (STRATA SEPM, 2015). This information is crucial for understanding depositional history, facies distribution, and stratigraphic architecture in a sedimentary basin (Al-Masgari et al., 2021).

Integrating well-log data with seismic data and outcrop studies allows for a comprehensive understanding of the sequence stratigraphy of an area (Catuneanu, 2022). Well-log data enable strata correlation in seismic lines, especially for thinner strata, as seismic resolution might not reveal thinner layers (Falcón, 2005). Hence, combining seismic and well-log data is essential for comprehensive chronostratigraphic unit correlation (Falcón, 2005). For example, a stratigraphic correlation between N-S wells is exhibited in Fig. 2.6 for Manabí basin (Benitez, 1995).

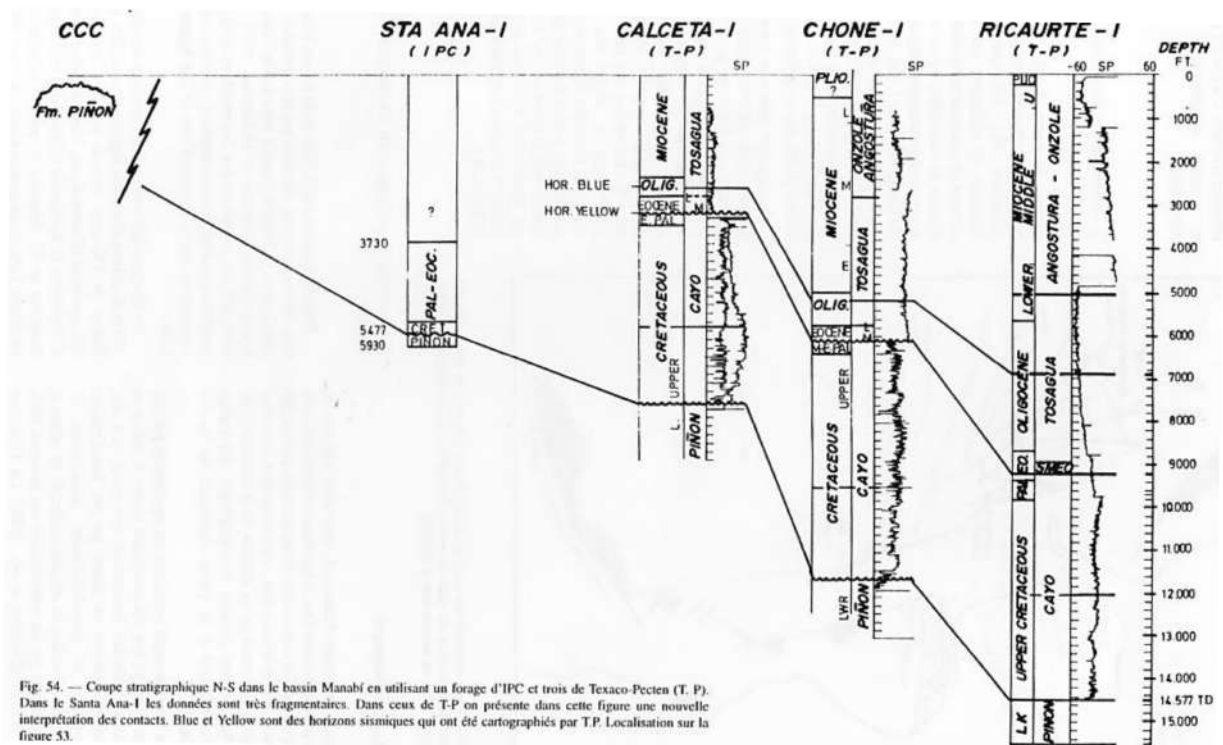


Figure 2.6: Stratigraphic cross-section and well correlations with the SP record between the boreholes in Manabí basin with N-S orientation. Taken from Benitez (1995)

Well-log analysis is centered to obtain lithology and grain size information, and used with biostratigraphic markers is helpful to identify stratigraphic sequence surfaces and stacking patterns (STRATA SEPM, 2013). Generally, the log records are the following:

Gamma Ray (GR)

It records the changes in the natural radioactivity that rocks emit and is commonly used to interpret grain size. For example, sandstones reflect lower values of gamma rays than shales, so GR is used to find sequence boundaries or unconformities with abrupt lithological changes. It is also valuable for identifying the accumulations of organic matter ([STRATA SEPM, 2015](#)).

Spontaneous Potential (SP)

The SP logs record the electrical potential of the formation caused by the variations of salinity from the water formation and mud filtration from the drilling. It is a permeability indicator and identifies bed boundaries ([STRATA SEPM, 2015](#)).

Density Logs (RHOB)

Density logs measure the bulk's density, and the matrix bulk's density will change with different lithologies. This record could be used to calculate the porosity ([STRATA SEPM, 2015](#)).

Resistivity logs

Resistivity logs record the properties of rocks that do not let the electrical current through them. It is helpful for grain size interpretation when the GR is unavailable, and these logs are used to determine the depth of hydrocarbon since the oil and gas present high resistivity values ([Posamentier and Allen, 1999](#)).

Sonic Logs (DT)

This log records the velocity of an elastic wave in rocks and is helpful for the calculation of mechanical properties of the rocks and porosity and lithology indicator ([STRATA SEPM, 2015](#))

2.4 Seismic-well tie

For a better sequence, stratigraphic analysis is necessary for well-log, seismic and outcrop data (STRATA SEPM, 2017). The connection between them should be made cautiously because it is the key to a fitting interpretation of a sedimentary basin infill. The seismic-well tie is the bonding of seismic and well-log data. It is the most crucial step because a good correlation between seismic and well-log data will provide an optimal geology analysis, with its formations, structures, and seismic reflections, and make reservoirs characterization. The link between these two data types is made with a synthetic seismogram to compare with the real data and approximate the geological features with the seismic. For this reason, the synthetic seismogram is a valuable tool for understanding the Earth's subsurface structure. The data and parameters that need to be considered for the synthetic seismogram are:

Well Logs

The essential information from healthy logs is the physical and chemical properties of the rocks recorded during drilling, such as lithology, porosity, density, and resistivity.

Seismic data

The characteristics of the seismic source, including its frequency content and amplitude, need to be considered when creating a synthetic seismogram.

Reflection Coefficients

Knowledge of the reflection coefficients at the interfaces between different rock layers is necessary for calculating the amplitude and phase of reflected seismic waves, significantly influencing the synthetic seismogram.

Wavelet

The wavelet represents the seismic pulse generated by the seismic source. Understanding the characteristics, like its frequency content and phase, is essential for accurately simulating the seismic signal recorded at the receivers.

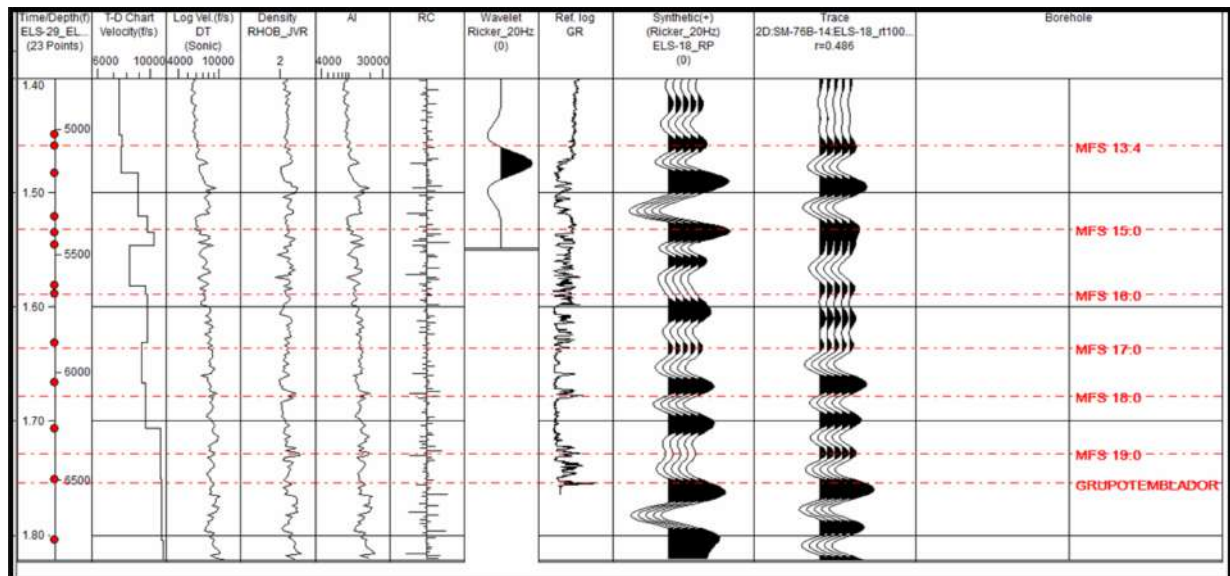


Figure 2.7: Synthetic seismogram from a well of a study in El Salto field, Venezuela, with a correlation coefficient of 0.486. Taken from Pérez and Richard (2015)

Creating a synthetic seismogram involves numerical modeling techniques that utilize the above data and parameters. The methods used are finite-difference modeling, ray tracing, or full waveform inversion to simulate the propagation of seismic waves through the Earth based on the input parameters. By iteratively adjusting the model to match observed seismic data, a synthetic seismogram that replicates the expected seismic response of the subsurface can be generated.

For the comparison of the synthetic and the real trace, the correlation coefficient is observed to get a quantitative value of the relation between these data (Fig. 2.7). However, it can also be analyzed qualitatively by matching the two traces. For a better correlation, both analyses should be made. The accuracy of the synthetic seismogram will depend on the quality and reliability of the input data; therefore, ensuring that the well logs and seismic data used in the modeling process are accurate and representative of the subsurface formations is fundamental. For this reason, it is important the improvement of quality data process.

Spectral Blueing (SB)

Seismic spectral blueing is a processing technique of seismic data that compensates for the attenuation of the high-frequency in rocks. As it helps the hydrocarbon industry,

this technique has been developed and improved gradually. This method increases the resolution of the seismic data by amplifying the attenuated high-frequencies and generating a better interpretation and finding of a reservoir (Villamizar et al., 2018). The attenuation of the frequency shows a whitening of the amplitude in the image of the seismic line. Since typical colors to the amplitude in seismic lines are blue (valleys) and red (peaks), this boost in the resolution will allow the “blueing” of those whitened parts. Thus, the seismic data will exhibit a better continuity of the horizons and a better interpretation of geological structures.

Self-supervised model

The seismic data processing includes noise removal to improve the data quality before building the synthetic seismogram. It is a deep learning model that only requires the dataset with noise, but has computational disadvantages because it demands a long amount of time and energy (Birnie et al., 2021). Birnie et al. (2021) found that deep learning techniques, such as Noise2Void (N2V), can be adapted and applied to seismic data for random noise suppression without the need for clean training data or pre-cleaning of field data. The N2V approach was tested on both synthetic and field datasets. It successfully suppressed random noise, increasing the signal-to-noise ratio (SNR) (Birnie et al., 2021).

Geohistory Analysis

Van Hinte (1978) proposed the stratigraphic technique to assess the evolution of a basin, useful for micropaleontological studies to determine the geological age of the units or hydrocarbon exploration to obtain data on the subsidence and sediment accumulation. The geohistorical diagrams represent this subsidence variation in time as a rate in mm/ka or m/Ma. This analysis takes into account the compaction values, porosity, lithology, sea level changes, paleo bathymetry, thickness, eustasy and age of units (Van Hinte, 1978).

Chapter 3

Geological Framework

Ecuador is in a convergent tectonic margin at the South American plate, with a subduction zone of the marine Nazca plate under the continental crust (Benitez, 1995). The subduction rate occurs at a velocity of 20-25 mm/yr (Jarrín Tamayo, 2021). Ecuador is formed by autochthonous and allochthonous terranes, such as the craton in the eastern part of the country and the oceanic terranes accreted in the western part of Ecuador. From west to east, there is the coastal Chongón Colonche Cordillera (CCC), the coastal plain (forearc basins), the western cordillera (WC), the inter-Andean depression (IAD), the eastern cordillera (ECE), the sub-Andean zone (SAZ), and the Amazonian lowlands (backarc basin) illustrate in Fig. 1.3.

The occurrence of a contractional period in Campanian times related to the collision of the Caribbean Large Igneous Province (CLIP) collision with the northwest of South America (Hernández et al., 2024) started the uplift process of the western cordillera around 75 Ma (Carrillo et al., 2022). After the accretionary processes, there were extension periods in the coastal basins due to the coupling and contraction periods that resulted in the inversion of previous geological structures. Crossing the Gulf of Guayaquil is the Grijalva Fracture zone with SW-NE orientation; the Nazca plate is split in the north, and the Farallon plate is in the south. Then, it is believed that the forearc zone was separated into various basins due to the entry of the Carnegie Ridge into the continental plate. This zone is divided into the Borbon, Manabí, Progreso, and Manta-Jama basins.

Forearc basins of the coastal region of Ecuador

The forearc coastal basins of Ecuador are delimited by the coastal cordillera at west, the western cordillera at the east, and it extends from Guayaquil at the south to San Lorenzo at the north. Moreover, [Benitez \(1995\)](#) established the boundaries of the basin by the faults in the area. These faults have major orientations of NW-SE and NE-SW. The tectonic setting of the region divides the north basins (Esmeraldas, Borbón, Manabí) from the south basins (Progreso, Jambelí). The northern basins have basement outcropping characteristics and low seismic activity; meanwhile, the southern basins have high seismic activity and high sedimentation rates ([Benitez, 1995](#)).

3.1 Manabí basin

The Manabí basin is delimited by the tectonic structures of displacement faults at the north by the Canandé fault, the Jama fault system at the west and the cordilleras at the east (WC) and at the south is the CCC ([Benitez, 1995](#)), which results in an elongated shape of the basin from N to S following the coastal margin. The basement of the basin corresponds to the Cretacic times (Fig. 3.1) with an estimated depth of 9 km ([Ordóñez et al., 2006](#)). Furthermore, [Reyes and Michaud \(2012\)](#) established the sedimentary fill composed of fourteen formations (Calentura, Cayo, Guayaquil, San Eduardo, Cerro, Zapallo, Punta Blanca, Pambil, Dos Bocas, Villingota, Angostura, Ónzole, Borbón, San Tadeo). According to [Reyes \(2013\)](#), the main faults in the Manabí basin are Canandé W-E-trending active thrust fault, Jama with NE-SW orientation is part of a belt of system faults with strike-slip movements, Flavio Alfaro normal fault from NE to SW, Pichincha NNE-SSW-trending thrust fault, Jipijapa is NNE-SSW-trending normal fault and Cascol of NW-SE orientation normal fault, other structures are the north are Tanigüe and Mataje fault in Fig. 3.1. The majority of these faults were normal deforming Cretaceous-Paleogene sediments but were reactivated as inverse of old faults uplifting part of the basement at NW and SW of the region ([Deniaud, 1998](#))

[Villitanga \(2020\)](#) made a tectonic analysis of the sequences in the Manabí basin, identifying five tectonic sequences (TS-1, TS-2, TS-3, TS-4, TS-5) and five unconformities (U0, U1, U2, U3, U4) as Figure 3.2 shown. The seismic-stratigraphic interpretation of the study

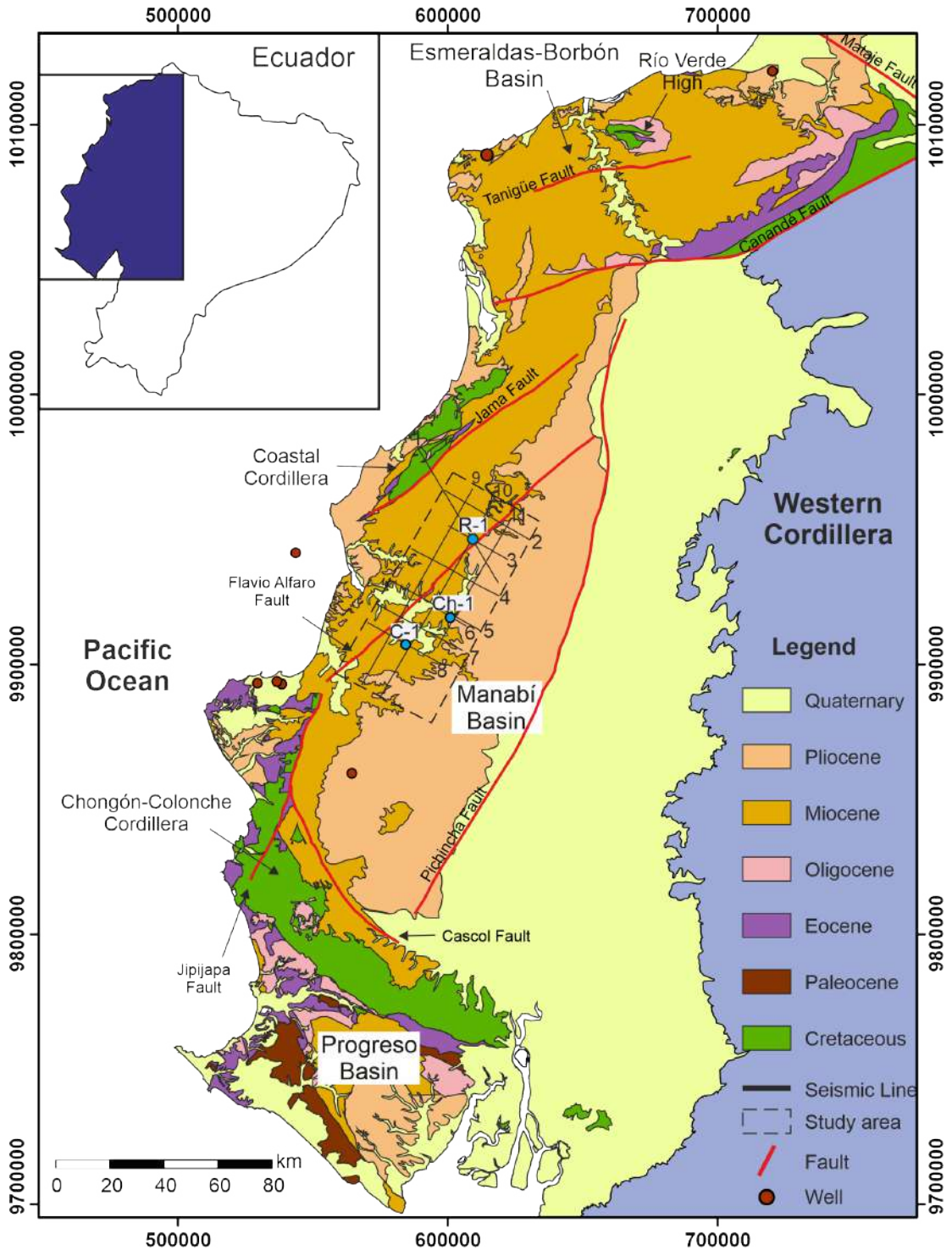


Figure 3.1: Geological map of coastal basins of Ecuador from Guayaquil Gulf to Esmeraldas, illustrating the main faults, basins and cordilleras of the coast, with the seismic lines (black lines) and the three wells (blue circles) analyzed delimited for the area of this study (dashed line). Other wells on the coast are represented by red circles. Modified from (Carrillo et al., 2022)

reveals the deposition of the units marked by different depositional events separated by the unconformities. These events are the accretion of oceanic terranes, the subduction of

the Nazca plate with strike-slip motion and shortening, and an extension period. Besides, [Villitanga \(2020\)](#) suggests that continental crust has around 20 to 40 km. of thickness in the coast region according to the gravimetric model. The positive and negative anomalies correspond to the geological structures in the areas, such as the outcropping of the basement at the NW of the basin is related to positive anomalies; meanwhile, the depocenters filled with Eocene-Miocene sediments coincide with the negative anomalies.

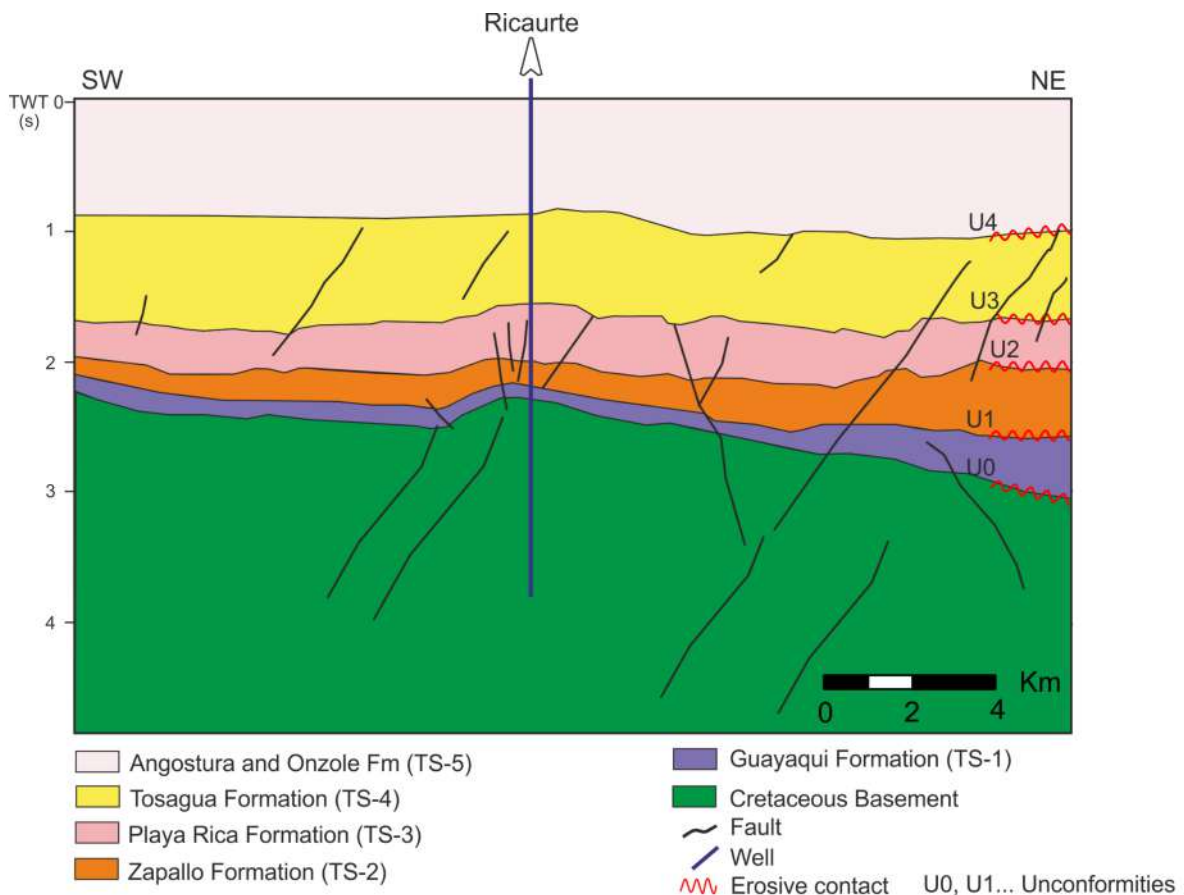


Figure 3.2: Seismic profile of line 553 with NW-SE orientation with the six seismic units and the regional discordance (U_b to U₅). Taken from ([Villitanga, 2020](#))

A recent study in the south of the Manabí basin is the undergraduate thesis of [Pazmiño and Tenelema \(2022\)](#), which characterizes the seismic stratigraphy and determines the structural boundaries of the southern part of the Manabí basin. In contrast, [Hernández et al. \(2020\)](#) analyzes the northern part and proposes a basin segmentation. They also postulate the possible segmentation between the north and south parts of the basin. This study examines three seismic profiles: the northern profile (968) cross from Sucre town to the Western Cordillera in SW-NE orientation, the profile 553 cross from Sucre county to

Palestina county in NW-SE orientation, and the 952 profile cross from Chongón Colonche Cordillera to Western Cordillera in SW-NE orientation. The study of the seismic lines determines seven seismic units above the basement, with five regional discordances and one local discordance.

Pazmiño and Tenelema (2022) described that the basement has a depth of approximately 2.2 seconds (TWTT) and is composed of the Piñón Formation with a regional unconformity (Ub) delimited by an onlap of the first seismic unit. The first seismic unit (S1), which likely corresponds to the Cayo Formation. This unit thins out towards the west and does not appear in the western profile 553. The second seismic unit (S2), interpreted as the San Mateo Formation, overlays the basement unconformably (U1) with a greater thickness of 0.4 seconds TWTT at the northern and western profiles (968 and 553). The third seismic unit (S3), likely the Dos Bocas Formation, unconformably overlays the basement only at the western and eastern ends of the basin in profile 952. It is unconformably deposited against S1 in the east and conformably against S2 along profile 968. It exhibits a similar thickness to S2. Its base has onlaps against Ub and U2, and its top has top laps with S4. The fourth unit (S4), interpreted as the Angostura Formation, displays a laminated layer of relatively constant thickness of 0.2 seconds TWTT at profile 553. It thins out towards the NE and reaches 0.4 seconds thickness at the center and west of profile 553. Its base has onlaps with S3 and top laps with S5 at the top. Seismic unit S5 is interpreted as the Ónzole Formation, with a maximum thickness of 0.4 seconds TWTT at the west of profile 553. U4 delimits its base, and U5 delimits its top. The sixth unit (S6), interpreted as the Borbón Formation, overlays S5 conformably in the western and central parts of the study area, reaching a maximum thickness of 0.5 seconds TWTT in the western part of profile 968. The last unit (S7) is only present in profile 968, overlaying the basement, S1, and S6 unconformably, denominated as U6, and its morphology resembles an outer fan that thins out towards the west.

Carrillo et al. (2022) study the tectonic-sedimentary evolution of the Manabí basin and Borbón basin since the Late Cretaceous to the present, which is defined by three main phases: alternating extension, quiescence-thermal subsidence, and tectonic inversion that is more present at Borbón basin. Carrillo et al. (2022) analyzed four seismic lines corresponding one to the Borbón basin, another crossing the Canandé fault, another across

the northeast of the Manabí basin, and the last one at the southernmost part of the Manabí basin. Seven seismic units (SES1-SES7) were identified and separated by three major unconformities, displaying transitional depositional and tectonic events.

The basement is described from discontinuous reflections of low amplitude. SES1 suggests erosion before the onset of deposition of the sequence, and the thickness of SES1-SES2 (Late Cretaceous-Paleocene) is 1100 and 750 ms, respectively; these sequences were reached by Ricaurte-1 well and show a composition of siliciclastic rocks. SES3 (Eocene age) has a thickness of 610-790 ms, and this sequence, which is truncated against SES4, is composed of shales with intervals of carbonates and a thin sequence of limestones at the base. SES4, discontinuous and chaotic, is Oligocene in age and reached a thickness of 1350 ms. SES5 and SES6 are Miocene in age and present continuous reflections with a thickness of 900 ms each, and the downward clinofolds indicate prograding sedimentation. SES7 is Pliocene-Quaternary in age and reached a thickness of 850 ms. with a composition of conglomerates underlying siltstones and shale successions up to the surface (Carrillo et al., 2022).

Moreover, Hernández et al. (2024) study the evolution of the Manabí basin with the 2D seismic lines, identify ten seismic units separated by nine unconformities, and describe the geodynamical process that determines the deposition of the basin.

Its major conclusions are that seismic unit 1 is the first depocenter caused by the oceanic plateau before the accretion process. The stages of evolution are delimited by a before, during, and after from this accretion of the Caribbean oceanic plateau as it revealed the sedimentary record (Hernández et al., 2024). In this pre- and post-accretionary period, the depocenters date the main collisional phases and the initiation of the Manabí forearc basin. Also, it shows the influence of basement structures on the building of the Coastal Cordillera. It discusses the potential geodynamic causes of the structural evolution of the central Ecuadorian forearc. The study also reports some positive anomalies for the outcropping of the basement at the Canandé and Jama mountain range and negative anomalies for the depocenters at the east of the Jama fault system and the south of Canandé fault (Hernández et al., 2024).

3.2 Lithostratigraphic units of Manabí basin

The Manabí basin is formed by the lithostratigraphic units of Piñón Fm. (KPñ), Calentura Fm. (KCa), Cayo Fm. (KCy), San Eduardo Fm. (ESe), Cerro Fm. (ECr), Zapallo Fm. (EZp), Punta Blanca Fm. (EOPb), Pambil Fm. (OPm), Tosagua Group (OMT) composed by Dos Bocas Fm. (MDb) and Villingota Fm. (MVg), Angostura Fm. (MAg), Ónzole Fm. (MOz), Borbón Fm. which is composed of three members: Lower Borbón (PLBi), Middle Borbón (PLBm), and Upper Borbón (QPBs), Balzar-San Tadeo Fm. (QPBz-ST), Tablazos Member (QTb). For this undergraduate thesis, the lithostratigraphic units from the Manabí basin were taken from previous research, as proposed by [Benitez \(1995\)](#) and [Reyes and Michaud \(2012\)](#). Following is a description of each unit, organized from the oldest to the most recent.

Piñón Formation (KPñ)

Piñón is an oceanic terrane accreted and forms the basement of the Manabí basin because it has been cut by the drilling of the wells (Fig.3.3). It is outcropping dispersed in the coastal area such as in the Chongón-Colonche Cordillera (CCC), in the Coastal Cordillera elevated by the Jama fault system and at the NE of Canandé fault (Fig.3.1). It comprises a sequence of basaltic pillow lavas tholeiitic in composition, hyaloclastite, sills and dikes of dolerite ([Kerr et al., 2002](#)). The fossils in the formation that help with the first approximation of the age are foraminifera and concluded an Early Cretaceous age for Piñón ([Aizprua et al., 2020](#)). According to [Luzieux \(2007\)](#) the age of Piñón is about Late Cretaceous, ~90-87 Ma, and has been constrained by the $^{40}\text{Ar}/^{39}\text{Ar}$. The new information on the Piñón block age indicates that it can be interpreted as a portion of the CLIP ([Vallejo, 2006](#); [Van Melle et al., 2008](#)). Thus, it is interpreted as a basaltic plateau from the abyssal environment.

Calentura Formation (KCa)

This formation overlies the Piñón formation, but it is not cut by the drillings, and it outcrops the north of Guayaquil and the eastern of CCC that thins to the west ([Luzieux, 2007](#)). The accretion of the oceanic terrane also formed San Lorenzo Member during the Late Cretaceous ([Kerr et al., 2002](#)). It is compounded by calcareous turbidites, black

shales, limestones, radiolarites and marl (Luzieux, 2007). According to Benitez (1995), it also has intercalated sediments in volcanic breccias. Luzieux (2007) date KCa from Coniacian-Santonian in age (89-84 Ma). It is interpreted as tholeiitic basalt from an island arc and abyssal paleo environment (Benitez, 1995).

Cayo Formation (KCy)

It overlies unconformably KPñ formation (Fig.3.3) and outcrops at the CCC and Jama system fault (Reyes and Michaud, 2012). It was cut by the three boreholes (R-1, Ch-1, C-1) to study. It has around 3 km in thickness of massive turbidites intercalated with basaltic lava flows (Reyes and Michaud, 2012). It is interpreted as a mega turbidite due to the finding of a fining upward sequence of high and low-density turbidites. The fossil content analyzed for KCy age were radiolarians, calcareous nanofossils, and foraminifera by Ordóñez et al. (2006), who concluded an age from Santonian to Lower Maastrichtian. The fossils analysis also indicates a bathyal to abyssal depth for the paleo-environment (Ordóñez et al., 2006). Benitez (1995) concluded that it registers the two pulses of insular arcs, and Deniaud (2000) mentioned that it may be caused by the Insular Arc rupture.

Guayaquil Formation (KGq)

Guayaquil Fm. is the last from Cretaceous times overlying the KCy after the hiatus interpreted as U-1 (Fig.3.3), and KGq is exposed at CCC (Reyes and Michaud, 2012). It has been cut by three wells: R-1, Ch-1, C-1. KGq has 400 m in thickness (Reyes and Michaud, 2012) of tuffaceous siltstones, bluish-grey shales and fine sandstones, with cherts on top of the sequence (Ordóñez et al., 2006). The sandstones become more calcareous and organic matter-rich (Luzieux, 2007). The fossil content present by nanofossils calcareous, scarce foraminiferous and radiolarious spumellarios provide an age from Campanian in the basal part and Paleocene in the upper part (Ordóñez et al., 2006; Benitez, 1995). It was deposited in a pelagic environment (Deniaud, 2000), and in an outer shelf to bathyal environment (200-500 m) according to Ordóñez et al. (2006); Luzieux (2007).

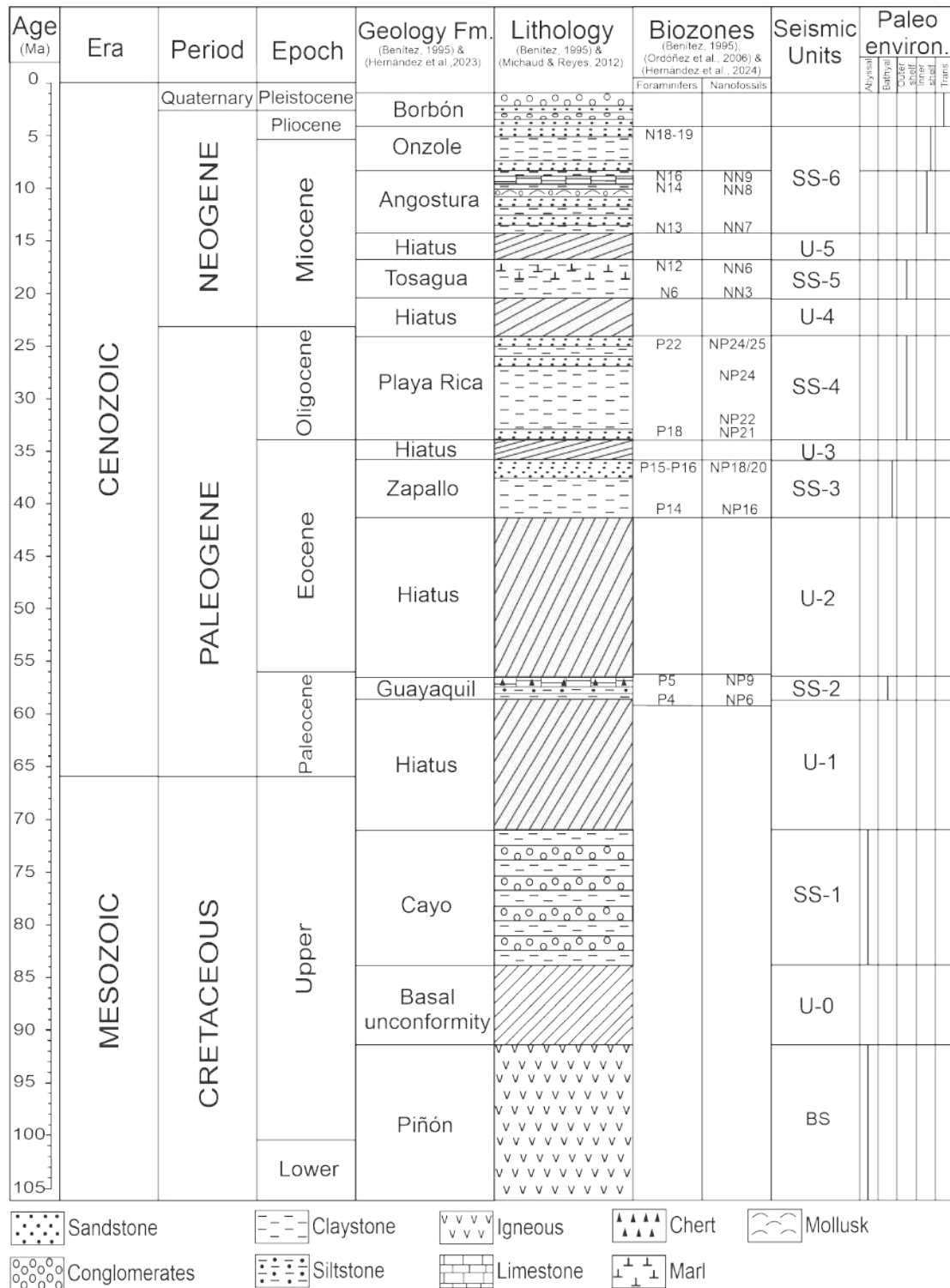


Figure 3.3: Stratigraphy of Manabí basin according to the Chone-1 drilling information and Reyes and Michaud (2012), the biozones according to Benitez (1995); Ordóñez et al. (2006), seismic sequences and unconformities codes analyzed in this work, the paleoenvironment from Ordóñez et al. (2006); Benitez (1995), the lithology according to Benitez (1995); Reyes and Michaud (2012)

San Eduardo Formation (ESe)

This formation is conformable overlying the cretaceous sediments. Still, it is not cut by the drillings, and it outcrops at the west of Jipijapa fault and in the CCC (Reyes and Michaud, 2012). Its thickness is 30-100 m of limestones, calcarenites, mudstones and siliceous claystone (Luzieux, 2007). ESe formation is a calcareous sequence formed from a post-accretionary process Hernández et al. (2020). This formation may be correlated with the Santiago and Ostiones formations in the Borbon basin, and its age is from Early Eocene (Reyes and Michaud, 2012). The paleo depth estimation by Luzieux (2007) indicates a 200-800 m of a bathyal paleo-environment.

Cerro Formation (ECr)

It is an 800 m sequence, which outcrops at the west of Jipijapa fault (Fig.3.1), of volcanoclastic sediments, shales, and tuffs (Reyes and Michaud, 2012). According to Deniaud (2000) and Benitez (1995), this is formed by ~100 m of light gray clastic rocks thinly laminated, that is rich in radiolarian content and slightly calcareous (Benitez, 1995; Deniaud, 2000). The age of Cerro Fm. is Middle Eocene (Reyes and Michaud, 2012; Deniaud, 2000; Benitez, 1995). It corresponds to an outer shelf to the upper bathyal paleoenvironment (Benitez, 1995).

Zapallo Formation (EZp)

EZp is unconformably overlying the KGq (Fig.3.3) at the three wells (R-1, Ch-1, C-1) that cut this formation. The outcrop is found in the north of Canandé fault (Fig.3.1) with a thickness of 500-1000 m Reyes and Michaud (2012). It is compound by a calcareous grey shale standing on the top of gray clay dark, soft and slightly calcareous, and it is biostratigraphically correlated to San Mateo formation (Ordóñez et al., 2006). The age of this formation was determined by Benítez using the foraminifers that date it as Middle to Upper Eocene (Benitez, 1995; Ordóñez et al., 2006). The paleo-environment of EZp is outer shelf to upper bathyal (Benitez, 1995) of warm waters (Ordóñez et al., 2006).

Punta Blanca Formation (EOPb)

Punta Blanca Fm. is not cut by the wells but is exposed and dispersed at the Jama fault system (Fig.3.1). Silicic and pelitic rocks form it with diatoms that have a marine origin, and its outcrop is found in discordance with older sediments over the Jama fault (Reyes and Michaud, 2012). Benítez described it as 60 m of calcareous sandstones with sedimentary structures of cross-stratification overlain by fine sandstones silicic, pelitic, and calcareous rich in microfauna (Benitez, 1995). Its age dates from the Late Eocene (Reyes and Michaud, 2012).

Playa Rica Formation (OPr)

OPr is unconformably overlying the EZp formation (Fig.3.3) and cut by the three wells. Outcropping dispersed at the Jama fault system, represented by 800 m in thickness of volcanoclastic sediments formed by intercalations of green and gray sandstones with shale limestones (Reyes and Michaud, 2012). Benítez described an outcrop at the Colonche fault of intercalation of 15m of tuffs with some calcareous nodules, bioturbation, and greenish-gray massive siltstones was found that corresponds to an upper bathyal paleo-environment (Benitez, 1995). The fossil content is represented by benthonic foraminifera and calcareous nanofossils, which indicates an age from the Oligocene, and a paleo-environment of the outer shelf to upper bathyal (Ordóñez et al., 2006).

Pambil Formation (OPm)

Pambil Fm. overlies the Playa Rica Fm. in concordant contact, but it is not cut by the wells (R-1, Ch-1, C-1). It outcrops east of the Jama fault and north of the Canandé fault (Reyes and Michaud, 2012). This is described as blueish-gray massive pelitic rocks. It is formed by the intercalation of siltstones and white tuff sandstones. The radiolarian studies from Luzieux (2007) suggest a Late Oligocene age and a paleo-environment of shallowing upward until bathyal depths.

Tosagua Group (OMT)

It is cut by the three wells (R-1, Ch-1, C-1) and unconformably overlying OPr (Fig.3.3). It was a pelitic deposition during the Miocene and has outcrops to the west of the Manabí

basin and the Coastal Cordillera. It is divided into Dos Bocas Fm. and Villingota Fm. (Hernández et al., 2020).

- **Dos Bocas Formation (MDb)**

In the area of Tosagua town, it is possible to find a massive outcrop of 2.5km of Dos Bocas Fm. and to the east of Jipijapa and Jama faults, or at the Santa Elena peninsula (Reyes and Michaud, 2012). It is composed of siltstones and brown mudstones with local sedimentary sandstones. It is altered by gypsum veins, calcareous concretions, iron oxide and sulfur (Reyes and Michaud, 2012). The biozone marker of the NN3 zone of *Sphenolithus belemnus* suggests a Lower Miocene age (Ordóñez et al., 2006).

- **Villingota Formation (MVg)**

It has local outcrops from the Santa Elena peninsula to Esmeraldas. Still, its main outcrop is north of the Manta peninsula (Reyes and Michaud, 2012). This formation overlies the Dos Bocas Fm. and it comprises the intercalation of blueish-gray laminated shales with diatoms and sandstones with calcareous concretions (Reyes and Michaud, 2012). The fossil content of the zone NN3 (**Sphenolithus belemnus**) and NN6 (Fig.3.3) indicates a Lower Miocene age (Ordóñez et al., 2006).

Angostura Formation (MAg)

MAg is cut by Chone well and exposed mainly at the Coastal Cordillera, east of the Jama fault system and extends to Esmeraldas (Fig.3.1). It also overlaps in disconformity with Piñón Fm., north of CCC. In this contact, there are 5 m yellow feldspathic sandstones and overlain a 20 m conglomerate with marine fauna (Benítez, 1995). The outcrop at the north of the Canandé fault is formed of intercalations of sandstones and conglomerates that are rich in marine fauna. To the east of the Jama, the fault comprises 1 m of turbiditic sediments in a fining-upward sequence of tuff and blueish volcanic sandstones at the base and light-yellow tuff shales at the top. Over the CCC and to the east of the Jipijapa fault, the deposits are intercalations of massive sandstones with continental conglomerates (Reyes and Michaud, 2012). The fossil content is represented by calcareous nannofossils and foraminiferas, which determine the age of the Middle to Upper Miocene. According

to the planktonic foraminifera, the paleoenvironment for Angostura at the base and the top provided an outer shelf environment. The central part has more benthic foraminifera that corresponds to the inner shelf, and the thickness for this formation is around 920 m (Benitez, 1995).

Ónzole Formation (MOz)

This formation is cut by Chone-1 well, and it is outcropping dispersed at the central and north of Coastal Cordillera (Reyes, 2013), at the western flank of Manabí basin, along the Jama fault, NW of Esmeraldas, at the south of Mataje fault, see Fig. 3.1; (Reyes and Michaud, 2012). In the Manabí basin, this is divided into two members. The lower member is composed of gray siltstones and white tuffs, with some gypsum and high content of microfauna. The upper member comprises mudstones and dark gray to greenish-gray siltstones rich in marine fauna and microfauna such as benthonic foraminifera and radiolarians (Reyes and Michaud, 2012). The fossil content indicates biozones N16-N19 dated MOz from the Upper Miocene to Lower Pliocene (Ordóñez et al., 2006; Reyes, 2013). The paleoenvironment of the lower member corresponds to deep marine deposits, and the upper member is a middle-shelf environment of 50-100 m in the Manabí basin (Benitez, 1995).

Borbón Formation (PLB)

PLB is not cut by any of the three wells used in this study, but it overlies in conformable contact with the MOz (Reyes, 2013). It is outcropping at the eastern flank of Coastal Cordillera or western side of Manabí basin, mainly at the central and northern part and at the SW of Jama fault, see Fig. 3.1, (Reyes and Michaud, 2012). This formation is divided into three members: the Lower Borbón member, defined by clastic deposits; the Middle Borbón member of volcanoclastic sediments; and the Upper Borbón member of volcanic deposits.

- **Lower member:**

According to Reyes and Michaud (2012), it is formed of massive sandstones with lenses of conglomerates. The characteristic outcrop is located between Canoa and

San Vicente. It may be correlated to the Progreso Fm. in the Progreso basin. Nannofossils data suggest an age of Uper Miocene to Middle Pliocene (Reyes, 2013)

- **Middle member:**

The middle member is outcropping at the south and central part of the Manabí basin and at the Bahía de Caráquez area (Reyes and Michaud, 2012). It is formed of intercalations of local tuffs and reworked medium-grained sandstones and coarse-grained conglomerates from volcanic origin and shows finning-upward sequences from several turbiditic cycles (Reyes, 2013). This member overlaps in discordant contact with the lower member west of Quinindé. It may be correlated with the Puná Fm. from the Progreso basin (Reyes and Michaud, 2012). The fossil content mainly represented by nannofossils provides an age range from the Middle Miocene to the Middle Pliocene.

- **Upper member:**

This member is mainly exposed along the eastern flank of the Manabí basin from N-S, but it is more dispersed at the south (Fig.3.1); (Reyes and Michaud, 2012). It is overlying in discordant contact with the middle and lower members. Intercalations of reworked tuffs, breccias, and local volcanic sandstones form it. The middle and upper Borbón members participate in alluvial fans (Reyes and Michaud, 2012). Reyes (2013) dated the upper Borbón member with an age of 0.803 ± 0.101 Ma obtained from a volcanic tuffaceous level with a $^{40}\text{Ar}/^{39}\text{Ar}$ method, and it is correlated to Canoa formation Pleistocene in age.

The paleo-environment for the Borbón formation corresponds to a shallow marine environment from regressive. After this, it is registered as a transgressive period, followed by an uplift (Benitez, 1995).

Bálar-San Tadeo Formation (QPBz-ST)

XReyes and Michaud (2012) described this formation, outcropping at the eastern side of the Pichincha fault, adjacent to WC (Fig. 3.1). It has an approximate thickness of 80m and is a massive brown mudstone that overlies the alluvial fans of Santo Domingo, which

are mapped as volcano-clastic sediments to the north of the coastal plain. Its age is dated from the Pleistocene (Reyes and Michaud, 2012).

Tablazos Member (QPTb)

Tablazos member also named as old terraces are fluvial deposits and marine sediments covering the southern part of the Progreso Basin, Santa Elena peninsula (Fig.3.1) and at the western side of Jipijapa fault in the Manta area. It is dated from the Late Pleistocene (Reyes and Michaud, 2012).

Chapter 4

Methodology

This study focuses on improving seismic data combined with well-log data for a broad interpretation of the geology of the Manabí basin. Figure 4.1 shows the workflow for the activities to improve the data, which begins with compiling the data necessary and the bibliographic revision and methodologies used before. Next, the geophysical and the geological work were separated for seismic-well tie and then combined for the interpretation, conclusions, and recommendations.

The geophysical work from the seismic-well tie includes analyzing the features to extract the resolution of the seismic data and extracting the wavelets for the first synthetic seismograms (phase I). Next, quality control of the logs is used to eliminate the noise, and a filter is applied to create a synthetic seismogram of one well (phase II). Then, the final synthetic seismogram filters were developed for the other wells after applying denoising and spectral blueing to the seismic data. The correlation coefficient from the seismic-well ties and the interpretation of previous works were verified to validate the improvement and interpretation of the data obtained. On the other hand, the geological work is based on the revision of biostratigraphic information and analysis of the well-log data, the digitalization of well-log data, and its correlations between wells to the definition of the stratigraphic sequences. Finally, the geophysical and geological information is used for interpretation and conclusions.

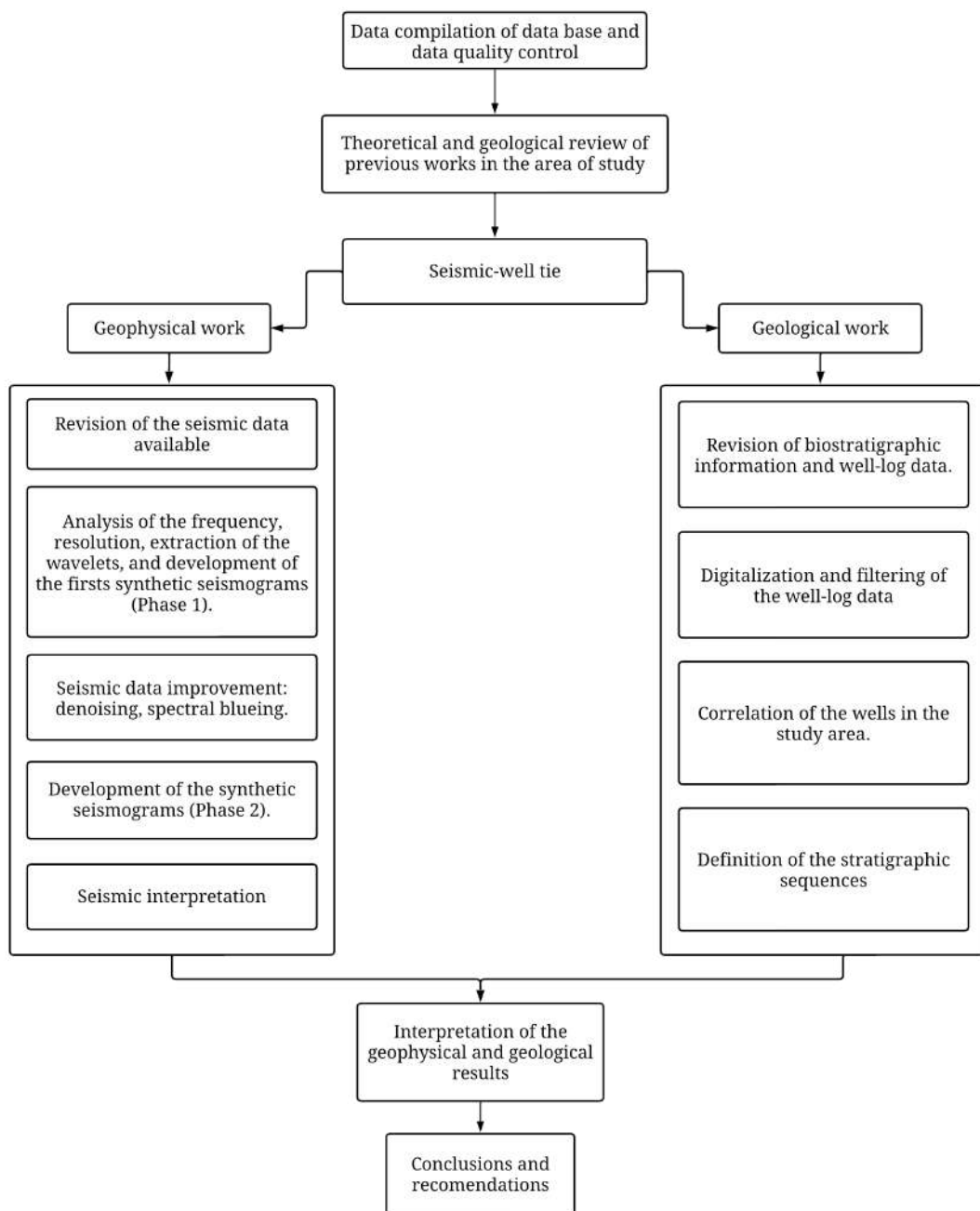


Figure 4.1: Workflow of the methodology of this project describing the geophysical and geological activities to develop for the improvement of the seismic-well tie.

4.1 Data Available and software

Data used is from seismic reflection surveys and information from well drilling. The data, which are confidential information, were provided under an agreement with the Secretariat of Hydrocarbons from Ecuador and Yachay Tech University. From the seismic survey, 2D

seismic data of eleven lines were used for the interpretation, and those lines sum up a total of 497.89 km with a reached depth of ~ 3.6 s of two-way traveltime (TWT). Additionally, the data from three wells (Ricaurte-1, Chone-1, and Calceta-1) was provided by the drilling of Texaco, and the top formations were from data from a previous study of SINOPEC. Ricaurte-1 (R-1) reached 4724.4 m cut the top of the following formations: Piñón, Cayo, Guayaquil, Zapallo, Playa Rica and Tosagua Gp.; Chone-1 (Ch-1) record data until 3621 m cutting Piñón, Cayo, Guayaquil, Zapallo, Playa Rica, Tosagua Gp., Angostura and Ónzole. Calceta-1 (C-1) well has 2682 m of data that cut the formations of Piñón, Cayo, Guayaquil, Zapallo, Playa Rica and Tosagua Gp. The information on wells, which was presented in scanned images but not digitalized, includes logs of gamma-ray (GR), sonic (DT), density (RHOB), spontaneous potential (SP), and resistivity important for the evaluation of the basin.

The seismic data was clean using deep learning denoising of an open-code self-supervising technique (Noise2void), which only requires a noisy data set. Besides, the main horizons and faults of the seismic lines were interpreted using the IHS Kingdom paid software, specialized for seismic interpretation in the oil and gas industry, in the School of Earth Sciences, Energy and Environment workstation computer.

4.2 Geophysical work

The map of the area with the seismic lines and the wells is represented in Fig. 1.4. The data of the seismic lines and the wells was processed to get a new correlation of the stratigraphic units. The correlations and interpretation of the tops were made of 11 seismic lines and three wells (R-1, Ch-1, C-1) in the software IHS Kingdom.

4.2.1 Analysis of the frequency and resolution of seismic data, extraction of wavelets and development of synthetic seismograms (Phase I).

The frequency of a seismic wave is its repetition of the complete wavelength (λ) measured in Hz ([Energy Glossary, 2023](#)). Analysis of the frequency for the seismic data was made for a ranging depth of 7200-14000 ft/s, which resulted in a bandwidth of ~ 5 -55 Hz and a

dominant frequency of 25 Hz for the original survey spectrum (Figure 4.2).

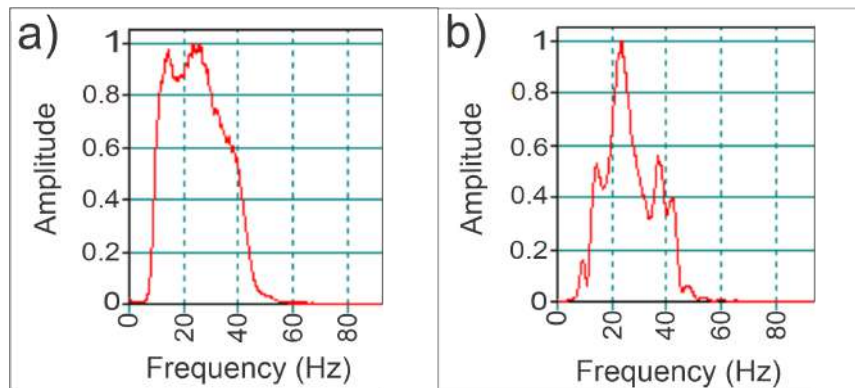


Figure 4.2: Survey spectrum of the seismic data. A) Survey the spectrum of seismic data before processing data. B) survey spectrum after applying spectral blueing.

Then, the resolution of the seismic data is how clearly the reflectors could be distinguished in detail. This resolution is inversely proportional to the bandwidth; thus, the lower the frequency, the higher the depth reached. Further, resolution will drop with depth because the reflection frequency decreases (attenuation of seismic waves). Hence, resolution analysis is based on the frequency and the sampling interval (Nanda, 2016).

There is the horizontal resolution, which is the ability to distinguish features laterally displaced, and the vertical resolution, which is the ability to differentiate features of two seismic events in different depth levels (Nanda, 2016). For the vertical resolution measurement, a quarter of the wavelength is used ($\lambda/4$). The vertical resolution of these seismic data was analyzed with the interval of seismic velocity and frequency. Since the sonic record of the wells determines the resolution, the velocity value is taken as a range from the top and the base of the sonic log. For this reason, the seismic resolution is calculated as follows:

$$\frac{\lambda}{4} = \frac{v}{f}$$

Where,

λ = Wavelength

f = Dominant seismic frequency

v = Seismic velocity

Seismic resolution ($\lambda/4$) for Ricaurte well, which values of the velocity in the sampling interval are 7200-14000 ft/s and an FDOM=25 Hz, is in the range of 288-560 ft or 87.78-170.68 m. Meanwhile, for Chone well, the values for the seismic velocity are 4000-9600 ft/s, and an FDOM = 25 Hz, and its resolution range is 160-384 ft or 48.77-117.04 m. At last, Calceta well uses a range value of 3200-7500 ft/s for the seismic velocity and an FDOM = 25 Hz, and the resolution of this well is 128-300 ft or 39.01-91.44 m.

In addition, control of the seismic velocity was carried out by a series of verification shots in the Ricaurte well detailed in Table 4.1, and these check shots were used to create the Time-Depth (TD) chart that was applied for the three wells (Fig. 4.3). This TD chart, combined with the sonic and density logs, was helpful in the generation of the first synthetic seismograms for all wells (Table 4.1).

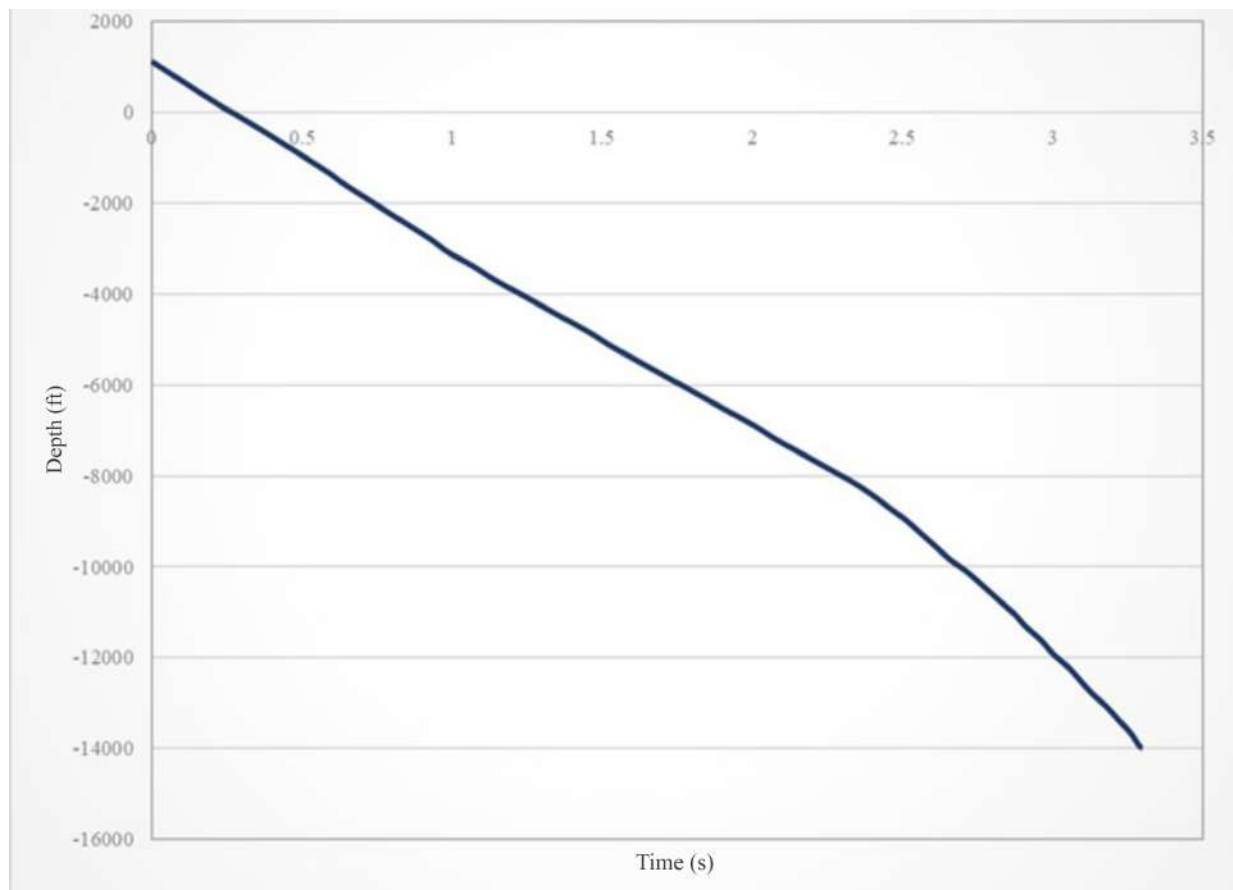


Figure 4.3: Time-Depth chart of Ricaurte well, used to create the first synthetic seismograms of the three wells.

The synthetic seismograms before improving the quality of data (phase I), which used the sonic log, density log, and the TD chart from Ricaurte, were created with an extracted

Table 4.1: Data available in the study area for the creation of synthetic seismograms

Wells	Verification	Sonic record	Density record	Synthetic seismogram
Ricaurte	Yes	Yes	Yes	Yes
Chone	No	Yes	Yes	Yes
Calceta	No	Yes	Yes	Yes

wavelet generated by Kingdom for the three wells. Then, a qualitative analysis was developed with synthetic and trace comparison; meanwhile, the quantitative analysis considers the correlation coefficient (Fig. 4.4).

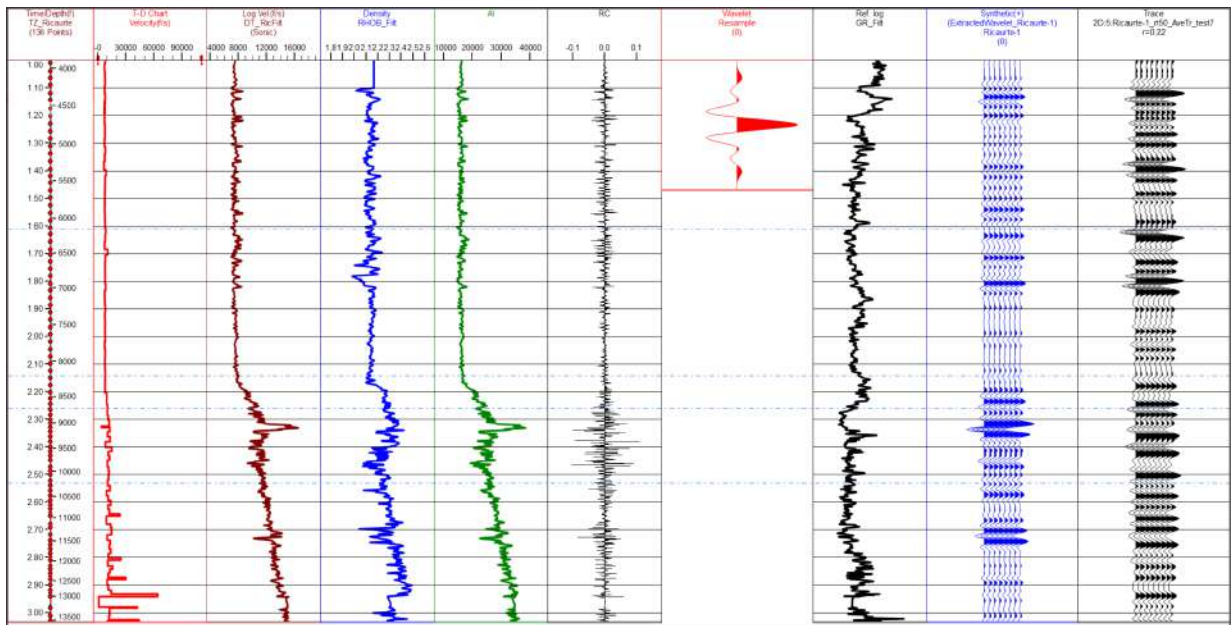


Figure 4.4: Synthetic seismogram of the first phase from Ricaurte-1 well shows the velocity, depth, density, gamma ray record, wavelet, synthetic trace and the trace with the correlation coefficient (r) at the last column.

4.2.2 Seismic data improvement: denoising, spectral blueing

This step is the most important to obtain a good result for the posterior interpretation. The denoising of seismic lines involves the self-supervised network, which works only with the noise data set. This process uses a blind-spot network that eliminates the random noise without replicating it. This method works by controlling the PSNR, checking the spectrum frequency plot, and examining the impedance inversion. It assumes that noise is random and that two noises are independent between the target and input. However, the assumption that noise is statistically independent between samples may only sometimes

hold for seismic data, and N2V may only partially suppress correlated noise. Nevertheless, this usually only occurs in applied geophysics, where the network cannot learn to replicate the noise. Thus, it will not predict random elements through a blind-spot network (Birnie et al., 2021). First, a noise (White or Band) or neither must be chosen. Then, it divides the data into a specific number of pixels of the seismic line. Next, the network will be trained in a particular number of epochs. For this study, ten proofs were made to look for the best combination of the division of pixels and the noise used. The combinations are shown in Table 3.2, and better results were given with combinations 6, 9, and 4. The filter for 11 seismic lines, chosen after a qualitative analysis, was the 6 with 32x32 pixels and without extra noise.

Table 4.2: Combination of the parameters for the denoising process

#	# de pixels	# de pixels	Noise
1	32	32	White noise
2	20	20	None
3	20	20	White noise
4	20	20	Band
5	32	32	Band
6	32	32	None
7	32	20	White noise
8	20	32	Band
9	20	32	None
10	40	40	White noise

The combinations were tested to recognize whether there is a pattern or change when applying different types of noise. The best combinations for denoising seismic data were numbers 6, 9, and 4 (in that order). It is important to note that these combinations divide the seismic lines into more patches than others, and it is better not to apply additional noise (6, 9). Birnie et al. (2021) mentioned in their article that seismic denoising increases the number of active pixels and reduces the number of epochs, which makes it difficult to replicate the noise due to the decreased epochs, but increasing the number of pixels will regularize the training Birnie et al. (2021). The number of epochs was fixed, and only the number of pixels and types of noise were changed to obtain the best-denoised data. Additionally, combination number 10 was tested to see if there was any improvement with increased pixels, but it resulted in a low suppression of noise.

Furthermore, another improvement process applied to the data was spectral blueing, which enhances the vertical resolution by shaping the seismic spectrum with a low noise level. The attenuation of high-frequencies will affect the vertical resolution and the identification of thinner beds. Still, this convolution with an operator from the sound data will result in a high frequency that will blue those parts and improve the continuity of the reflector in the line (Villamizar et al., 2018). This filter process of spectral blueing for the deconvolution was applied with a Matlab code.

4.2.3 Development of synthetic seismograms (Phase II)

The second phase of the development of the seismograms was made with the seismic-well tie with the same information (sonic, density, and the same TD chart from the Ricaurte well). Still, this second time, we used the processed data, which was the denoised seismic lines, applying spectral blueing. The wavelet was extracted from the processed data at the borehole. Also, a filter was applied for the well-logs to improve the TD chart, so a better seismic-well tie is created, and the synthetic seismogram is quantitatively and qualitatively enhanced, which is possible to see with the increase of the correlation coefficient.

4.2.4 Seismic Interpretation

The seismic interpretation follows the improvement of the data to construct a geological model of the subsurface describing the stratigraphic units or sequences found, the structural features seen and its depositional settings. For this reason, the interpretation is based on determining the tops and base formation with the help of well-log data and analyzing the reflections by its parameters (see Chap. 2). The seismic interpretation of the 11 lines was made by identifying the structural features like faults and folds and the stratigraphic units as shown in Fig. 4.5.

Stratigraphic interpretation

The analysis of the continuity of the reflectors was made to reveal the stratigraphic units that evolve with the basin. The top formation was interpreted with information about the wells that pass through three lines, and then it was connected to the rest of the lines in the Kingdom software. Table 4.3 shows the characteristics of seismic units, and Fig.

Table 4.3: Seismic characteristics of the interpreted sequences for the 11 lines. These characteristics are generally evaluated according to the parameters described in the chapter 2 and an example is present in Fig. 4.5

Seismic sequence	Polarity	Character (Intensity of reflection)	Reliability
SS-6	Negative (Valley)	Strong	Strong reflector in the major area, but it is uncertain near to the surface
SS-5	Negative (Valley)	Strong	Strong reflector in the major of the area, but it loses intensity at some points
SS-4	Negative (Valley)	Strong	Strong reflector in the major of the area, but it loses intensity at some points
SS-3	Negative (Valley)	Strong	Strong reflector in the major of the area, but it loses intensity at some points
SS-2	Negative (Valley)	Weak	Reflector of high uncertainty
SS-1	Negative (Valley)	Weak	Reflector of high uncertainty
Basement	Negative (Valley)	Weak	Reflector of high uncertainty

4.5 exhibits its structural interpretation from a seismic line of NW-SE orientation. These horizons were interpreted as the basement, and the six seismic sequences (SS-1, SS-2, SS-3, SS-4, SS-5, SS-6) were stated, and a specific color was used for each. Moreover, the isopach and isochore maps of each sequence were developed. The isopach maps show the true stratigraphic thickness of the sequence; meanwhile, the isochore maps show the true vertical thickness (TVT) of the sequence.

Structural interpretation

The interpretation of the seismic lines involves delimiting the faults and horizons. The faults were assigned with the Kingdom software in the 11 seismic lines for the structural part. Then, the previous works on this structural data will be revised and compared with the main faults in the region. This understanding of faults simplifies the interpretation of sequences in the following step because a fault could cut the continuity of the reflectors Fig. 4.5.

4.3 Geological work

This part revises the study's geological work, mainly revising biostratigraphic information to correlate with the data processed. Then, the stratigraphic sequences are defined according to the units, and the thickness variations of each sequence along the basin are analyzed

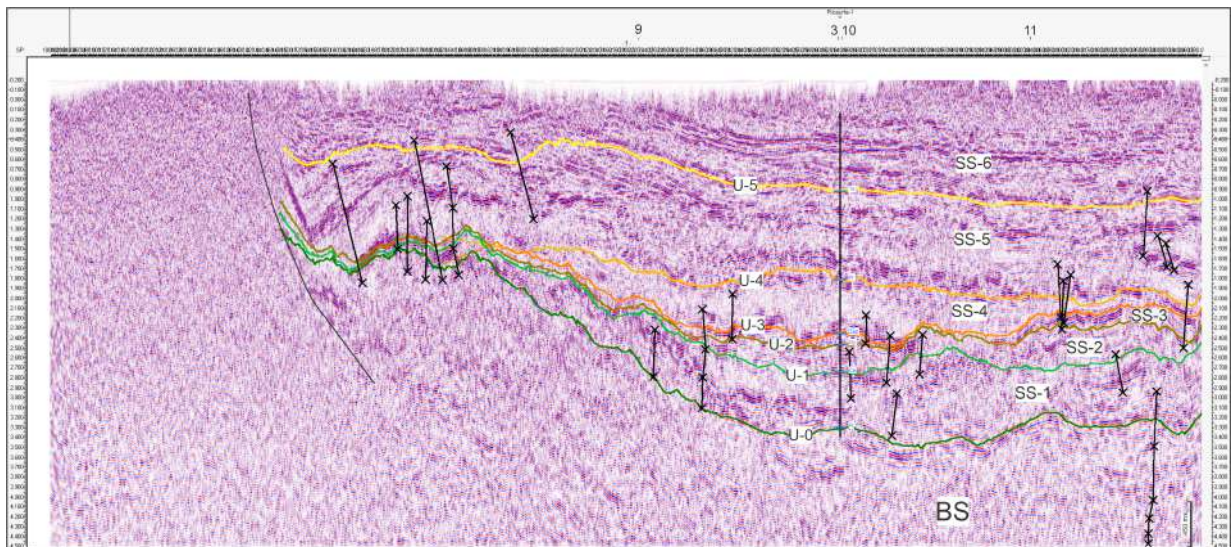


Figure 4.5: Seismic interpretation example of line 1 (see location in Fig. 1.4) with NW-SE orientation, crossing line 9, line 3, Ricaurte-1 well and line 11. Faults (black lines), stratigraphic sequences and unconformities are represented.

with the isochore maps. Besides, the evolution of the basin's subsidence was evaluated with the geohistorical graphs.

4.3.1 Digitalization and filtering of well-log data

The well-log data provided by the Secretariat of Hydrocarbons from Ecuador was the scanned logs from the three wells. This information was digitalized with the Kingdom software. The well-log data was also processed with a Butterworth filter for noise elimination and smoothing of the data to clear fluctuations in the general trend of the records.

4.3.2 Correlation of wells in the study area

The wells correlation is made by matching the tops of the formation using the log data as indicators where there are peaks, as is shown in Fig. 2.6. It is important to understand the causes of the record variations to determine the seismic units, such as the gamma-ray representing sandstone for the low values and shales for the high ones. The SP values at the baseline represent sandstones in the unit and shales on the contrary. This information was used along with the gamma-ray log for the eustatic analysis and to define the cycles in which the units were deposited.

Besides, it was used for the analysis of the evolution of the basin, including the cal-

culuation of the subsidence and representing it in a geohistorical graphic with the data of three wells. These geohistorical graphics correlate the changes in the subsidence of a basin with time. So, tectonic and total subsidence evolution was calculated for the three wells: Ricaurte-1, Chone-1, and Calceta-1. The data necessary for the geohistorical graphs are the lithology, age, thickness, compaction constant, density values, porosity, sea level changes, and paleo-bathymetry. This data was obtained from different sources. The age, thickness, porosity values, and lithology were obtained from the well-log record; meanwhile, values of density, compaction constant, and initial porosity were taken from [Gallagher and Lambeck \(1989\)](#), and the sea level variations were taken from the eustatic curve from [Haq et al. \(1987\)](#). Finally, the paleo-bathymetry values were estimated from the facies paleo-environment analysis.

The calculations were based on the concepts presented by [Van Hinte \(1978\)](#). The sum of the corrected thickness at each unit plus the paleo-bathymetry values minus the sea level changes obtained the total subsidence. For the backstripping or tectonic subsidence, the density values were necessary to calculate the sum of the thickness and for the sea level changes. The current final porosity values were obtained from the GR and RHOB log record for each formation, and the other values were calculated by the formula presented by [Sclater and Christie \(1980\)](#).

4.3.3 Definition of stratigraphic sequences

The definition of the stratigraphic sequences was made with the information provided by the well-logs and the interpretation of the 2D seismic data and the biostratigraphic and sedimentological information from previous studies made in the area as [Benitez \(1995\)](#); [Ordóñez et al. \(2006\)](#); [Hernández et al. \(2024\)](#). The sequences were regionally correlated along all seismic lines, and their geometry is proposed based on the interpretation of the seismic data using sequence stratigraphy techniques to describe it.

Chapter 5

Results and Discussion

To describe the results accomplished, a review of the objectives is important to develop. These encompass data improvement through denoising and spectral blueing techniques applied to seismic data, digitalization, and filtering of well-log data. Additionally, isopach and isochore maps are created based on the interpretation. Finally, the geo-historical graphics with the stratigraphic sequence model contribute to the comprehensive description of the basin.

5.1 Enhancement of seismic and well-log data

The seismic data were improved by applying the self-supervised denoising for the noise suppression and SB to increase the intensity of the reflectors used for the 11 seismic lines. This processing enhances the signal-noise ratio and the continuity of the reflectors, as Fig. 5.1 shows an example of the difference between before (Fig. 5.1.a) and after processing of seismic data (Fig. 5.1.b) in a portion of line 1 of NW-SE orientation (see location in Fig. 1.4). These changes of continuity are more visible at time 1.0 s and the shot point 2040 (left circle); 0.65 s and 2120 shot point (central circle); 0.87 s and 2180 shot point (right circle). This improvement was applied to all seismic lines, and those changes in the amplitude and continuity of the horizons allow for a reliable interpretation of the top formations and geological structures.

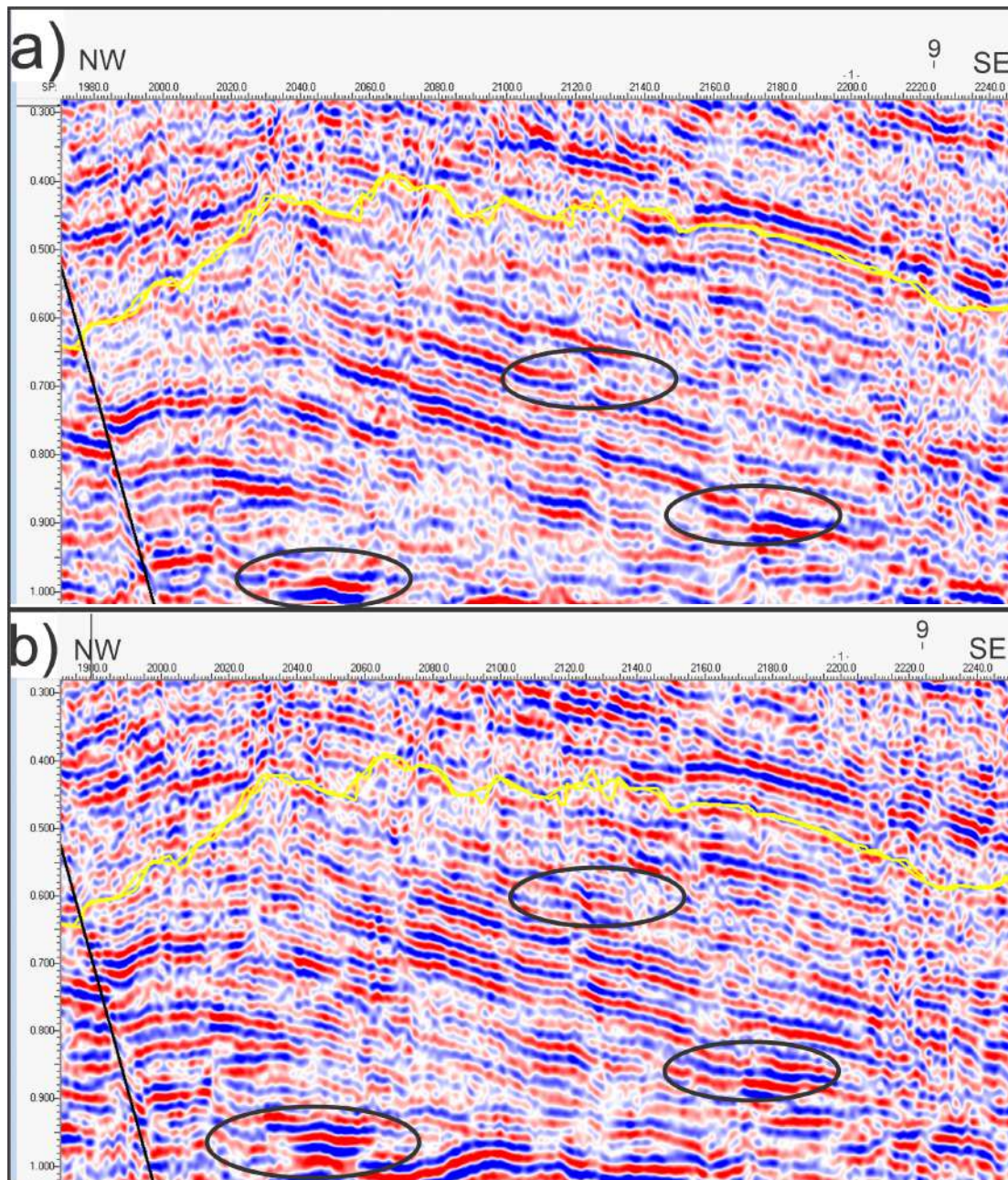


Figure 5.1: Portion of a seismic line 1 with NW-SE orientation (Fig. 1.4) that crosses the line 9. A) Seismic raw data B) Data denoised with proof 6 of 32x32 pixels, with no extra noise and SB. The yellow line represents the top of SS-5, and a fault is found at the northwestern part (black line.)

Moreover, the well-log data processing starts with its digitalization of the records from the scanned images as Fig. 5.2.a that shows an example of the logs data collected and the digitalized (Fig. 5.2.b) from the Ricaurte-1.

After the processing of seismic and well-log data, the synthetic seismogram was created. The data enhanced was used to calculate the synthetic trace and increase the correlation

coefficient of the seismograms; for R-1, the increment was of $\sim 41\%$. This process obtained a visible quantitative (Table 5.1) and qualitative improvement as the trace appears similar to the synthetic trace for the wells (R-1, Ch-1, C-1) as Fig. 1, 2, 3 in Appendix 1 exhibit. These improvements in the correlation coefficient of Table 5.1 indicate that the processing of each data set enhances the correlation between the traces. Therefore, the synthetic trace created is reliable for simulated real trace and has a better seismic-well tie. Thus, the denoising, SB of seismic data, digitalization, and filtering of well-log data results in a better interpretation of the geological characteristics of the subsurface of the Manabí basin.

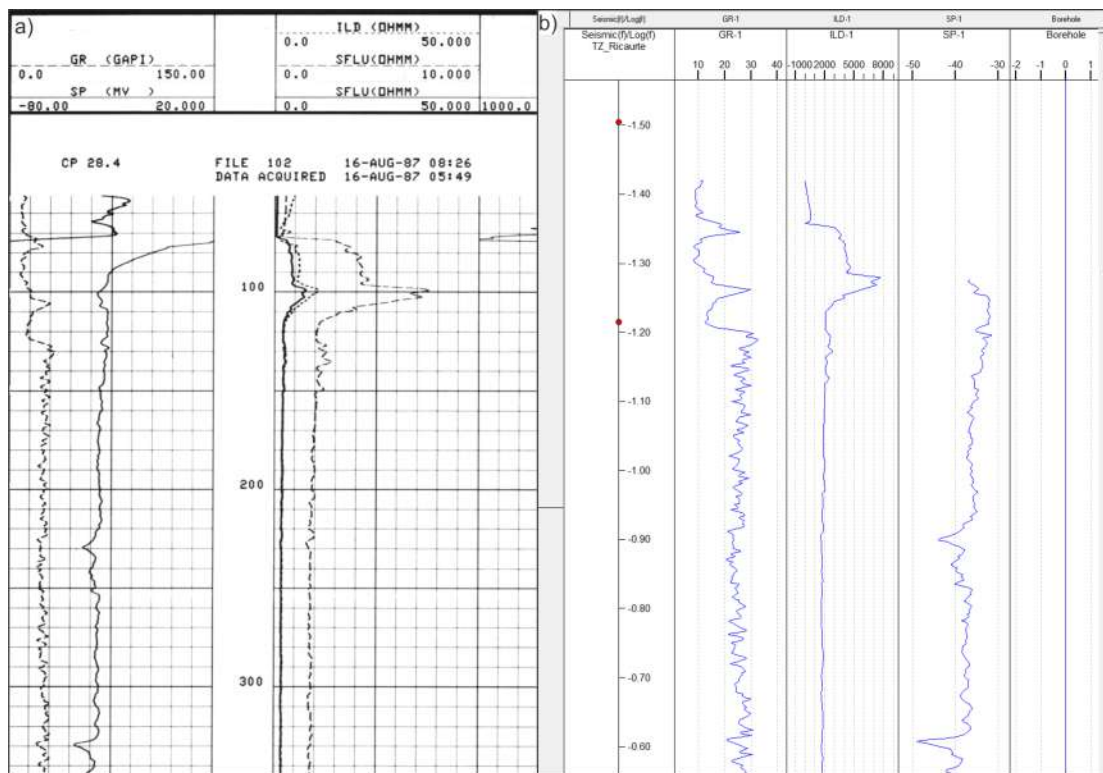


Figure 5.2: Well-log of GR, SP and resistivity ILD records of Ricaurte-1. A) Segment of data scanned from logs of Ricaurte-1 well of 340 m. B) Segment of well data digitalized of Ricaurte-1 from -1.40 to -0.60 s. Some of the first part of the records (SP) were skipped because of the distortion of superficial conditions

5.2 Seismic interpretation

After the improvement, the interpretation of horizons in seismic lines results in the definition of 6 seismic sequences (SS-1, SS-2, SS-3, SS-4, SS-5, SS-6) were established overlying

Table 5.1: Correlation coefficients of the synthetic seismograms for the three wells before (phase I) and after (phase II) the improvement of data.

	Correlation coefficient of the first seismogram	Correlation coefficient of the seismogram after the improvement of data
Ricaurte-1	0.22	0.31
Chone-1	-0.13	0.42
Calceta-1	-0.30	0.42

the basement and five unconformities (U0, U1, U2, U3, U4, U5) that are delimiting the sequences as Fig. 5.3 illustrate (see location Fig.1.4). The seismic analysis of the horizons with the code of the interpreted seismic is presented in Table 5.2. In general, SS-3, SS-4, SS-5, and SS-6 are well-defined with higher amplitude, and it is possible to follow the top of the sequences due to its continuity after the improvement of the data. However, the basement, SS-1, and SS-2 are the horizons more chaotic and difficult to distinguish structures due to the attenuation of the signal at greater depths (Table 5.2).

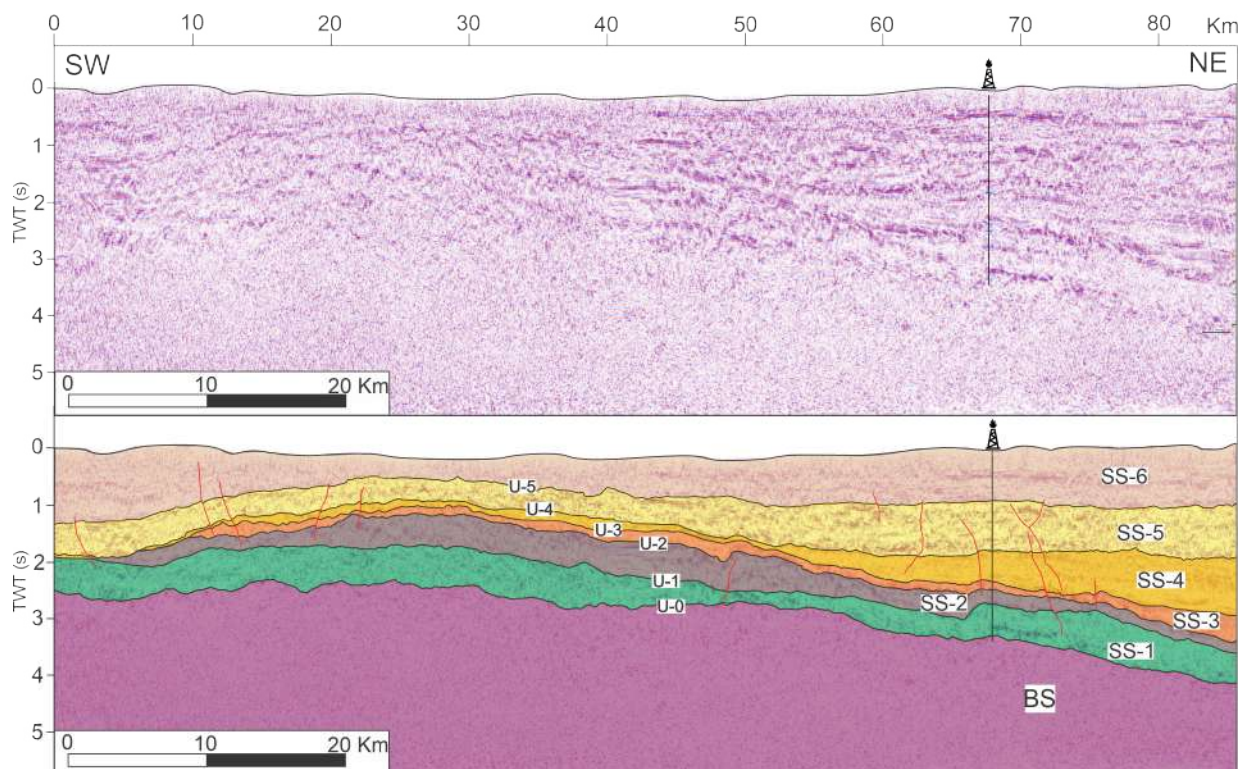


Figure 5.3: Seismic line 10 with SW-NE orientation (see location in Fig. 1.4). Above the data without interpretation, and below the seismic line with the sequences and unconformities identified. Faults are represented with red lines.

Further, the interpretation of the seismic lines allows the development of the isopachs

and isochore maps, the flattened horizons of the correlation between wells, to observe the lateral variations of the sequence's thickness.

Table 5.2: Analysis of the horizons, generally described according to their frequency, amplitude, and continuity.

Seismic sequence	Description of horizon
SS-6	It is continuous of moderate amplitude and high frequency.
SS-5	This horizon is continuous of high amplitude and high frequency with only a few discontinuous patches.
SS-4	It is mainly continuous with some chaotic parts parallel to sub-parallel reflectors of low frequency and low amplitude. This attenuation could be related to the texture of the rock type
SS-3	The horizon is continuous of parallel to sub-parallel reflectors, moderate amplitude and low frequency.
SS-2	This horizon is less chaotic, continuous with low frequency and moderately amplitude.
SS-1	It has more continuity, amplitude and frequency than the BS.
Basement	Very chaotic, discontinuous of high amplitude and low frequency because it is the deepest sequence, so the signal is attenuated

5.2.1 Basement (BS)

The basement of the Manabí basin corresponds to the Piñón Fm., whose top boundary is around 3.3 s TWT from ~ 93 Ma., but the base has not been defined. BS coincides with the cretaceous series mega-sequences and a sequence of the second order of a transgressive system (Fig. 5.4). The sequence has a negative polarity that represents a valley reflector of weak intensity and high uncertainty (Table 4.3).

The top of the BS described a decrease in thickness from Calceta to Ricaurte as the seismic line of Figure 5.19 exhibit (see Fig. 1.4 for location). Moreover, the basement shows variations of low values of TWT of 1.303 s at the northwestern part and 4.152 s at the northeastern part of the grid (Fig. 5.5). There are low values of 2.253 s at the Calceta well; as it goes to the NE, the values are moderate from 2.633 s through the Chone well and 3.202 s at Ricaurte-1. Hence, the basement has a higher thickness at SW of the area, and it thins towards NE, which coincides with the observations of Fig. 5.19 and Fig. 5.3.

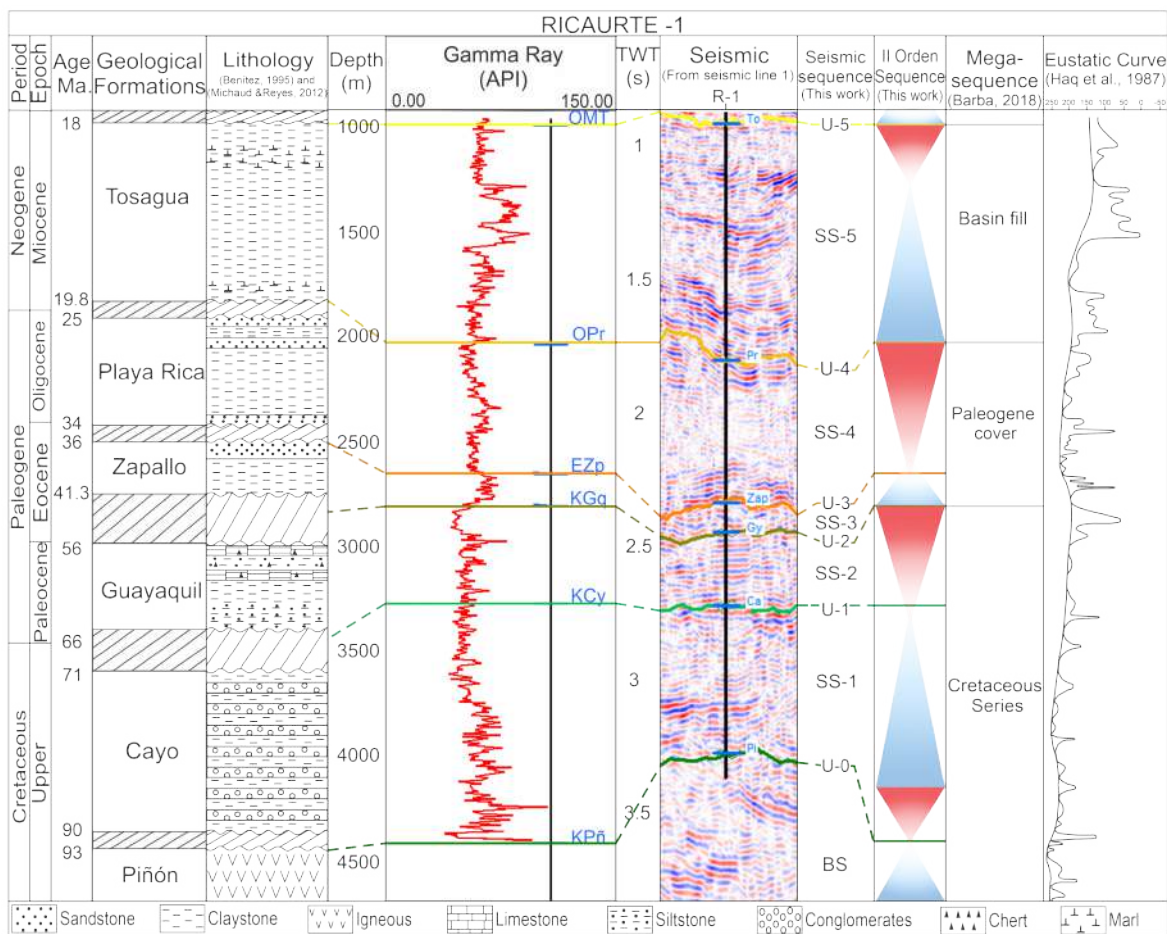


Figure 5.4: Transgressive-Regressive cycles of the second order from the Gamma Ray record of Ricaurte well and the correlation with the seismic sequences, seismic portion of line 1 (see Figure 1.4 for location) from this work with its time in two-way traveltime, eustatic changes of Haq et al. (1987), the mega-sequences of Barba (2018), the geological formations that Ricaurte-1 cut and the lithology from Benitez (1995); Reyes and Michaud (2012)

5.2.2 Seismic sequence 1 (SS-1)

The basin sedimentary fill is separated from the basement by unconformity U-0. SS-1, documented in three wells, was deposited over U-0 and delimited at the top by the U-1 (Fig. 5.19). The Cayo Fm. represents this sequence and the age boundaries are from ~ 86 Ma to 65.6 Ma. The reflectors are of weak intensity, negative polarity, and high amplitude. This second-order sequence is also part of the cretaceous series mega sequence (Fig. 5.4) and a transgressive system that moves the margin landward. It is characterized by discontinuous shale depositions until the upper Campanian and sand (Maastrichtian-Lower Paleocene) (Fig. 5.4) deposited in a bathyal-abyssal paleoenvironment with an

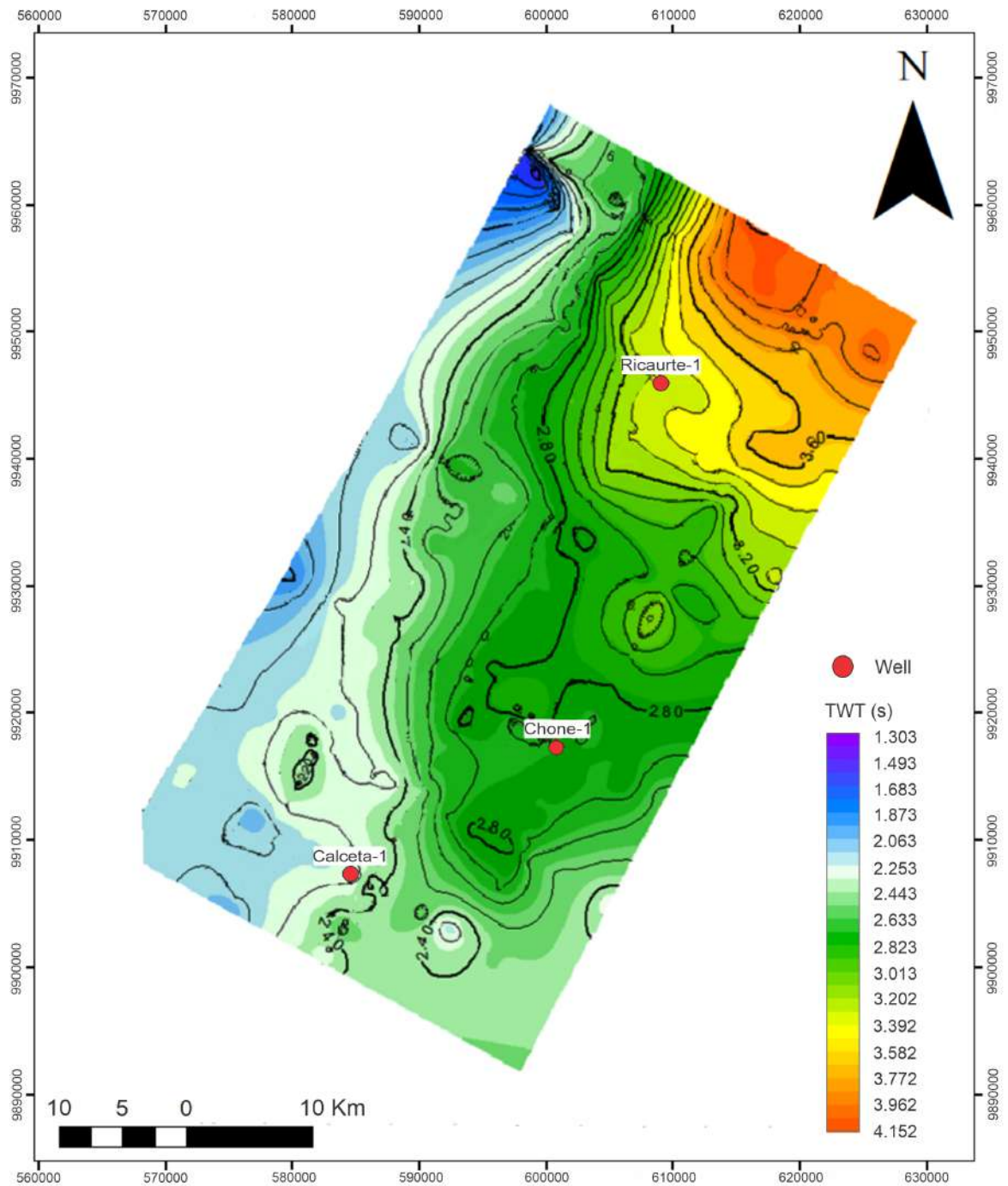


Figure 5.5: Isopach map of the basement (BS) in the study area showing two-way travel time in s (TWT).

average porosity of 0.20848789.

According to the isochore map, the thickness is constant in the area, but it thins towards NW and at the east of seismic line 4 (Fig. 5.7). The TWT of SS-1 at Calceta well is 0.550

s and a TVT of 670.6 m, which changes to 0.881 s TWT and 1325.9 m TVT at Chone, and Ricaurte has values of 1158.24 m in TVT and 0.560 s of TWT. Thus, the thickest part of SS-1 is NE and along line 5 (see Fig. 1.4 for location). In addition, the isopach map shows the changes of TWT in SS-1, where the depocenters are at the NE (Fig. 5.6). The correlation panel shows the same deepening to the NE as the isopach map, and Fig. 5.3 shows the reduction in thickness at the central part of line 10.

5.2.3 Seismic sequence 2 (SS-2)

SS-2 is delimited at the base by U-1 and U-2 at the top, documented in the three wells. It corresponds to the top of the Guayaquil formation over Cayo with age boundaries of lower Paleocene to lower Eocene (62-53 Ma). It is the last sequence from the Cretaceous series mega sequence, a regressive second-order sequence characterized by sands of low gamma-ray values at the three wells. Still, Chone and Ricaurte have a small raise of the gamma-ray at $\sim 56Ma$. (Fig. 5.4). This sequence has an average porosity of 0.25896060. The reflectors in this sequence are of negative polarity and weak intensity, with high uncertainty, which loses continuity.

The thickness variations, illustrated in the isochore and isopach maps (Figure 5.9, Fig. 5.8) as well as the correlation panel (Fig. 5.19) and line 5 (Fig. 5.3), show higher thickness at the central part, but it thins at the SW and NE. The isopach map shows low values of 0.905 s at the Calceta well in the SW and at the NW of the grid. The values are increasing in the northeast direction, where the highest values are around 3.424 s. The values are 1.577 at the Chone well and 2.416 s at the Ricaurte well.

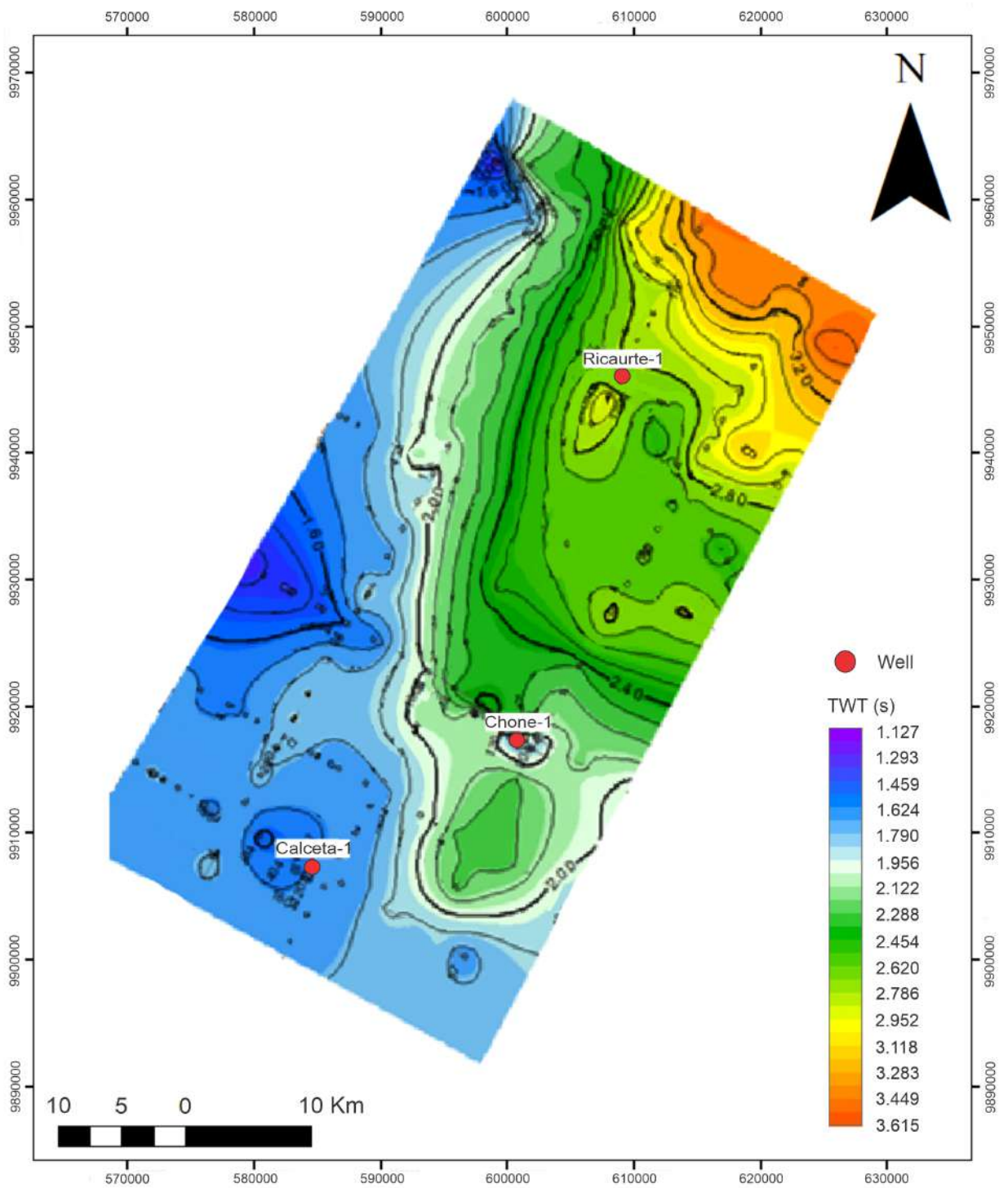


Figure 5.6: Isopach map of SS-1 in the study area showing the two-way traveltime (TWT) of the seismic waves in s.

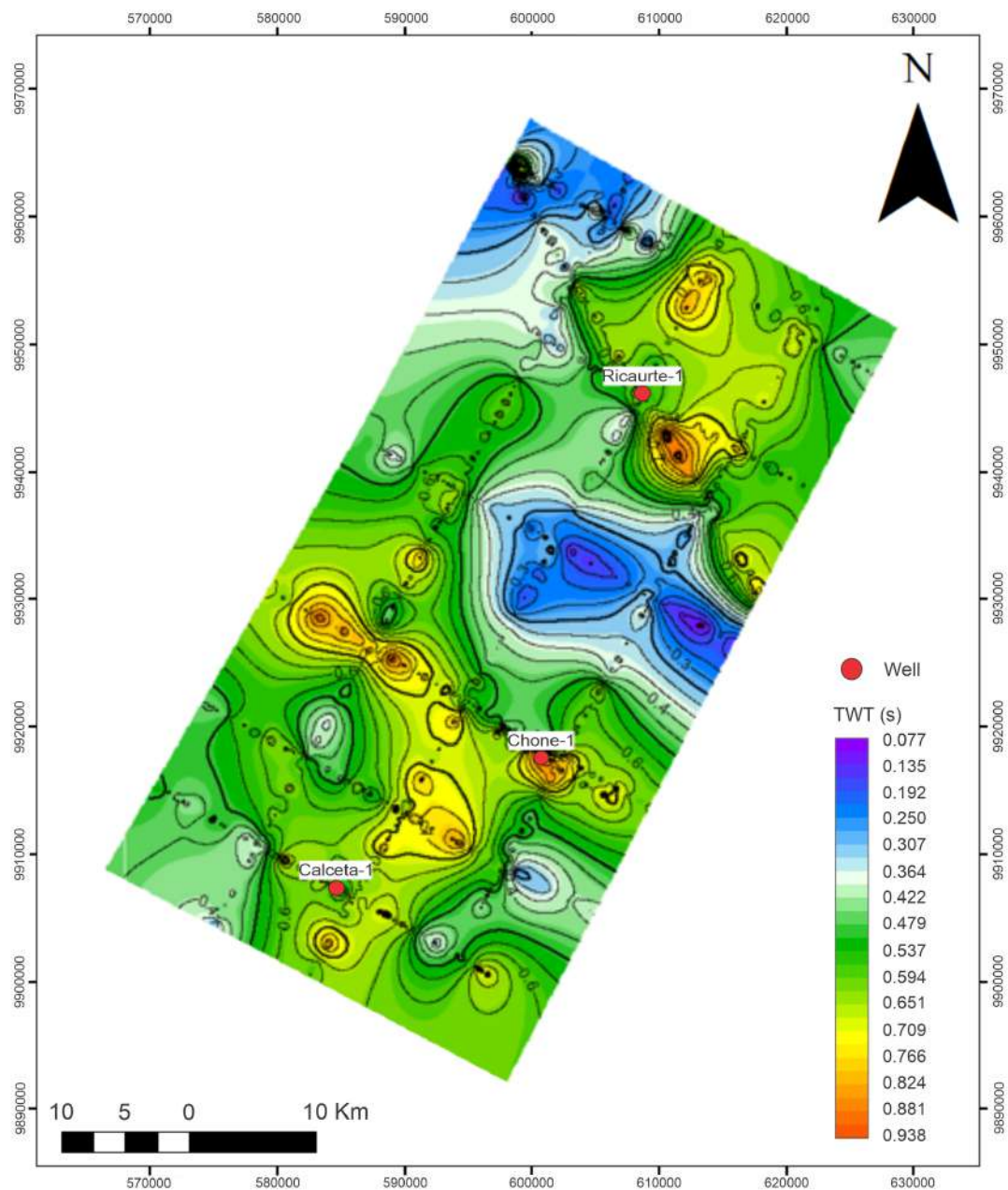


Figure 5.7: Isochore map of SS-1 and the basement showing the two-way traveltime (TWT) of the seismic waves in s.

The isochore map has a range of values from -0.079 s to 0.809 s. For this case, the lowest values are at NW and the eastern side of the grid; meanwhile, the highest values are at the SW and in the center of the grid. Ricaurte and Chone have relatively small values of around 0.23 s, and Calceta has a vertical thickness of 0.6 s. Guayaquil Fm sequence has a major thickness drop from 0.640 s or 713.2 m at the Calceta to 0.280 s or 354 m at the Chone well and an equal thickness to the North in the Ricaurte well with 0.280 s

(457.2 m). These indicate variations of the depocenters with higher deposition of SS-2 at the central and south part of the area (Fig. 5.10) due to a change in the accommodation space because of a tectonic control in the Paleocene.

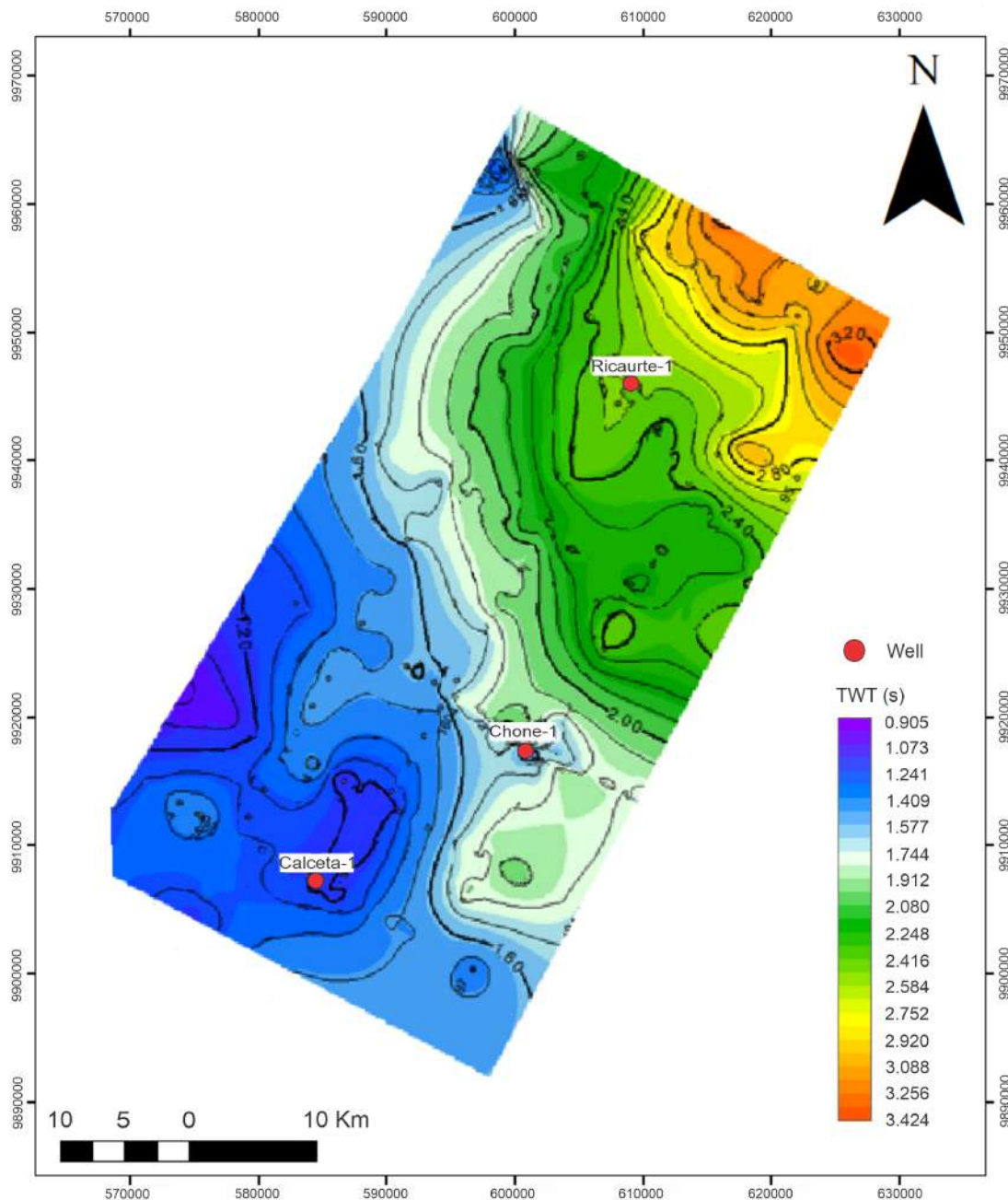


Figure 5.8: Isopach map of SS-2 in the study area showing the two-way traveltime (TWT) of the seismic waves in s.

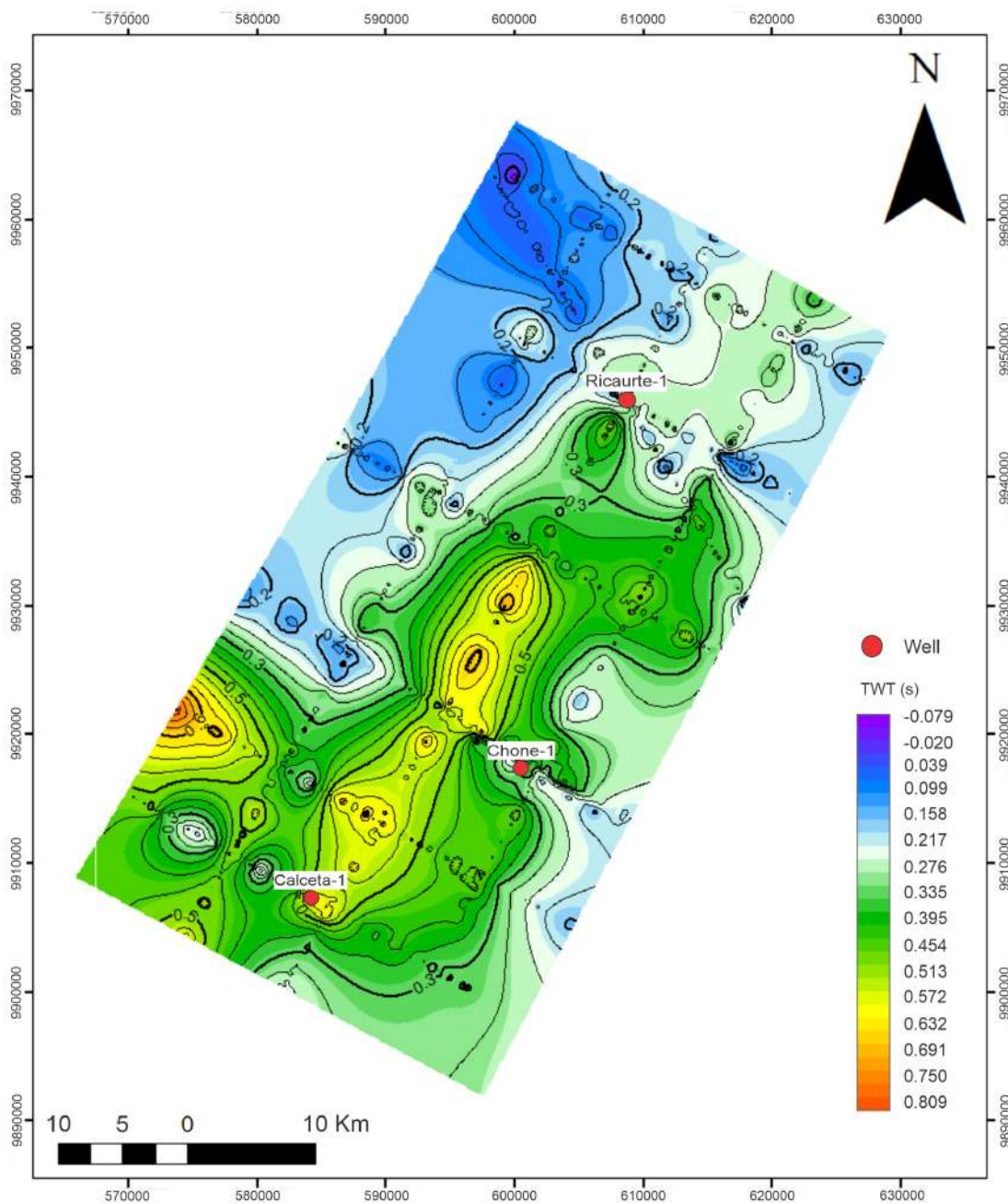


Figure 5.9: Isochore map of SS-2 and SS-1 showing the two-way traveltime (TWT) of the seismic waves in s.

5.2.4 Seismic sequence 3 (SS-3)

SS-3 is delimited at the base by U-2 and at the top by U-3; it overlies the Guayaquil Fm. with age boundaries of Middle to Upper Eocene (41.3-36 Ma). This sequence corresponds to the top of Zapallo Fm., which belongs to the Paleogene cover mega sequence and from a transgressive sequence of second order (Fig. 5.4). Shales at Chone and Ricaurte wells

dominate it, but there is only a slight increase in gamma-ray for the Calceta well, the log values from the three wells resulted in an average porosity of 0.3115032862.

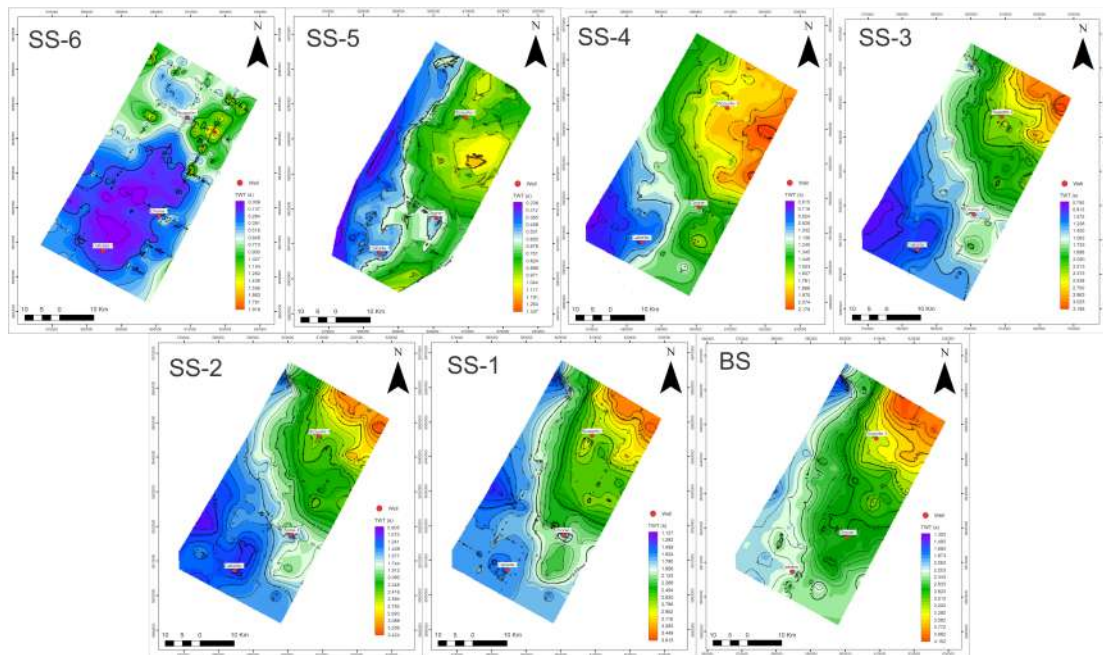


Figure 5.10: Isopach maps of each sequence (BS, SS-1, SS-2, SS-3, SS-4, SS-5, SS-6) in the study area showing the two-way traveltime (TWT) of the seismic waves in s.

The thickness variations of SS-3 show a thickening at the SW (Fig. 5.19). The isopach map (Fig. 5.11) indicates a thickness range from 0.750 to 3.188, with the lowest being from the SW, and it increases northeastwards. The Calceta well has 0.913 s, Chone has 1.563, and Ricaurte has 2.375 s thickness. Meanwhile, the isochore shows the lowest value of -0.298 s at the northwestern part of the grid and the highest value of 0.571 at the southwestern part of the area. The three wells have similar values of around 0.136 s. Figure 5.12 shows the changes in the thickness of the seismic line passing through three wells. The thickness at Calceta is 0.080 s (91.4 m), 0.080 s (91 m) at Chone and 0.110 s (152.4 m) at Ricaurte well. There are variations of depocenters to the SW part of the area (Fig. 5.12) and the thickest part at SW (Fig. 5.19)

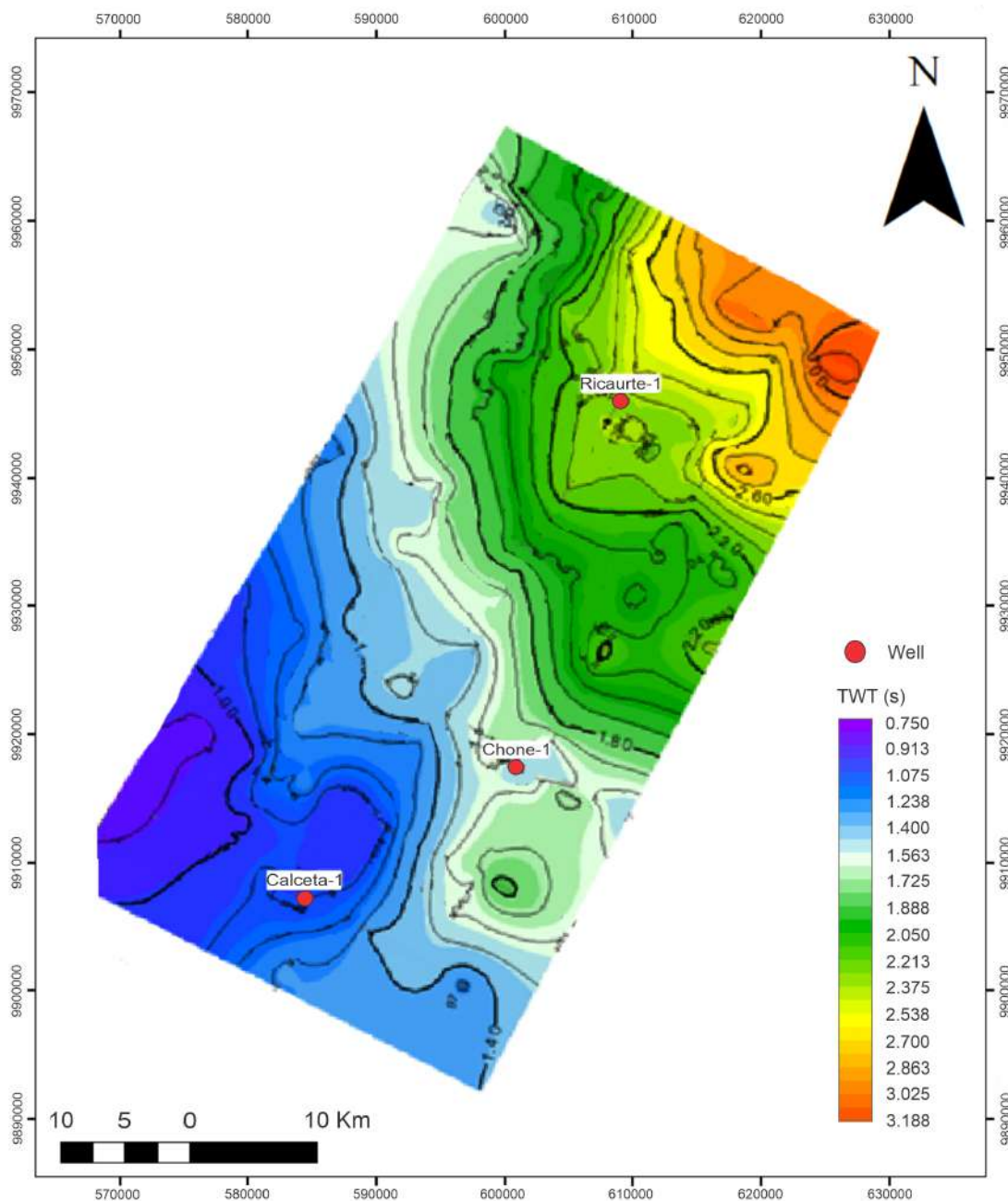


Figure 5.11: Isopach map of SS-3 in the study area showing the two-way traveltime (TWT) of the seismic waves in s.

5.2.5 Seismic sequence 4 (SS-4)

This sequence overlies the U-3 and is delimited at the top by U-4. It corresponds to the Playa Rica formation, whose age boundaries are from the Lower to Upper Oligocene (34-25 Ma). It forms part of the last mega-sequences of the Basin fill, and it shows a regressive sequence of second order dominated by sands with some increase of gamma-ray values at

the Calceta well. For the Chone well, in the lower to middle Eocene, there is an increase of gamma-ray and sands deposited in the Upper Eocene and a rise again near the top of the formation. For the Ricaurte well, the gamma-ray log is similar to the Calceta well (Fig. 5.4). The porosity calculated from the three wells for Playa Rica is 0.3410477, which is an increase compared with the oldest units.

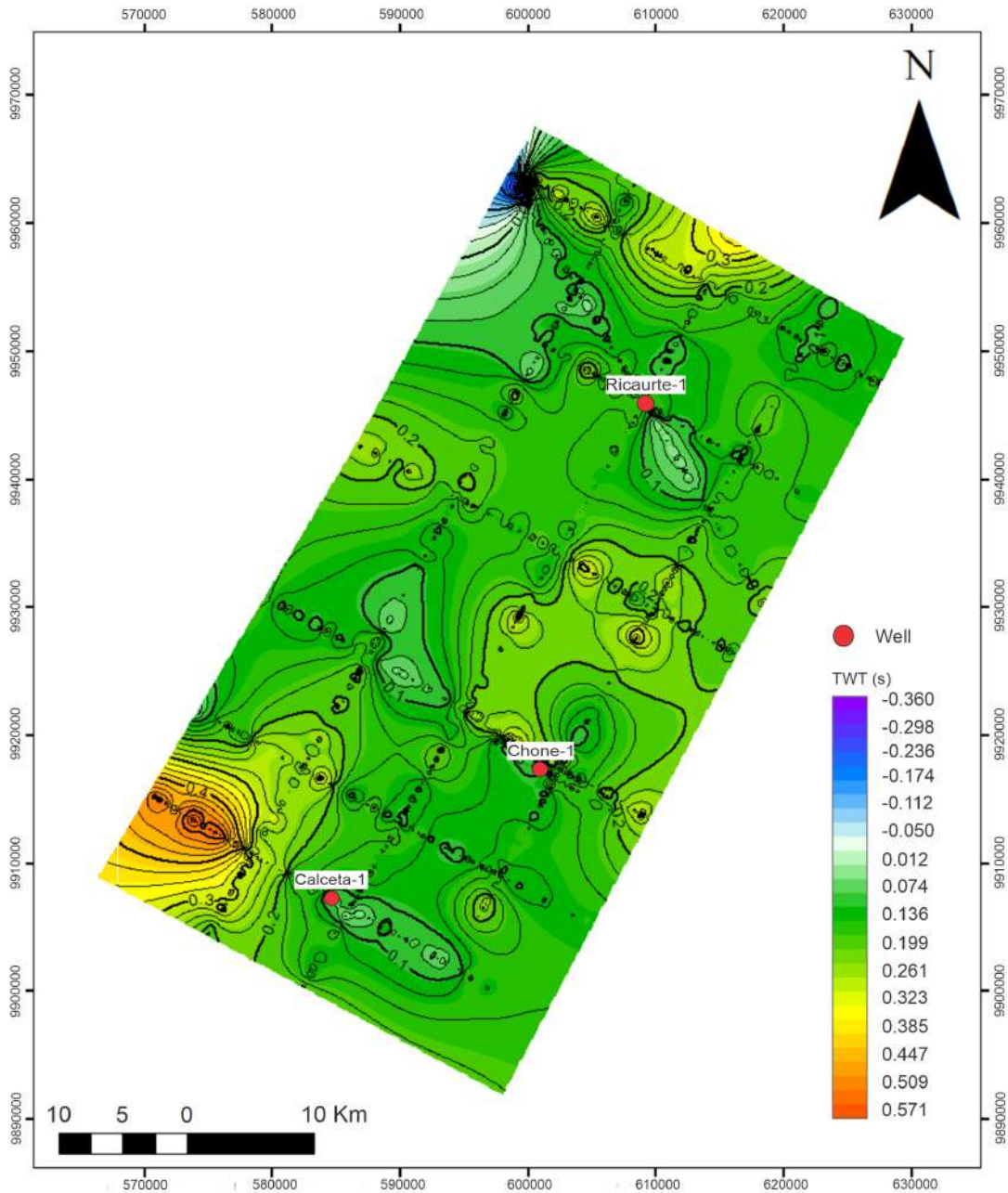


Figure 5.12: Isochore map of SS-3 and SS-2 values showing the two-way traveltime (TWT) of the seismic waves in s.

SS-4 is thickening to the NE (Fig. 5.19). The thickness variations range from 0.615

s to 2.178 s for the isopach map of the sequence (Fig. 5.13). The figure shows that the lowest values are at the southwest and the highest at the northeast of the grid. For the vertical thickness (Fig. 5.14), the low values are all over the grid (0.057 s) until around line 3, which starts to increase to the northeast corner of the grid with values of 1.272 s. The Calceta well has a value of 0.928 s (171 m), the Chone well has 1.240 s (268.2 m) of thickness, and 1.866 s (622 m) of Playa Rica thickness at Ricaurte. Fig. 5.10 indicates a depocenter at the NE part and a thinner TVT at the south (Fig. 5.14).

5.2.6 Seismic sequence 5 (SS-5)

The seismic sequence 5, overlying U-4 and the top delimited by U-5, also appears at the three wells. It corresponds to the Tosagua formation, which has age boundaries from Lower to Middle Miocene (19.8–18 Ma). It also forms part of the last mega sequence of basin fill, and it has a major transgressive sequence of second order characterized by an overall pattern of sands, shales, and sands deposition according to the gamma-ray record (Fig. 5.4). Calceta well shows the sand deposition until around the upper Oligocene and increased gamma-ray values until the Miocene times. Chone well has general sand sediments with some raised values of gamma-ray. Ricaurte well has low gamma-ray values, an increase of gamma-ray at the lower Miocene, and a drop until the Upper Miocene. The porosity value for this unit is 0.32749167.

SSS-5 is thickening at the NE (Fig. 5.19 and Fig. 5.3). The isopach map has a range of true thickness from 0.238 s to 1.337 s, and the low values are on all the western sides of the grid and increase to the east. Calceta well has a thickness of 0.458 s (564 m), Chone well has a thickness of 0.531 s (732 m), and Ricaurte well has a value of 0.971 s (1044 m) (Fig. 5.15). The isochore map shows a range value of the vertical thickness of 0.181 s - 1.228, distributed in the southwestern area. The low values then increase northwards; the highest values are at the NW and NE corners of the grid. Calceta well has a value of 0.460 s, Chone well has a value of 0.669 s, and Ricaurte well has a value of 0.949 s (Fig. 5.16). It also shows a slight rise of thickness from Calceta to Chone and a major increase northwards at Ricaurte. The depocenter of this sequence is similar to the SS-4, but it is thickening to the western side of the area (Fig. 5.10). SS-3, SS-4 and SS-5 show similar deposition patterns, which could be interpreted as syn-tectonic sequences. Besides, SS-5 deposition

might be related to the uplift of the cretaceous basement changing the morphology at the NW, and causing the shallow deposits that Fig. 5.15 shows.

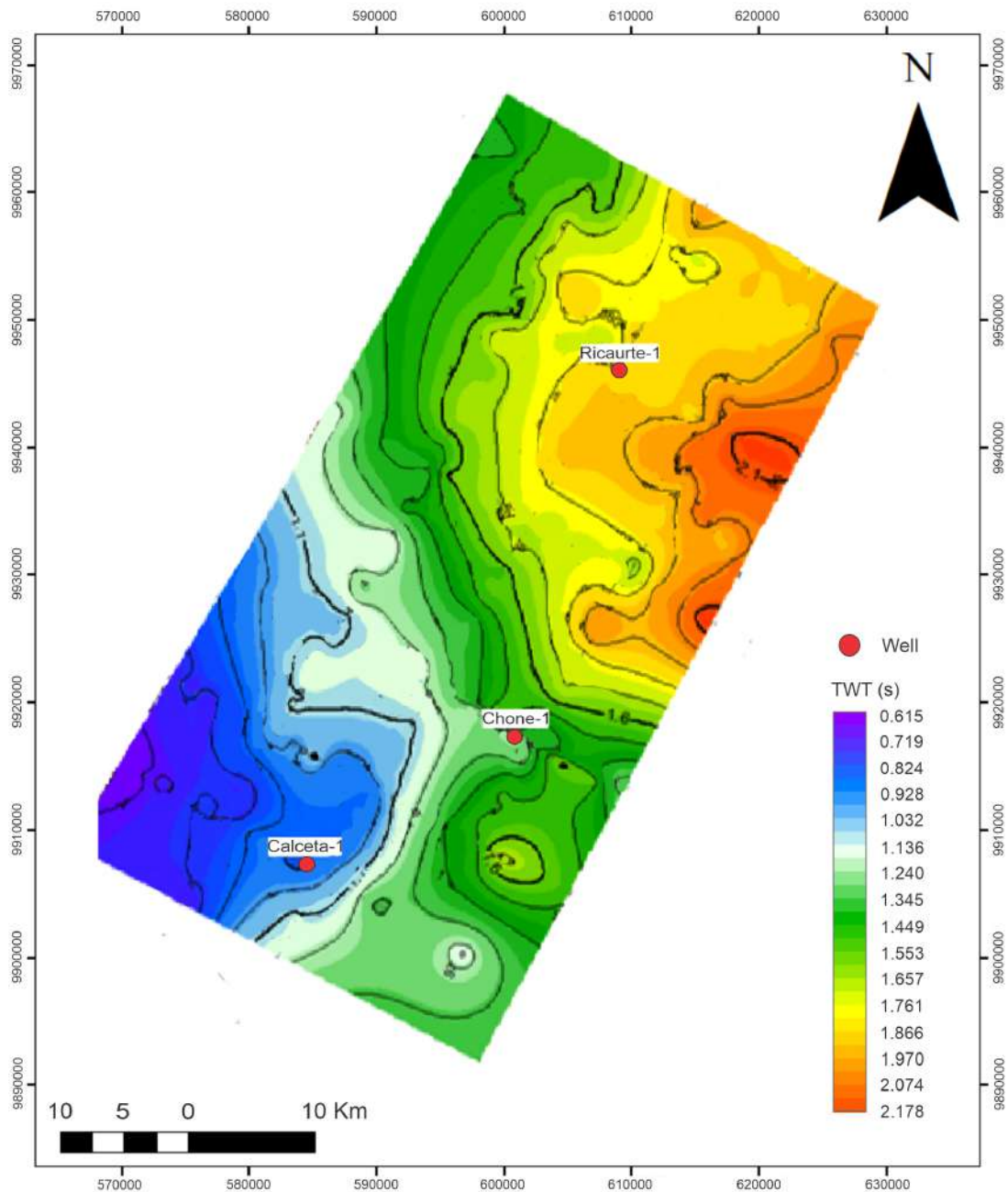


Figure 5.13: Isopach map of SS-4 in the study area showing the two-way traveltime (TWT) of the seismic waves in s.

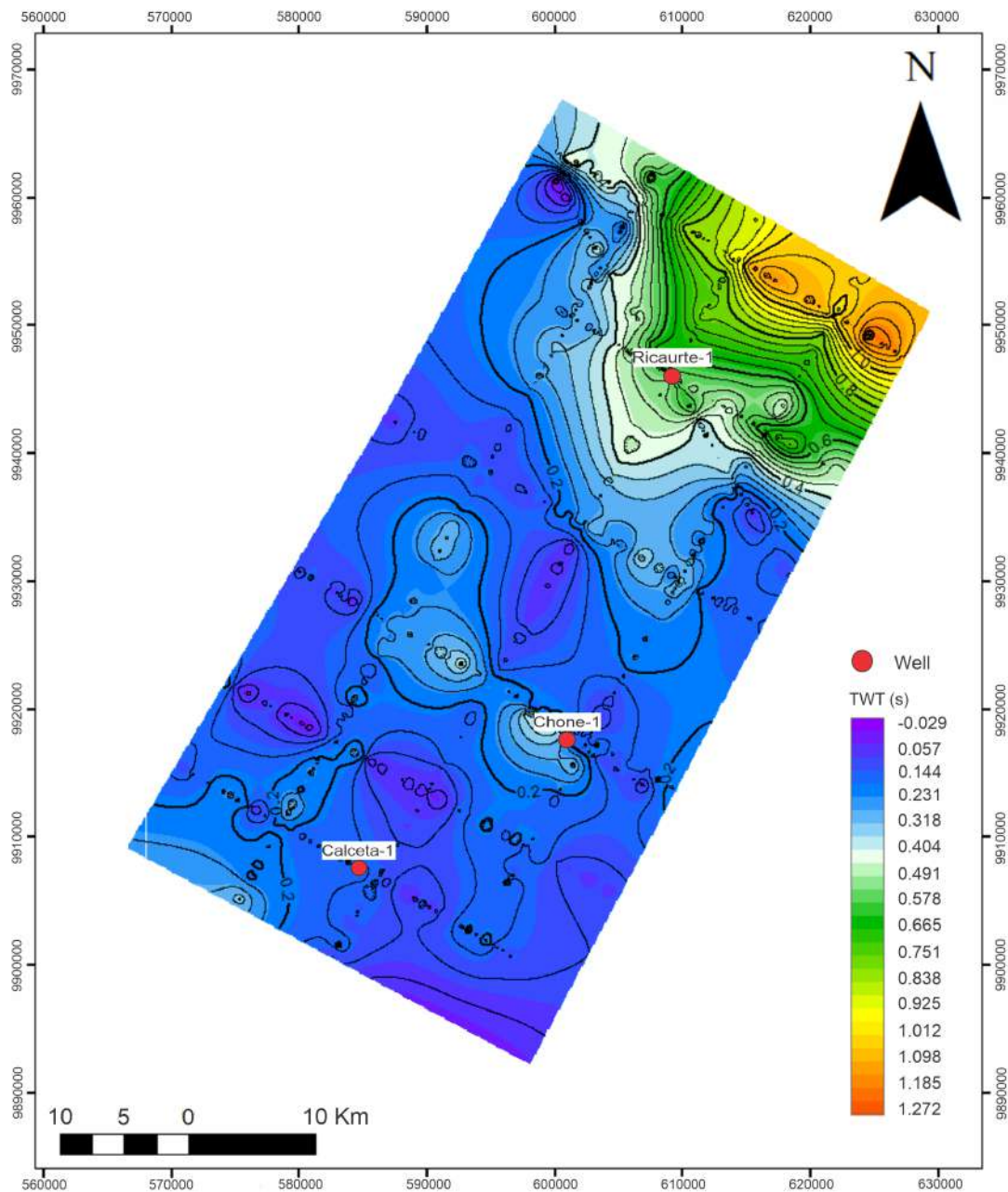


Figure 5.14: Isochore map of SS-4 and SS-3 values showing the two-way traveltime (TWT) of the seismic waves in s.

5.2.7 Seismic sequence 6 (SS-6)

The seismic sequence 6, overlying U-5 and the top delimited by surface, also appears at the three wells. It corresponds to the Angostura and Ónzole formation but is recorded by the Chone well. It has the age boundaries from the Middle Miocene to the Lower Pliocene (15–4 Ma). It forms part of the last mega sequence of basin fill (Fig. 5.4). Its paleo-environment

corresponds to the inner shelf. The porosity measurements for Angostura y Ónzole were obtained from the Chone well, as it is the only well that penetrates these formations. The porosity value for Angostura is 0.32609537, and for Ónzole, it is 0.29334404. It is worth noting that the porosity of these units is lower than that of the previous formations.

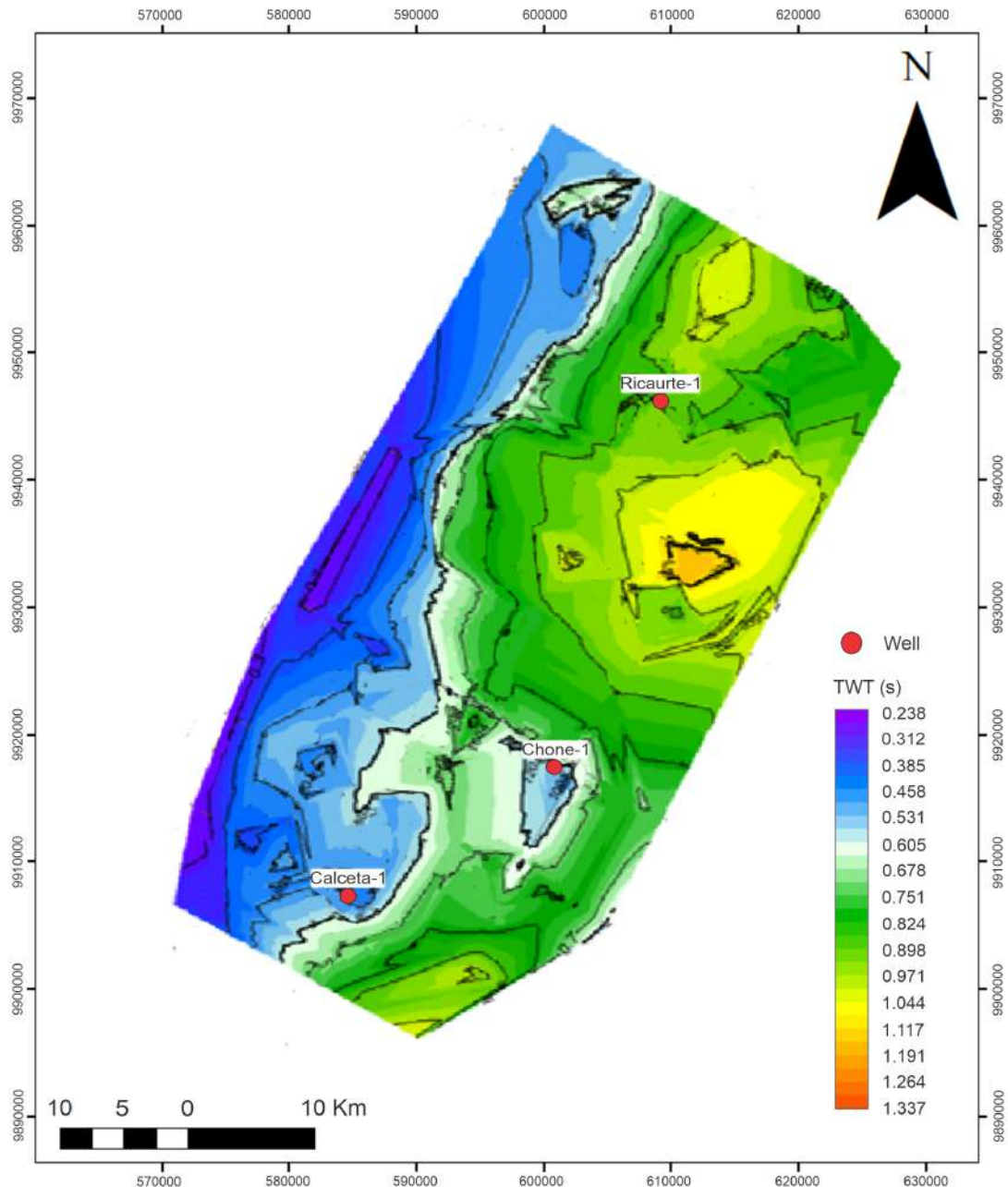


Figure 5.15: Isopach map of SS-5 in the study area showing the two-way traveltime (TWT) of the seismic waves in s.

SS-6 is thick at the NE and SW, but it thins at the central part (Fig. 5.3). The isopach map has a range of true thickness from 0.009 s to 1.918 s, and the low values are in all the

southern side of the grid and increase to the North. Chone well has a thickness of 0.264 s (625 m), and Ricaurte well has a value of 0.63 s (966 m) (Fig. 5.17).

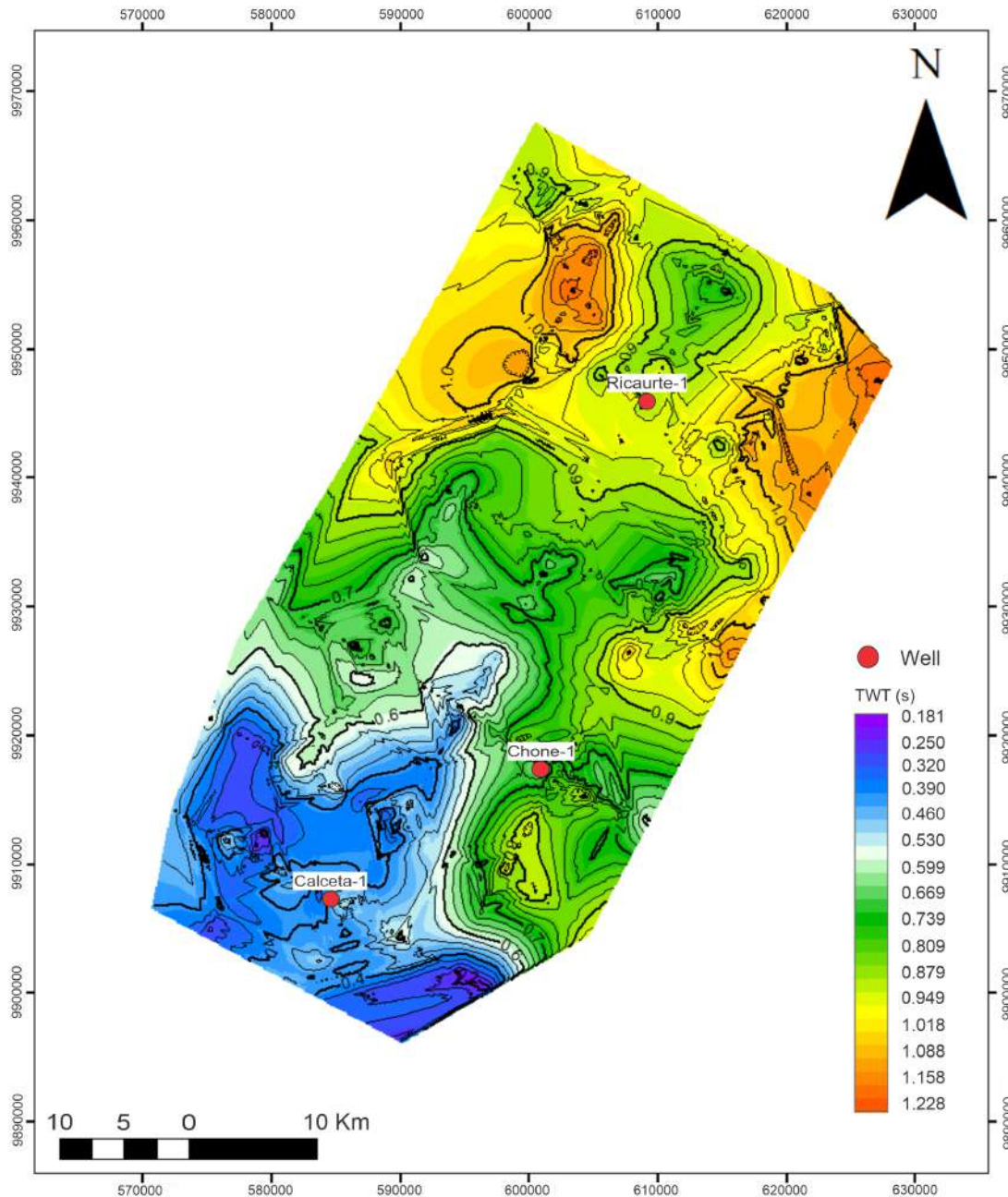


Figure 5.16: Isochore map of SS-5 and SS-4 values showing the two-way traveltime (TWT) of the seismic waves in s.

The isochore map shows a range value of 0.317 s - 2.903 vertical thickness. The highest values are at the NE part of the grid. Calceta well has a value of 0.317 s, Chone well has a value of 0.662 s, and Ricaurte well has a value of 1.696 s (Fig. 5.16). The depocenter is at

the NE along line 11; it is thickening to the north and south part of the area (Fig. 5.10).

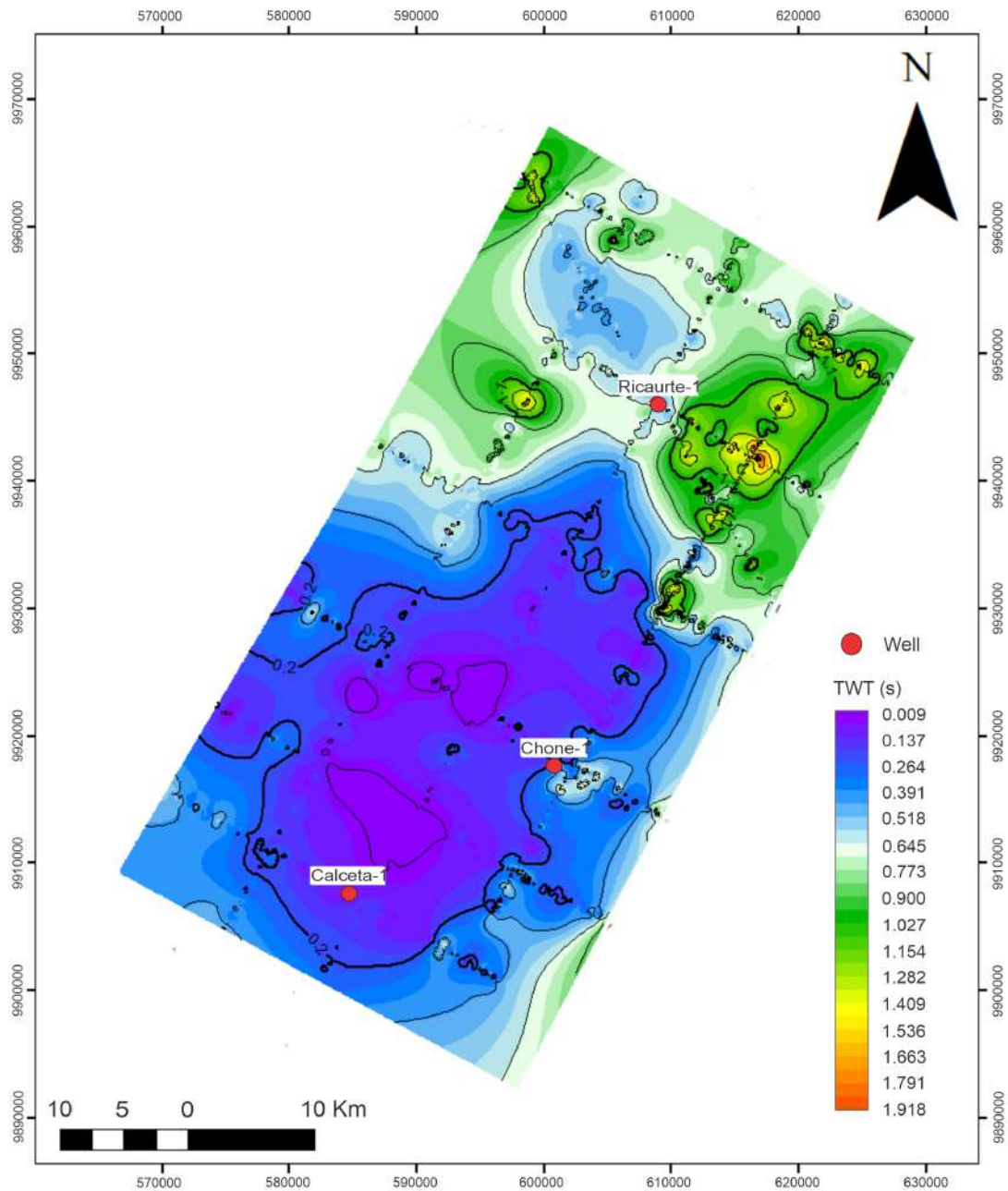


Figure 5.17: Isopach map of SS-6 in the study area showing the two-way traveltime (TWT) of the seismic waves in s.

5.2.8 Correlation Panel

The correlation panel shows a scheme of the geometry of the seismic stratigraphic units and their lateral changes across the area in the Manabí basin. The panel connects the three boreholes through seismic lines, resulting in a cross-section of Calceta-Chone-Ricaurte wells

in an SW-NE orientation and the distance between Ricaurte and Chone is 29787 m., and from Chone to Calceta is 19253 m. It also allows one to analyze the thickness change of the seismic sequences.

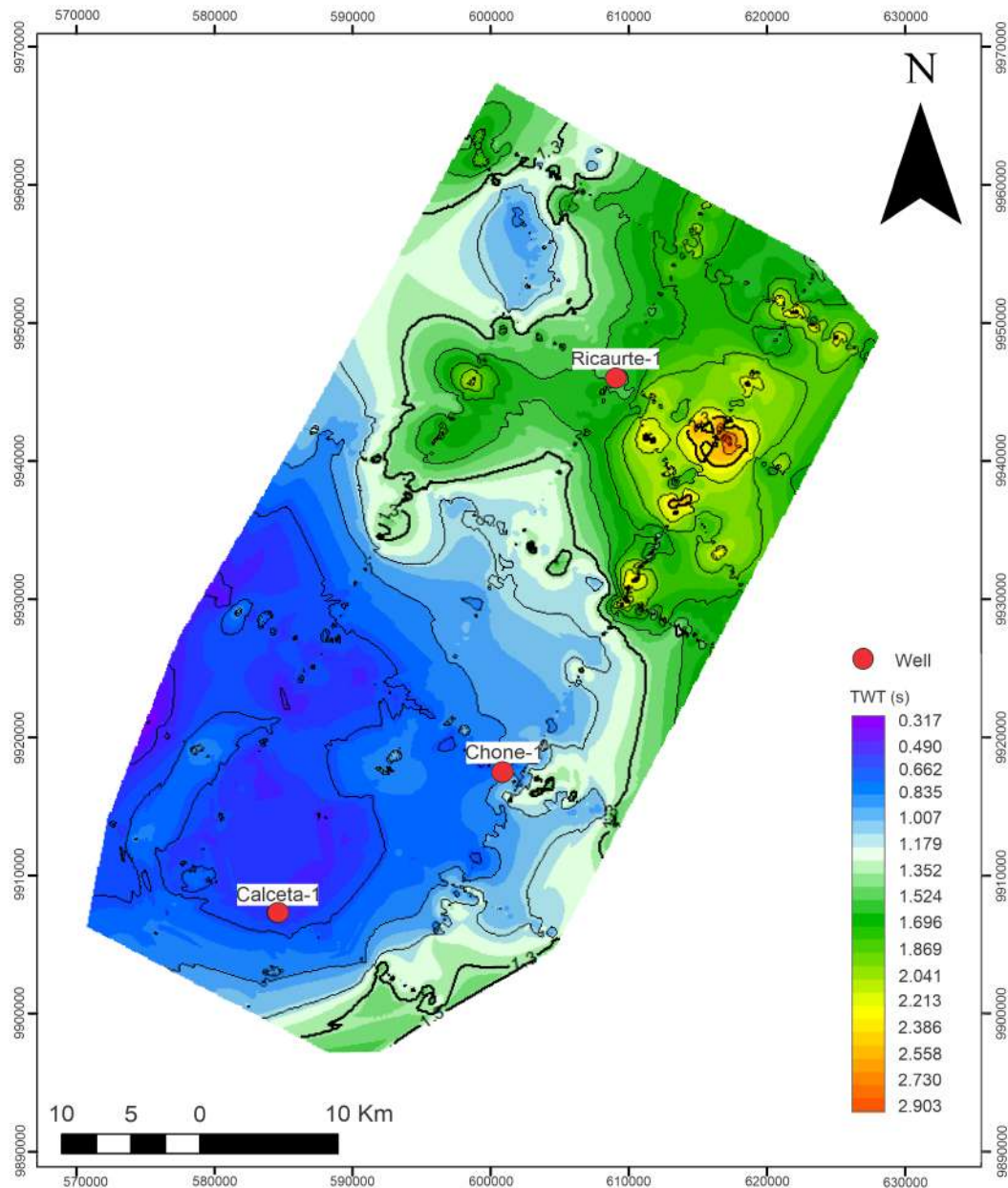


Figure 5.18: Isochore map of SS-6 and SS-5 values showing the two-way traveltime (TWT) of the seismic waves in s.

The panel goes from Calceta-1 at the south of the area, moving to the east up to the Chone-1 borehole, and it goes for the easternmost seismic line to the North until it reaches

the line that passes through Ricaurte-1 well to the NW as indicated in Fig. 5.19 (See Fig.1.4 for location).

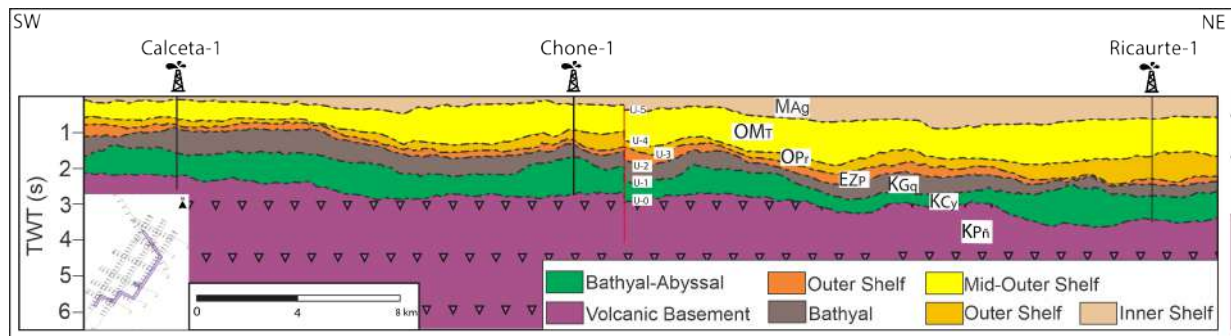


Figure 5.19: Correlation panel of the three wells Calceta-1, Chone-1, Ricaurte-1. Formation's code: KCy = Cayo Fm., KGq = Guayaquil Fm., EZp = Zapallo Fm., OPr = Playa Rica Fm., OMT = Tosagua Gp, MAg= Angostura Fm. with its depositional setting, and the unconformities U-0, U-1, U-2, U-3, U-4. Fault in red line

5.3 Basin Analysis

The geo-historical graphs consider the factors mentioned by [Posamentier and Allen \(1999\)](#) to understand the determinant agent controlling the evolution of the basin through time. Moreover, climate and biological factors also could indirectly control the evolution of the basin. For example, a rise in precipitation could generate more erosion, increasing the sediment supply that will be transported to the basin, or an increase in sea temperature could cause a rise in the sea level, which generates more load on the basin, increasing its subsidence in both cases. For the analysis of the evolution of the subsidence in the Manabí basin, the results from the total and tectonic subsidence were plotted in the geohistorical graphics for each well (Ricaurte-1, Chone-1, Calceta-1).

5.3.1 Geo-historical results and basin fill evolution

The geohistory from the drilling of Ricaurte-1 (Fig. 5.20) shows intense positive subsidence at the beginning of the curve (86 to 71 Ma.), which corresponds to the sedimentation of the seismic SS-1 (Cayo Fm.); followed by a significant decrease in the subsidence of the basin from 71 to 58.4 Ma., that correspond to the unconformity U-1. After this, there is a minor period of subsidence, in which the seismic sequence two was deposited (Guayaquil Fm.; 58.4 to 56.5 Ma.), followed by a slight decrease in the subsidence values from 56.5 to

41.3 Ma. It corresponds to the unconformity U-2. Then, there is a general tendency to increase the subsidence during the sedimentation of Zapallo Fm. (SS-3; 41.3 to 35.5 Ma.), Playa Rica Fm. (SS-4; 33.9 to 25 Ma.), and Tosagua Fm. (SS-5 from 19.8 to 18 Ma.); separated by the unconformities U-3 (35.5 to 33.9 Ma.) and U-4 (25-19.8 Ma.). Next, unconformity U-5 and the sedimentation of SS-6 (MAg and MOz) from 15 Ma-4 Ma.

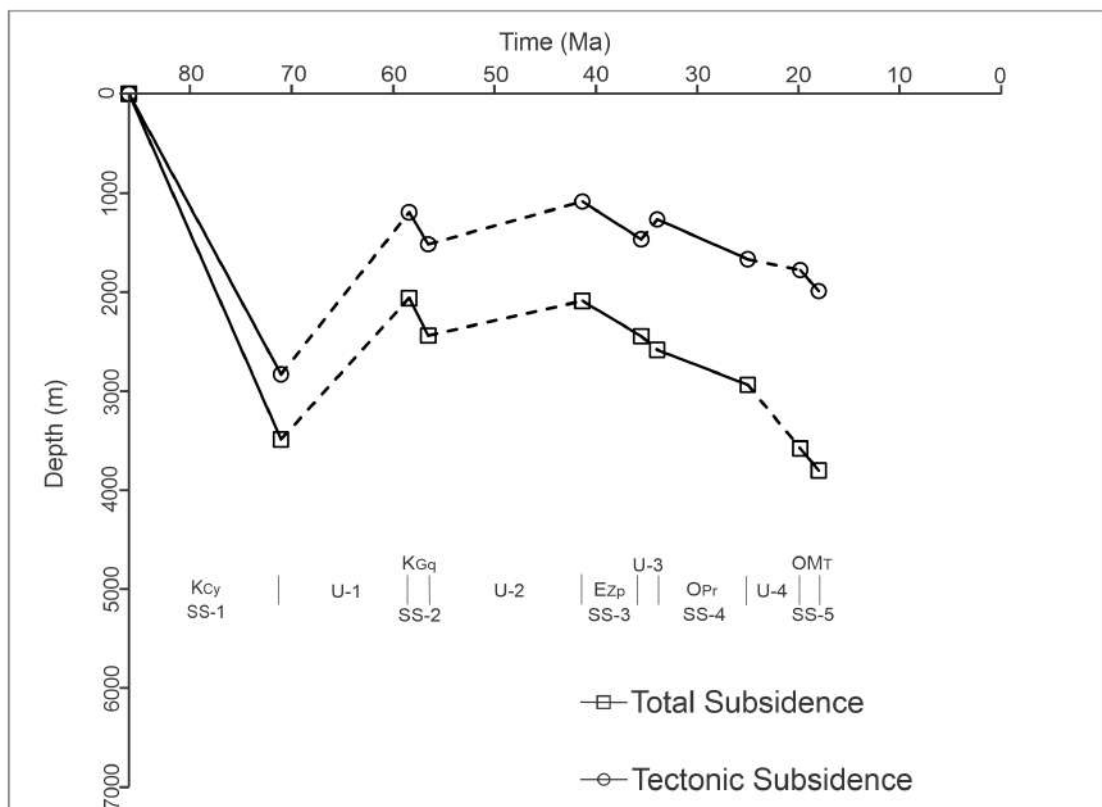


Figure 5.20: Geohistorical graphic of Ricaurte-1 well. Formation's code: KCy = Cayo Fm., KGq = Guayaquil Fm., EZp = Zapallo Fm., OPr = Playa Rica Fm., OMT = Tosagua Fm. It shows the seismic sequences SS-1, SS-2, SS-3, SS-4, SS-5, which correspond to each formation, and the unconformities U-0, U-1, U-2, U-3, U-4.

According to the eustatic curve of [Haq et al. \(1987\)](#) in Fig. 5.4, in the first period of the sedimentation of the turbidites from Cayo, there was a fall of the sea level and deep tectonic subsidence that is similar to the total subsidence (Fig. 5.20), which indicates a low rate of sediment supply and low deepening of the basin and that it was controlled by tectonism. It suggests an extension period during the Upper Cretaceous in the Manabí

basin. After this, U-1 shows negative values for subsidence and a rise of sea level until 66 Ma (Fig. 5.4), and this unconformity could occur in compression. Hence, it is a period of uplifting and shows a low sediment supply.

In addition, Fig. 5.20 indicates positive subsidence during the sedimentation of Guayaquil Fm. (SS-2), Zapallo Fm (SS-3), Playa Rica Fm. (SS-4), and Tosagua Gp (SS-5). The values of tectonic subsidence are decreasing from SS-3 to SS-5, which suggests an increase in the sediment supply to the young sediments. For the sedimentation of SS-4, an increase in the sea level occurs, but the tectonic subsidence is lower than the initial, which could indicate a thermal subsidence at this time. During the SS-3 deposition occurred a decrease in the sea level and also a decrease of the tectonic subsidence; SS-4 deposition has a similar tendency to a reduction of the tectonic subsidence and also of the sea level, but there was an increase of the sea level for the SS-5 deposition with a more visible increase of the total subsidence. However, they are minor for the tectonic values, which could indicate a rise in the sediment supply and deepening of the basin.

The unconformity U-2 occurred in an increase of the accommodation space around 58.4-41.3 Ma. (Fig. 5.4). Fig. 5.20 shows negative subsidence during this period, which suggests an uplifting due to a compressive regime to have a higher control during U-2. The unconformity U-3 experienced an increase in the accommodation space, and the total subsidence has a positive curve, but not with tectonic control. This subsidence could indicate a climate factor, such as a period of the thermal expansion of water. This factor will increase the sea level and cause subsidence, and it coincides with the thermal maximum of the Paleocene-Eocene, described by [Li et al. \(2022\)](#). During the U-4, accommodation space increased, and the total subsidence showed positive values but with low tectonic control. Finally, the U-5 occurred in an increase of accommodation space, showing high subsidence probably caused by thermal subsidence or growth of the sediment rate to the basin.

Chone-1 well shows a geohistory represented in Figure 5.21, and the curves also describe deep initial subsidence from 93 to 71 Ma. which correspond to the basal unconformity and the sedimentation of the Cayo Fm. (SS-1). Then, there is a fall in the important decrease in the subsidence of the basin (71 to 58.4 Ma.) corresponding to the unconformity U-1, followed by low values for the subsidence with slight changes such as the curves illustrated

during the sedimentation of SS-2 (Guayaquil Fm.; 58.4 to 56.5 Ma.), SS-3 (Zapallo Fm.; 41.3 to 35.5 Ma.), SS-4 (Playa Rica Fm.; 33.9 to 25Ma.) and SS-5 (Tosagua Fm.; 19.8 to 18 Ma.). These seismic sequences are separated by the unconformities U-2 (56.5 to 41.3 Ma.) and U-3 (35.5 to 33.9 Ma.) with a tendency of negative subsidence and U-4 (25-19.8 Ma.) that show a difference in the tendency of the total subsidence curve.

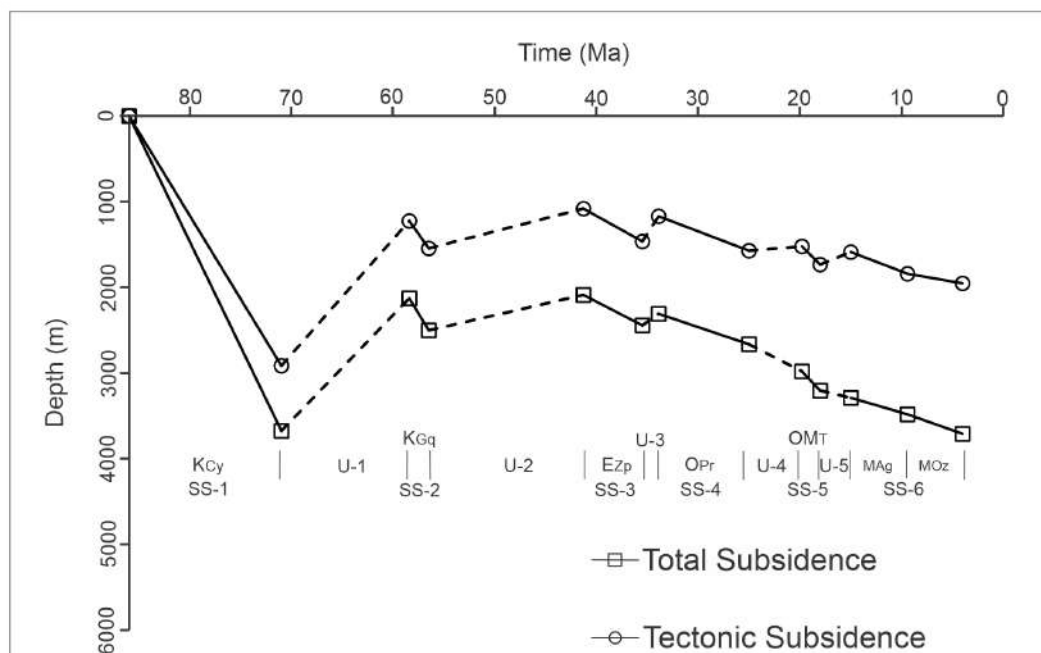


Figure 5.21: Geohistorical graphic of Chone-1 well. Formation's code: KCyl = Cayo Fm., KGq = Guayaquil Fm., EZp = Zapallo Fm., OPr = Playa Rica Fm., OMT = Tosagua Fm. It shows the seismic sequences SS-1, SS-2, SS-3, SS-4, SS-5, which correspond to each formation, and the unconformities U-0, U-1, U-2, U-3, U-4.

There is a decrease in the accommodation space during the sedimentation of the turbidites from Cayo Fm. (SS-1) due to a fall in the sea level (Fig. 5.4). The tectonic and total subsidence are positive and indicate higher tectonic control than the sediment load. Then, there was a fall in the sea level during U-1, which means a lower accommodation space was probably caused by a compression period with a low sediment supply.

Subsequently, there is an increase in the total subsidence, which suggests a control by the load of sediments in a sea level rise during the sedimentation of SS-2. U-2 curves show negative subsidence values like the Ricaurte well curves, where the positive slope indicates a compression period. Therefore, SS-3 and SS-4 exhibit similar tendencies for the tectonic and total subsidence, but SS-4 appears to have more sediment supply control than the tectonic subsidence. However, the unconformity U-3 splitting the two sequences shows negative subsidence more visible in the tectonic, indicating a compression period. The sedimentation of SS-5 takes place during a rise of the sea level, and its subsidence curves point to a high rate of sediment supply and possible climate control due to an increase in temperature. The unconformity U-4 has a negative tectonic subsidence tendency; meanwhile, the total subsidence is positive, suggesting a compression period. Then, the U-5 curve shows low subsidence and negative tectonic control, and SS-6 conformed by Angostura Fm. and Ónzole Fm indicate moderate subsidence with tectonic control but a higher sediment supply.

The geohistory information from the Calceta well (Fig. 5.22) shows a high subsidence controlled by the tectonic during the sedimentation of the SS-1 (Cayo Fm.) from 86-71 Ma. Therefore, there is a major drop in the basin subsidence values (71 to 58.4 Ma), corresponding to the sedimentary hiatus between SS-1 and SS-2 (U-1), and a change in the tectonic subsidence is observed. This is followed by low values for subsidence during the sedimentation of SS-2 (Guayaquil Formation; 58.4 to 56.5 Ma), which shows values between 1000 and 2000 m. of depth, which are lower than the other wells. SS-3 (Zapallo Fm.; 41.3 to 35.5 Ma.) exhibit positive tendencies of subsidence parallels between them; SS-4 (Playa Rica Formation; 33.9 to 25 Ma) and SS-5 (Tosagua Formation; 19.8 to 18 Ma) shows similar positive curves for total and tectonic subsidence. These seismic sequences are separated by the unconformities U-2 (56.5 to 41.3 Ma), U-3 (35.5 to 33.9 Ma) with negative subsidence, and U-4 (25-19.8 Ma), which shows a difference in negative tectonic subsidence from the total subsidence curve.

Cayo Fm. (SS-1) sedimentation occurred in a fall of the sea level (Fig. 5.4), and the tectonic subsidence curve is controlling the subsidence in the basin with a low rate of sediment supply; meanwhile, the total subsidence reached values of almost 3000 meters of depth suggesting a period of extension. Then, SS-2 (Guayaquil Fm.) exhibits a decrease

in subsidence compared to SS-1. However, the tendency is still positive for the tectonic, and higher values for total subsidence with a rise in sea level indicate an increase in the sediment supply with a possible climate factor and lower tectonic control. SS-3 (Zapallo Fm.) has parallel curves of tectonic and total subsidence with a smoother slope than SS-2, and the basin has been shallower since the Paleocene. However, the sediment supply seems to be constant between SS-2 and SS-3, and there is a decrease in the sea level. For SS-4 (Playa Rica Fm.), there was a fall in the sea level, and the total subsidence is parallel to the tectonic subsidence curve, implying a constant sediment supply. However, the basin deepens around 25 Ma and a quiescence period is inferred for the last three seismic sequences (SS-2, SS-3, SS-4). SS-5 (Tosagua Fm.) takes place with a rise in the accommodation space, and the tectonic curve has lower values in contrast with the total subsidence. It implies that the sediment supply rate increased and a higher load due to the rise of the sea level during the sedimentation of SS-5.

The unconformities between the seismic sequences show tendencies similar to the Chone-1 well. U-1 unconformity shows a negative tectonic and total subsidence curve that indicates a shallowing of the basin and a period of compression with uplifting. Then, the unconformity U-2 exhibits negative subsidence values, but the tectonic curve describes a reduction in the subsidence, which implies a compression period and shallowing of the basin. The unconformity between SS-3 and SS-4 (U-3) occurs during a sea level rise, which may be controlled by a climate factor in a compression interval. Finally, the unconformity U-4 happened with a decrease in the sea level, and as the tectonic subsidence values diminish, the total subsidence increases in time, indicating a compression period.

In the Calceta-1 and Chone-1 wells geohistory, the unconformity U-3 curves describe negative values for both subsidence plots. Meanwhile, the Ricaurte-1 exhibits a negative curve for tectonic subsidence but positive values for total subsidence.

In Figure 5.23, the results of the three geo-historical data have been plotted to discuss the contrast of subsidence between the wells. The plot shows an interval of high subsidence during the sedimentation of Cayo Fm. (SS-1), then an unconformity and a phase of short periods of subsidence in the deposition of SS-2, SS-3, SS-4, SS-5 and SS-6 for all boreholes. The initial phase indicates intense subsidence, but Chone exhibits a deeper value than the other wells (3700 m of the basin depth), followed by Ricaurte, with total subsidence of

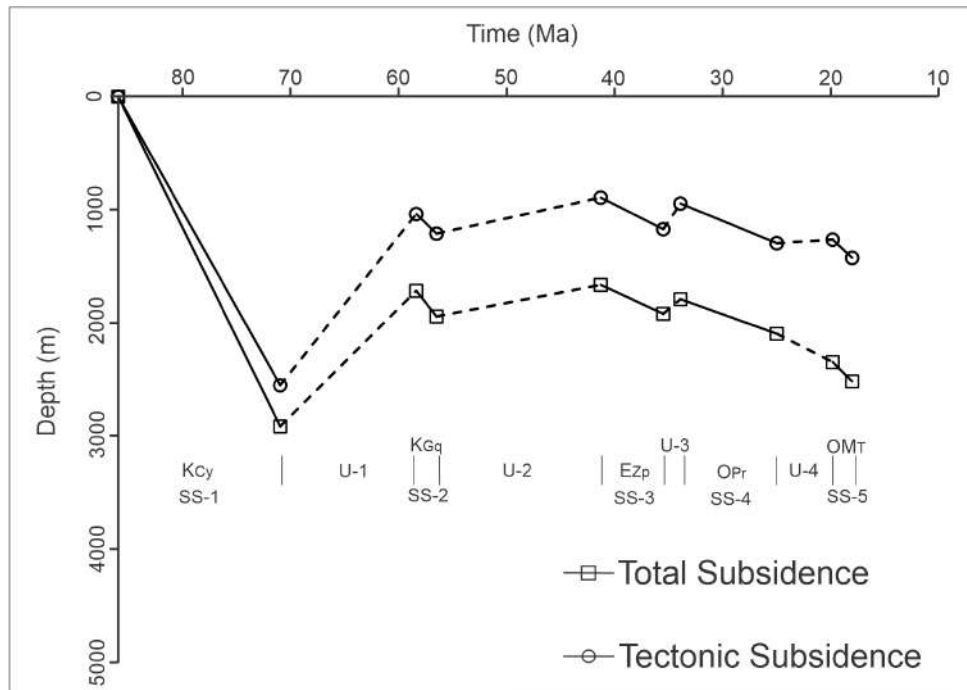


Figure 5.22: Geohistorical graphic of Calceta-1 well. Formation's code: KCy = Cayo Fm., KGq = Guayaquil Fm., EZp = Zapallo Fm., OPr = Playa Rica Fm., OMT = Tosagua Fm. It shows the seismic sequences SS-1, SS-2, SS-3, SS-4, SS-5, which correspond to each formation, and the unconformities U-0, U-1, U-2, U-3, U-4.

3513 m, and Calceta reached 2923 m. of depth at Cretaceous times (90 to 71 Ma). This implicates a deepening of the basin in the eastern part of the study area, especially in the southeast, where Chone-1 was drilled. Moreover, the tectonic subsidence curve for Calceta-1 suggests a higher tectonic control at the southwest of the basin; meanwhile, subsidence is driven by another factor at Ricaurte and Chone, such as the sediment supply. The basal unconformity (U-0) corresponds to the 93 to 90 Ma and could be related to a rift in the Lower Cretaceous. The following unconformity (U-1) described a shallowing of the basin due to the negative subsidence curves caused by an uplifting of the basin in a compression period.

During the sedimentation of Guayaquil Fm (SS-2), there is an increase in accommoda-

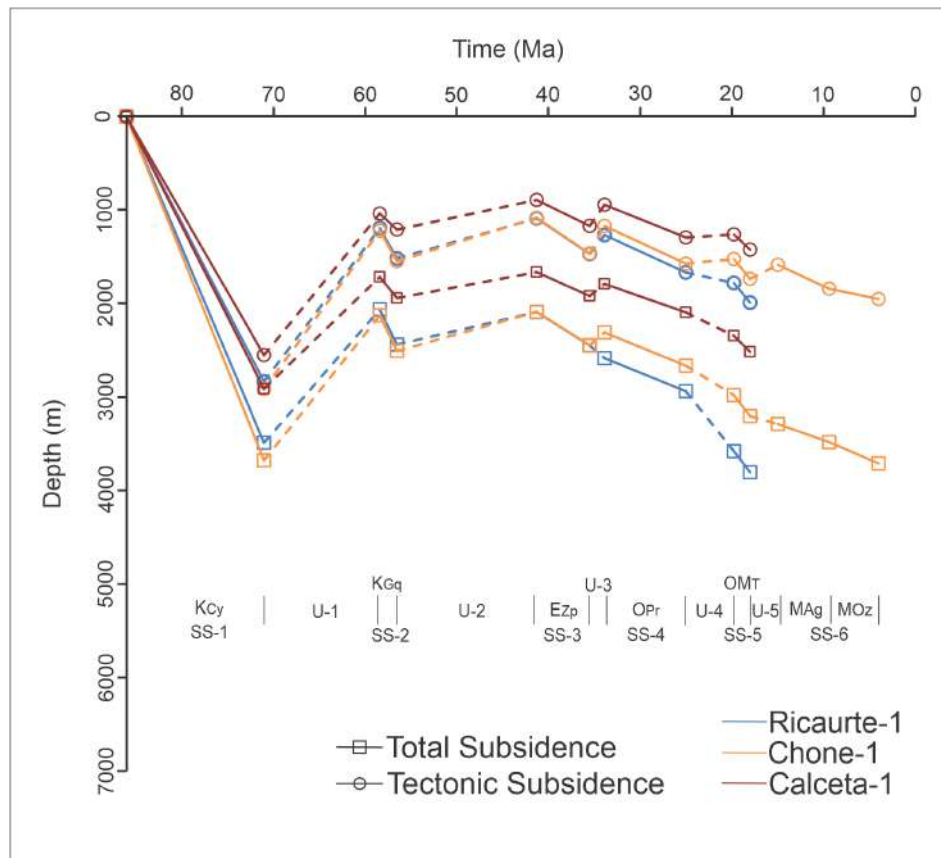


Figure 5.23: Geohistorical graphic of three wells (Ricaurte-1, Chone-1, Calceta-1). Formation's code: KCy = Cayo Fm., KGq = Guayaquil Fm., EZp = Zapallo Fm., OPr = Playa Rica Fm., OMT = Tosagua Fm. It shows the seismic sequences SS-1, SS-2, SS-3, SS-4, SS-5, which correspond to each formation, and the unconformities U-0, U-1, U-2, U-3, U-4.

tion space and subsidence controlled by a climatic factor. Then, U-2 suggests a compression period due to the negative subsidence. Jaillard et al. (1995); Jaillard (2022) stated that it was followed by emersion of the area, which coincides with the negative subsidence during U-2 at the Lower to Middle Eocene. Then, Jaillard et al. (1997) mentioned syn-sedimentary structures that show an extensive regime at the Middle to Upper Eocene corresponding to the deposition of Zapallo Fm (SS-3). Zapallo has a positive subsidence parallel between the three boreholes with a low accommodation space; also, there is a decrease in the tectonic control for the Calceta, suggesting a rise in the sediment supply and accommodation space. For unconformity (U-3; 35.5 Ma), Ricaurte evidences a positive value of total subsidence; meanwhile, the rest of the curves plot negative values for both subsidence.

Playa Rica Fm (SS-4) sedimentation has positive subsidence for all the curves. The U-4 shows a deepening of the basin with positive curves for the subsidence, mainly controlled by the Farallon plate's fragmentation at the beginning of U-4. [Hernández et al. \(2024\)](#), mentioned this sedimentary gap as the final of the accretion and a transitional stage after the collision. Tosagua Group (SS-5) plots positive subsidence curves for all the wells, indicating a deepening of the basin that exceeds the initial Cretaceous subsidence for Ricaurte-1, reaching more than 3700 m. of depth. Since the unconformity U-3, the Ricaurte-1 total subsidence curve reached deeper values than Chone-1, which suggests an increment of the sediment supply at the North of the basin caused by a possible change of the source because of the closing of the accretion process.

The geohistory of the three wells describes the evolution of the Manabí basin in a general way, still, the gathering of seismic and isopach information provides a comprehensive analysis of its evolution. The chart integrating the geohistory of the subsidence of the three wells (Fig. 5.23) corroborates that they belong to the same tectonic block. The mafic igneous rocks form the basement of the basin from an old insular arc accreted to continental crust, and its depocenters are at the northeastern part of the study area, which could be generated by the uplifting of BS at the NW of the basin in the Miocene-Pliocene. Then, U-0 delimits the base of SS-1, and the onlap of SS-1 reflectors suggests an erosion period. The SS-1 fining upward sequence indicates a high subsidence period controlled by tectonics and a transgressive sequence. [Carrillo et al. \(2022\)](#) stated a period of extensive kinetics in the Late Cretaceous, but [Hernández et al. \(2024\)](#); [Jaillard et al. \(1995\)](#) proposed a shortening period as the first stage of an accretion process. However, seismic profiles do not show any thrust fault or fold that evidences a compression period. Instead, the high subsidence and normal faults indicate an extensive period. Delimiting the top of SS-1 is U-1, which coincides with the sedimentary hiatus reported by [Ordóñez et al. \(2006\)](#) (66-58.4 Ma), and its negative subsidence curve represents the collision of the remanent arc with the Andean margin. Nevertheless, [Hernández et al. \(2024\)](#) stated this period as the second stage of the accretion process. After, SS-2 was deposited during regression and a subsidence period controlled by tectonics. The top of SS-2 is delimited by U-2 (56-41.3 Ma) unconformity, also reported by [Ordóñez et al. \(2006\)](#). U-2 suggests a compression period that shallows the basin, and [Hernández et al. \(2024\)](#) attributes it to

the final stage of the accretion of the Caribbean plateau with the continental crust. Then, the deposition of SS-3 was homogeneous over the area with higher vertical thickness at SW and occurred during a transgressive sequence and tectonic subsidence. SS-3, SS-4 and SS-5 are syn-tectonic sequences showing continuous depositional characteristics. Delimiting the top of SS-3 is the sedimentary hiatus U-3 (35-33.9 Ma), stated by [Ordóñez et al. \(2006\)](#), and a thermal maximum of the Paleocene-Eocene controlled its subsidence. [Carrillo et al. \(2022\)](#) mentioned a quiescence period or thermal subsidence during the Late Eocene. SS-4 deposition was also homogeneous TWT, thickening to NE, but there is a change in the depocenters in the study area. [Hernández et al. \(2024\)](#) mentioned this sequence is the transitional stage of post-accretion. Next, U-4 (23-19.8 Ma) was characterized by the subsidence caused by a load in the basin by rising sea level. A thickening to the North and a change of depocenters occurred during SS-5 deposition. The U-5 (17.8-15.9 Ma) mentioned by [Ordóñez et al. \(2006\)](#) shows low subsidence and a quiescence period. Finally, SS-6 was deposited during moderate subsidence caused by a load of sediments in a regressive sequence. [Hernández et al. \(2024\)](#); [Carrillo et al. \(2022\)](#) report clinoforms geometries of a prograding sequence to the west that create accommodation space. Additionally, [Carrillo et al. \(2022\)](#) describes a tectonic inversion at Upper Miocene that causes the structural deformation and reactivation of faults.

The basin assessment offers insights into the discontinuous sedimentation processes within its geological framework. Such discontinuities may pose challenges to hydrocarbon formation within the basin. However, the optimal conditions for the generation of a hydrocarbon reservoir were possible. Then, the exploration needs a meticulous and multidisciplinary approach. In this context, this sequential stratigraphy study has provided significant data suggesting that Tosagua Gp (SS-5) could be a promising prospect for exploration. Analyses of well-log data revealed significant porosity of sandstones in this formation. Moreover, the isopach map and seismic data provide the highest thickness and major structural features that serve as a seal layer at the NE of the study area. Furthermore, these results can help as a solid basis for future hydrocarbon prospecting studies, providing a valuable framework for research in the petroleum industry.

Chapter 6

Conclusions

The Manabí basin is a forearc basin that forms part of the coastal basin system of Ecuador and has recorded the tectonic evolution in its sediments. The study area represents the western central part of the basin, as studied by information from the Ricaurte-1, Chone-1, and Calceta-1 wells and eleven seismic lines. The sedimentation occurs over a Cretaceous igneous basement. The sedimentary fill has been delimited into five seismic stratigraphic sequences (SS-1, SS-2, SS-3, SS-4, SS-5, SS-6) from Late Cretaceous to Lower Pliocene divided by six unconformities (U-0, U-1, U-2, U-3, U-4, U-5).

The basement of the basin (BS) is delimited at the top by the basal unconformity (U-0), corresponding to Piñón Fm. from the Upper Cretaceous age. It is mainly composed of an igneous complex of basaltic pillow lavas. The base of the Piñón has not been identified, but the top shows a deepening of the basin towards the NE and a greater thickness at the eastern side of the area. This basement has been uplifted by the reactivation of the Jama system fault at the northwest of the basin, causing the overlying of a young sequence above the basement.

The first seismic sequence (SS-1) is defined by the basal unconformity (U-0) at the base and by U-1 at the top. Its age is from the Late Cretaceous (Santonian to lower Maastrichtian). It comprises volcanoclastic turbiditic deposits of conglomerates, siltstones, and sandstones, and Cayo Fm represents it. The depocenters around 0.938 s (TWT) are marked at Chone-1 and especially in the line that passes through Ricaurte-1, and that elongates SE-NW orientation. The geo-historical plots also confirm an intense subsidence caused by a tectonics.

The second seismic sequence (SS-2) is delimited by the unconformity U-1 at the base and U-2 at the top, with a Paleocene age. Its composition is tuffaceous siltstones, gray claystones, fine sandstones, and chert at the top, representing the Guayaquil Fm. The lateral variation indicates the geometry of the sequence, which suggests a shallowing of the basin with depocenters at the Calceta-1 and elongated to the north. The geo-historical plots also describe this shallowing, an increase in the sediment supply rate, and tectonic dominance.

The U-2 delimits the seismic sequence SS-3 at the base and the top by U-3 with an age of Middle Eocene to Lower Oligocene and a lithological composition of claystone and shales with a low content of limestone, which corresponds to the Zapallo Fm. This sequence is deepening to the NE, and it shows a depocenter at SW due to the increase in thickness. This suggests a change in the depocenters of the area. The subsidence is controlled by the sediment supply rate and tectonics during the deposition of SS-3.

The seismic sequence SS-4 is outlined by the unconformity U-3 at the base and the top by U-4, and Oligocene in age; it is lithologically composed of tuffaceous sandstones and claystone calcareous. The geometry of the sequence reveals depocenters at the northeasternmost part of the area grid that reached values of around 1.27 s (TWT). The geo-historical data indicate a deepening of the basin until around 3000 m of depth. Its main control is the sediment supply, followed by tectonism.

The seismic sequence SS-5 is defined by the U-4 at the base and the top by U-5, with age from Oligocene to Miocene. The Tosagua Group comprises coarse to fine sandstones, claystone, and marl at the base. The variations in thickness analysis exhibit a deeper deposition at the north, with depocenters at the northwest and the northeast of the area. Geo-historical data shows the basin's deepening and reduced subsidence's tectonic control.

The seismic sequence SS-6 is defined by the U-5 at the base, with age from the Middle Miocene to the Lower Pliocene. It encompasses two formations: Angostura and Ónzole, which are sandstones, conglomerates, siltstones and tuffs rich in marine fauna. The variations in thickness analysis exhibit a deeper deposition at the northeast, with a depocenter at the intersection of lines 11 and 3. Geo-historical data from Chone shows a deepening of the basin similar to the initial one of the Late Cretaceous subsidence (4000 m), with less tectonic control over the subsidence and more sediments carried to the basin.

The evolution of the basin was determined by different tectonic events produced by the accretion of the oceanic terrane, including thermal subsidence and compression periods, which are represented mainly by the unconformities bounding the seismic sequences. However, it also shows climate and sediment control in more recent times. Moreover, the data provides some important characteristics for a hydrocarbon reservoir that delimited the Tosagua group as a potential target for hydrocarbon exploration in the northeast of the studied region.

Bibliography

- Aizprua, C., Witt, C., Brönnner, M., Johansen, S. E., Barba, D., Hernandez, M. J., and Billi, A. (2020). Forearc crustal structure of ecuador revealed by gravity and aeromagnetic anomalies and their geodynamic implications. *Lithosphere*, 2020(1).
- Aizprua, C. A. (2021). Forearc crustal structure and controlling factors on basin formation across the southernmost northern andes: Geophysical and geological investigations.
- Al-Masgari, A. A.-S., Elsaadany, M., Abdul Latiff, A. H., Hermana, M., Hamzah, U. B., Babikir, I., Adeleke, T., Sohail Imran, Q., and Al-Bared, M. A. M. (2021). Seismic sequence stratigraphic sub-division using well logs and seismic data of taranaki basin, new zealand. *Applied Sciences*, 11(3):1226.
- Banco Central del Ecuador, D. T. (1990). *La Actividad Petrolera en el Ecuador en la década de los 80*.
- Barba, D. (2018). Estudio geologico de la cuenca manabi.
- Benitez, S. (1995). *Evolution géodynamique de la province côtière sud-équatorienne au Crétacé supérieur-Tertiaire*. PhD thesis, Université Joseph-Fourier-Grenoble I.
- Birnie, C., Ravasi, M., Liu, S., and Alkhalifah, T. (2021). The potential of self-supervised networks for random noise suppression in seismic data. *Artificial Intelligence in Geosciences*, 2:47–59.
- Carrillo, E., Barragán, R., Vázquez-Taset, Y., Almeida, R., Chalampunte, A., and Martín, G. (2022). The manabí and esmeraldas-borbón forearc basins of ecuador. pages 249–262.
- Catuneanu, O. (2020). Sequence stratigraphy. In *Regional Geology and Tectonics*, pages 605–686. Elsevier.

- Catuneanu, O. (2022). Chapter 1—introduction. In *Principles of Sequence Stratigraphy (Second Edition)*, pages 1–22. Elsevier, second edition edition.
- Catuneanu, O., Abreu, V., Bhattacharya, J., Blum, M., Dalrymple, R., Eriksson, P., Fielding, C. R., Fisher, W., Galloway, W., Gibling, M., et al. (2009). Towards the standardization of sequence stratigraphy. *Earth-Science Reviews*, 92(1-2):1–33.
- Cediel, F., Shaw, R. P., and Cceres, C. (2003). Tectonic assembly of the northern andean block.
- Central Bank of Ecuador (2023). Report on the evolution of the ecuadorian economy in 2022 and outlook for 2023 - central bank of ecuador. BCE.
- Deniaud, Y. (1998). Evolucion tectono-sedimentaria de las cuencas costeras neogenas del ecuador.
- Deniaud, Y. (2000). Enregistrements sédimentaire et structural de l'évolution géodynamique des andes équatoriennes au cours du néogène: étude des bassins d'avant-arc et bilans de masse.
- EIA (2023). Frequently asked questions - u.s. energy information administration (eia). U.S. Energy Information Administration (EIA) website.
- Energy Glossary (2023). Frequency.
- Eriksson, P. G., Muhongo, S. M., and Catuneanu, O. (2006). Editorial. *Journal of African Earth Sciences*, 46(3):173–179.
- Falcón, R. (2005). Seismic stratigraphy. Lecture.
- Gallagher, K. and Lambeck, K. (1989). Subsidence, sedimentation and sea-level changes in the eromanga basin, australia. *Basin Research*, 2(2):115–131.
- Galloway, W. E. (1989). Genetic stratigraphic sequences in basin analysis i: architecture and genesis of flooding-surface bounded depositional units. *AAPG bulletin*, 73(2):125–142.

- Haq, B. U., Hardenbol, J., and Vail, P. R. (1987). Chronology of fluctuating sea levels since the triassic. *Science*, 235(4793):1156–1167.
- Hernández, M. J., Michaud, F., Collot, J.-Y., d’Acremont, E., Proust, J.-N., and Barba, D. (2024). Evolution of the manabí forearc basin in ecuador: From the collision of caribbean oceanic plateau to the build up of the andes and coastal cordilleras. *Tectonophysics*, 870:230133.
- Hernández, M. J., Michaud, F., Collot, J.-Y., Proust, J.-N., and d’Acremont, E. (2020). Evolution of the ecuador offshore nonaccretionary-type forearc basin and margin segmentation. *Tectonophysics*, 781:228374.
- Hessler, A. M. and Sharman, G. R. (2018). Subduction zones and their hydrocarbon systems. *Geosphere*, 14(5):2044–2067.
- International Energy Agency (IEA) (2023). Oil market report - august 2023 – analysis.
- Jaillard, E. (2022). Late cretaceous-paleogene orogenic build-up of the ecuadorian andes: Review and discussion. *Earth-Science Reviews*, 230:104033.
- Jaillard, E., Benitez, S., and Mascle, G. H. (1997). Les déformations paléogènes de la zone d’avant-arc sud-équatorienne en relation avec l’évolution géodynamique. *Bulletin de la Société géologique de France*, 168(4):403–412.
- Jaillard, E., Ordoñez, M., Benitez, S., Berrones, G., Jiménez, N., Montenegro, G., and Zambrano, I. (1995). Basin development in an accretionary, oceanic-floored fore-arc setting: southern coastal ecuador during late cretaceous-late eocene time.
- Jarrín Tamayo, P. (2021). *Current kinematics in the Northern Andes by GPS*. Theses, Sorbonne Université.
- Kerr, A. C., Aspden, J. A., Tarney, J., and Pilatasig, L. F. (2002). The nature and provenance of accreted oceanic terranes in western ecuador: geochemical and tectonic constraints. *Journal of the Geological Society*, 159(5):577–594.
- Koutsoukos, E. A. (2005). Stratigraphy: Evolution of a concept. In *Applied Stratigraphy*.

- Li, M., Bralower, T. J., Kump, L. R., Self-Trail, J. M., Zachos, J. C., Rush, W. D., and Robinson, M. M. (2022). Astrochronology of the paleocene-eocene thermal maximum on the atlantic coastal plain. *Nature communications*, 13(1):5618.
- Lonsdale, P. (1978). Ecuadorian subduction system. *AAPG Bulletin*, 62(12):2454–2477.
- Lowrie, W. (2007). *Fundamentals of Geophysics*. Cambridge University Press, 2 edition.
- Luzieux, L. (2007). *Origin and Late Cretaceous-Tertiary evolution of the Ecuadorian fore-arc*. PhD thesis, ETH Zurich.
- Mitchum, R. M. (1977). Seismic stratigraphy and global changes of sea level, part 6: Stratigraphic interpretation of seismic refraction patterns in depositional sequences. *Seismic Stratigraphy Applications to Hydrocarbon Exploration*, 26:117–133.
- Nanda, N. C. (2016). *Seismic Data Interpretation and Evaluation for Hydrocarbon Exploration and Production*.
- National Oceanic and Atmospheric Administration (2019). What is subsidence?
- Octavian, C., Galloway, W., Kendall, C., Miall, A., Posamentier, H., Strasser, A., and Tucker, M. (2011). Sequence stratigraphy: Methodology and nomenclature. *Newsletters on Stratigraphy*, 44:173–245.
- Ordóñez, M., Jiménez, N., and Suárez, J. (2006). Micropaleontología ecuatoriana: Petroproducción (filial de petroecuador). *Centro de Investigaciones Geológicas de Guayaquil, Guayaquil, Ecuador*, pages 61–64.
- Organization of the Petroleum Exporting Countries (2023). Energy asia. Lee Ying Shan.
- Pazmiño, F. W. and Tenelema, G. D. (2022). Estudio sismoestratigráfico y estructural de la parte sur de la cuenca de manabí mediante el análisis de 2-d msc data.
- Pérez, R. and Richard, A. (2015). *Integración de estratigrafía secuencial y atributos sísmicos para la caracterización del campo El salto, estado Monagas*. PhD thesis.
- Posamentier, H. W. and Allen, G. P. (1999). *Siliciclastic sequence stratigraphy—concepts and applications*. SEPM Society for Sedimentary Geology.

- Reyes, P. (2013). *Évolution du relief le long des marges actives: étude de la déformation Plio-Quaternaire de la cordillère côtière d'Équateur*. PhD thesis, Université Nice Sophia Antipolis.
- Reyes, P. and Michaud, F. (2012). *Mapa Geologica de la margen costera ecuatoriana (1:500000)*.
- Slater, J. G. and Christie, P. A. (1980). Continental stretching: An explanation of the post-mid-cretaceous subsidence of the central north sea basin. *Journal of Geophysical Research: Solid Earth*, 85(B7):3711–3739.
- Selley, R. and Sonnenberg, S. (2023). *Sedimentary Basins and Petroleum Systems*, pages 419–472.
- SEPM STRATA (2014). Sequence stratigraphic framework - sepm strata. Available online: <http://www.sepmstrata.org/page.aspx?&pageid=410&3>.
- Smith, S. (2006). Renewable and nonrenewable resources.
- STRATA SEPM (2013). Use of well logs for sequence stratigraphic interpretation of the subsurface. Well log sequence stratigraphy.
- STRATA SEPM (2015). Well log suites. Well log suites.
- STRATA SEPM (2017). Introduction to sequence stratigraphy - sepm strata.
- The Observatory of Economic Complexity (2022). Ecuador (ecu) exports, imports, and trade partners. The Observatory of Economic Complexity.
- Vallejo, C. (2006). *Evolución de la Cordillera Occidental e los andes del Ecuador (Cretácico tardío–paleógeno)*. PhD thesis, Tesis doctoral. Swiss federal institute of technology zürich. Suiza.
- Van Hinte, J. E. (1978). Geohistory analysis—application of micropaleontology in exploration geology. *AAPG Bulletin*, 62(2):201–222.
- Van Melle, J., Vilema, W., Faure-Brac, B., Ordonez, M., Lapierre, H., Jimenez, N., Jaillard, E., and Garcia, M. (2008). Pre-collision evolution of the piñón oceanic terrane of sw

ecuador: stratigraphy and geochemistry of the “calentura formation”. *Bulletin de la Société géologique de France*, 179(5):433–443.

Villamizar, B., Hanyang, L., and Cheng, N. (2018). Increasing the value of seismic data with pre-stack spectral blueing. In *SEG 2018 Workshop: Reservoir Geophysics, Daqing, China, 5-7 August 2018*, pages 24–27. Society of Exploration Geophysicists and the Chinese Geophysical Society.

Villitanga, Rubén, M. (2020). Tectonosequence analysis of the manabi basin, ecuador. B.S. thesis, Universidad de Investigación de Tecnología Experimental Yachay.

Worldometer (2017). Oil left in the world. Worldometer website.

Appendices

Appendix 1.

The appendix shows the final seismograms used for the well-tie of the wells: Ricaurte-1, Chone-1 and Calceta-1.

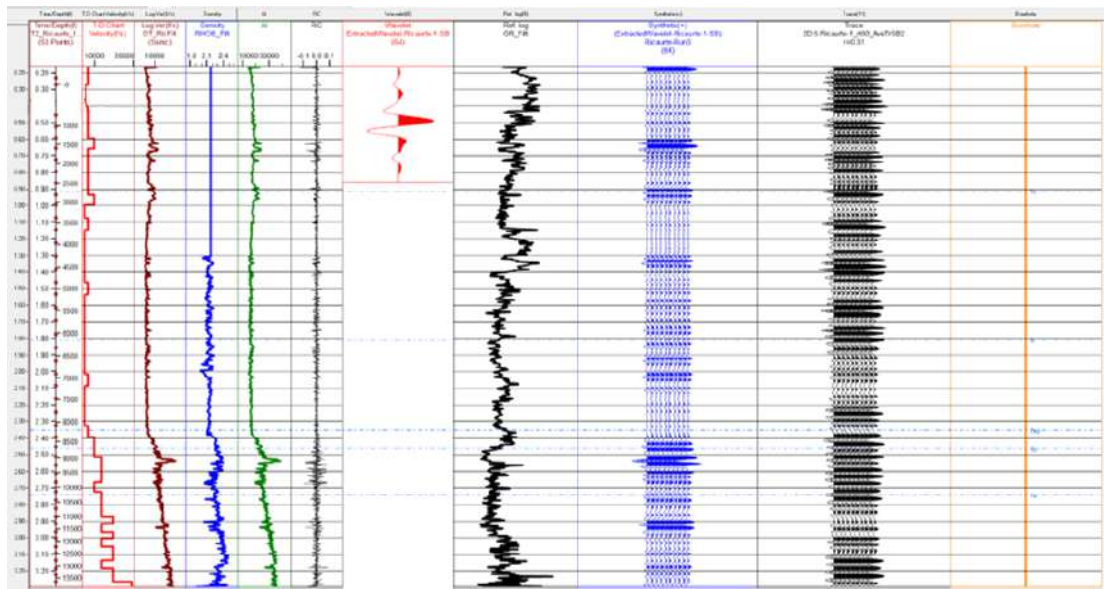


Figure 1: Synthetic seismogram of Ricaurte-1 well after the improvement of data.

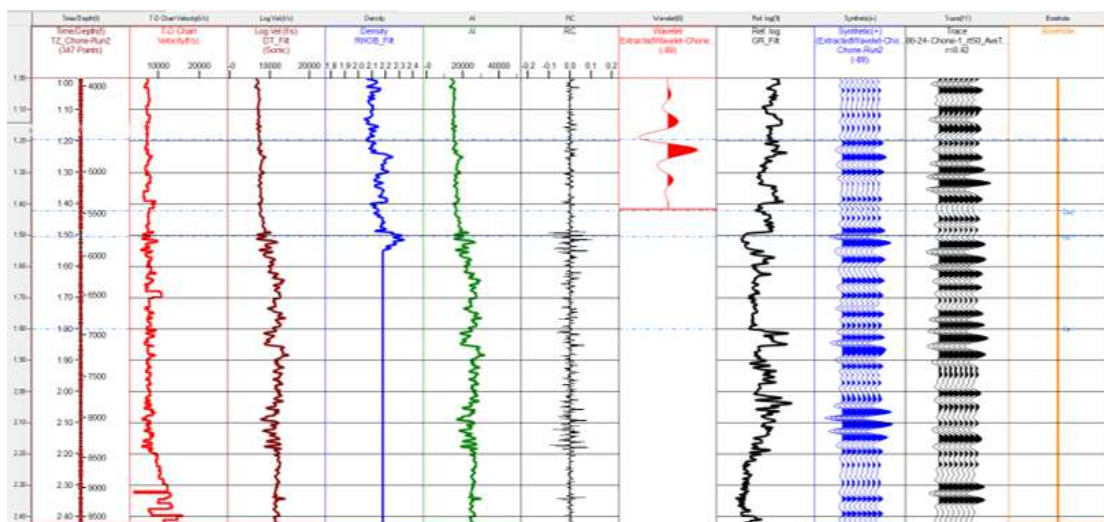


Figure 2: Synthetic seismogram of Chone-1 well after the improvement of data

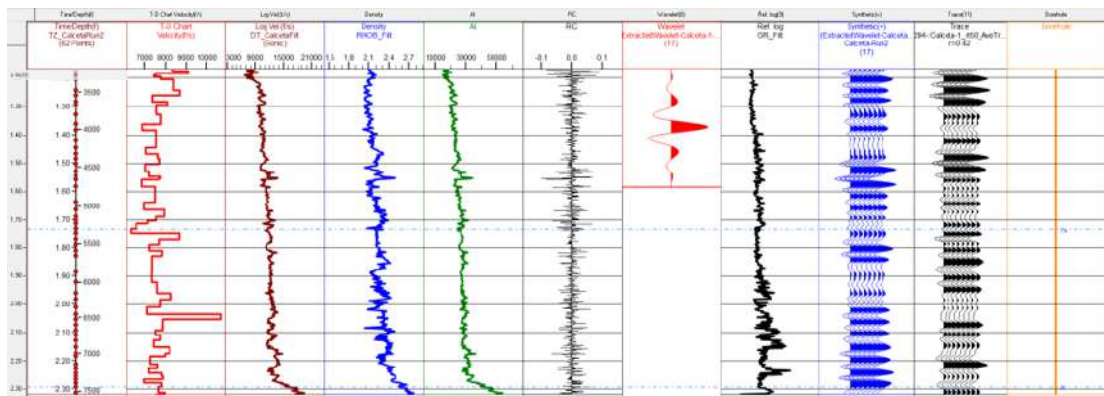


Figure 3: Synthetic seismogram of Calceta-1 well after the improvement of data